UNIVERSITA' POLITECNICA DELLE MARCHE

FACOLTA' DI INGEGNERIA

Corso di Laurea Magistrale in Biomedical Engineering

Finite Element Analysis of an innovative Mandibular Advancement Device for people suffering from Obstructive Sleep Apnea Syndrome combined with Periodontitis.

Relatore:

Prof. Marco Mandolini

Tesi di Laurea di:

Maddalena Barocci

A.A. 2019 / 2020

Abstract

The Obstructive Sleep Apnea (OSA) is a respiratory disorder very common among the population, characterized by episodes of complete or partial obstruction of the upper airways during the sleep. Nowadays, people who suffer from this respiratory disorder are able to cohabit with it without altering too much their day life thanks to non - invasive devices as the Mandibular Advancement Device (MAD).

In this work the finite element method has been used to carry out static structural simulations to evaluate the mechanical interaction, in terms of stress and deformation, between the MAD and the anatomical components of the oral cavity. The innovation of this work is the investigation of the OSA syndrome in a condition of periodontitis, an inflammatory disorder that affects the periodontium. In particular, a comparison analysis has been performed between a healthy model and a model where periodontal ligaments and mandibular bone are affected by the first stage of periodontitis (characterized by 15% bone reduction). The 3D models of the MAD and the dental arches representing both a healthy and an inflammatory condition are obtained by means of a Reverse Engineering technique and computer-aided design modelling software. Subsequently, the finite element analyses have been performed through Ansys software and the results obtained for the healthy and pathological condition have been compared. By evaluating the stress and the deformation of teeth and periodontal ligaments, a direct relationship can be established between bone resorption and an increase in stress and deformation in the affected area. The results achieved in this work show that the mandibular teeth deformation increases in the periodontitis condition with respect to the healthy model, ranging between 9% and 11%, while in the maxillary teeth the range is between 3% and 14%. For what concerns the stress over ligaments, the trend is a little bit swinging. The stress value of the mandibular periodontal ligaments of the periodontitis condition ranges between -16% and 24% with respect to the healthy model and between -24% and 14% for the maxillary periodontal ligaments. The results of this work are in line with the articles describing a situation of bone resorption, since greater deformation and stress values are documented in the most worn areas as might be expected. However, not all the results of this work are comparable with the results found in the literature, since this is the first study that investigates the biomechanical effects of a MAD to treat the OSA syndrome coupled with periodontitis making this work innovative. Further studies are planned to analyze in deeper all the other staging of periodontitis and consequently, to evaluate the edentulism phenomenon associated with this disorder.

Summary

1. Introduction

The Obstructive Sleep Apnea Syndrome (OSAS) is a respiratory disorder very common among the population, characterized by episodes of complete or partial obstruction of the upper airways during the sleep. The factors associated with OSAS are multiple, first among all: the obesity, which reduces the expansive force of the pharyngeal dilator muscles and it generates an accumulation of adipose tissue in the neck region, provoking a reduction in the lumen of the airway tract. Nowadays the treatment of OSAS is built up by several devices that allow patients to cohabit with this pathology without altering their day life too much. The Mandibular Advancement Device (MAD), a non-invasive device, with its induced movement of the mandible forward has gained popularity and it has been widely studied by researchers worldwide for evaluating the benefits and also the drawbacks of this approach. But what happens if an OSA patient suffers also from another pathology that affects its oral cavity, like the periodontitis? What are the consequences of the MAD usage in this case?

First of all, the periodontitis is an inflammatory dental pathology that is characterized by several stages of wearing out of the periodontium, the structural unit of teeth. This condition is determined by a lot of factors such as the poor hygiene, the poverty, a diet rich in sugar and even systemic diseases.

Periodontitis affects the periodontium and, as a result, reduces the height of the alveolar bone around the tooth. The initial stage of this pathology begins with a slight inflammatory activity at the gingival level: gingivitis; then periodontitis proceeds wearing down the periodontium more, until at the most severe stages (staging III and staging IV) the loss of some teeth occurs. As the severity increases, greater percentages of alveolar bone and teeth are lost. In this work is evaluated a staging I of periodontitis that is characterized by a 15% of reduction in the height of the alveolar bone with no loss of teeth in both the dental arches.

The evaluation of the consequences of a new MAD in a condition of periodontitis is analyzed for the first time in this work, as no one until now has ever gone to evaluate periodontitis associated with OSAS. In this work has been introduced a new MAD no yet on the market called the new SomnoDent Avant.

Since in vivo experiments that test behaviors of anatomical structures of the oral cavity in relation to a MAD are not practicable both in healthy or unhealthy conditions, the Reverse Engineering (RE)

technique allows to model all the anatomical structures and the MAD in order to obtain a 3D model to be simulated through the ANSYS software. In fact, by using the RE technique a tridimensional prototype of the anatomical structures is reconstructed from Cone Beam Computer Tomography (CBCT) scans of an OSA patient. Whereas the re-modelling of the new SomnoDent device occurs by means of laser scans over its geometry.

Subsequently, through the Finite Element Method (FEM) it is possible to make a structural analysis of the mechanical behaviors of the anatomical structures during the application of this specific MAD. The anatomical components that interact with the MAD are not only the periodontal ligaments (PDLs) and teeth, but are also the Mandible and Maxilla, both composed by cancellous and cortical bones.

In this work the attention goes to the evaluation of the mechanical interactions between this non-invasive device and the anatomical parts of the oral cavity both in the condition that sees healthy dental arches and worn by periodontitis. The anatomical parts affected by this dental disorder were not acquired by means of CBCT scans but were remodeled through a CAD approach, starting from the healthy anatomical structures get with this Computer Tomography technique.

Therefore, through the RE and FEM technique, it was possible to carry out an exhaustive analysis on the mechanical consequences caused by the application of this new MAD in patients suffering not only from OSA syndrome but also from Periodontitis.

This innovative approach will take further studies to analyze in deeper all the other staging of periodontitis and consequently, to evaluate the edentulism phenomenon associated with this disorder.

2. Chapter 2: Medical Background

The **tooth** is one of the most individual and complex anatomical as well as histological structures in the body. The tissue composition of a tooth is only found within the oral cavity and is limited to the dental structures. Each tooth is paired within the same jaw, while the opposing jaw has teeth that are classified within the same category. However, they are not grouped according to structure, but rather by function. They are settled within the upper and lower alveolar bone in the maxilla and mandible respectively and this exclusive type of joint is known as **gomphosis**.

The teeth are divided into four quadrants within the mouth, with the division occurring between the upper and lower jaws horizontally and down the midline of the face vertically. This leaves up to eight adult teeth in each quadrant and separates the opposing pairs within the same alveolar bone as well as their counterparts in the opposing jaw. Each quadrant contains: a medial incisor, a lateral incisor, a canine, two premolars and between two and three molars. The incisors are used for cutting and biting, the canines are used for gripping, as well as the premolars and the molars are used for grinding.

The main functions of the teeth include:

- chewing food into a bolus that can be easily swallowed for further digestion,
- giving structure, tissue support and shape to the face,
- aiding in the pronunciation of sounds during speech.

2.1 Tooth Anatomy

The structure of teeth is built up by articulating surfaces on the most superior part of the crown, designed to accommodate the function of the tooth. Therefore, the anterior teeth, from the right canine to the left canine, have a **single incisive edge** that can clamp down upon and tear away at a piece of food, whilst the premolars and molars have **cusps**, **pits** and **fissures** that are able to grind and mash a mouthful of food so that it is edible.

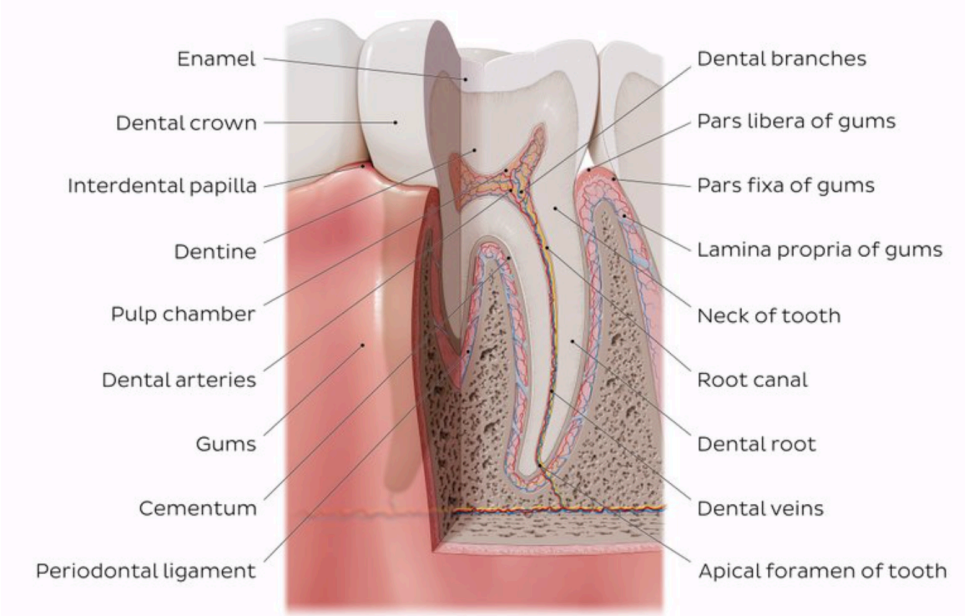

Figure 1 Structure of a tooth.

Each tooth is composed by four dental tissues visible in *Figure 1*. Three of them are hard tissue: enamel, dentin and cementum; while the fourth tissue is a soft, or non-calcified, tissue: the pulp. This latter one constitutes the center of the tooth and it contains nerves, blood vessels and connective tissue.

The **enamel** is the outer layer of the tooth that covers the dentin in the crown. It is a hard calcified tissue that contains no living cells and for this reason a damage of it cannot be self-repaired but needs a dentist intervention. The thickness of the enamel together with other factors like oral hygiene, lifestyle and age influences the color of the **crown**, the visible part of the tooth. In fact, the crown could vary its color from a pearl white to a yellow. Underneath this tough external layer there is a second softer layer with a structure of microscopic tubules (small hollow tubes or canals), that is slightly darker in color and it is known as **dentine.** This is the capsule that separates the hard outer tissue from the most inner layer, the **pulp cavity.** It is a soft tissue which contains blood vessels, nerves and connective tissue. The enamel and the dentine must be intact in order for the tooth to stay alive and healthy, if bacteria enter the pulp chamber, the damage is irreversible. The pulp chamber originates at the visible level of the tooth but it continues down till arrives at the apex of the root where there is an opening which allows the structures of the pulp to exit and enter. The area that signs the connection between the visible and hidden parts of tooth is defined **neck of the tooth** and is located between crown and root. The **root** of the tooth, whether it is single or multiple in number, is protected by soft tissues called gums. At the level of root, a portion of the pulp chamber continues down inside the **root canal** which is surrounded by dentine that finishes just

before the apex, where the root is surrounded not by enamel, but by cementum. The **cementum** is a hard connective tissue which gives attachment to the **periodontal ligament**, a thin layer of dense soft connective tissue interposed between tooth root and alveolar bone [1]. The viscoelastic properties of the periodontal ligament can be explained in terms of the different components composing it and their interaction *(Figure 2).*

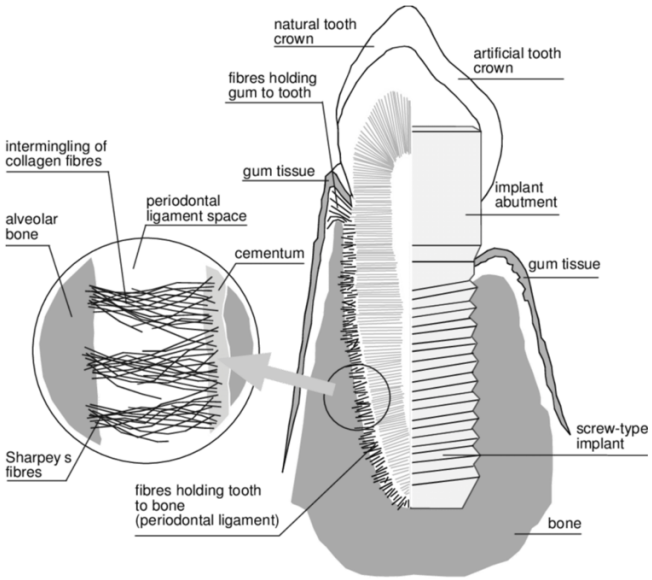

Figure 2 Representation of a PDL.

It is mainly comprised of structurally aligned collagen fibers (50-75%) along with fibroblasts, epithelial cells, osteoblasts, cementoblasts, and mesenchymal stem cells. Most of the collagen fibers are arranged in bundles extending from the cementum to the alveolar bone in a complex three-dimensional network. By transmitting forces acting externally on the tooth to the alveolar wall, these fibers bundles support the tooth in the bony socket and protect the tooth unit from intrusive, extrusive and rotational movements [2]. PDLs transmit the occlusal forces to the bone acting as a shock absorber in order to protect the vessels and nerves from injury by mechanical forces. They also maintain the gingival tissues in their proper relationship in the teeth and play a crucial role in sustaining tooth in the bone socket. Irreparable damages of this tissue provoke tooth loss, causing a decreased quality of life. Besides these physical properties, they also provide nutrients to the cementum, the bone and the gingiva by way of blood vessels. The thickness of human PDL ranges from 0.20 to 0.25 mm depending on the specific tooth position around the root and varies with age and healthy condition of the subject. PDL together with cementum, alveolar bone and gums forms the **periodontium**, a specialized structure that surrounds and supports the teeth. Each of these components that built up the periodontium is distinct in location, architecture, and biochemical

properties, which adapt during the life of the structure. For example, as teeth respond to forces or migrate medially, bone resorbs on the pressure side and is added on the tension side. Cementum similarly adapts to wear on the occlusal surfaces of the teeth by apical deposition. The periodontal ligament in itself is an area of high turnover that allows the tooth not only to be suspended in the alveolar bone but also to respond to the forces. Thus, although seemingly static and having functions of their own, all of these components function as a single unit.

2.1.1 Tooth Surfaces

The crown of each tooth is divided into five surfaces which are named according to the direction in which they face. This subdivision is made in order to better identify a specific section of the tooth. The surfaces are termed as following [3]:

- **Occlusal/Incisal surface** – the biting surface. The cutting edge of the anterior teeth that is used for mastication is defined *incisal edge*, while in the posterior teeth it is termed the *occlusal surface*.

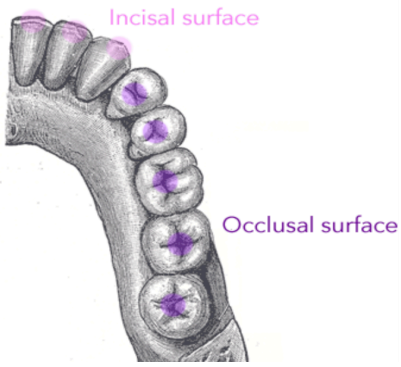

Figure 3 Representation of Occlusal/Incisal surface.

- **Mesial surface** – surface toward the midline of the mouth.

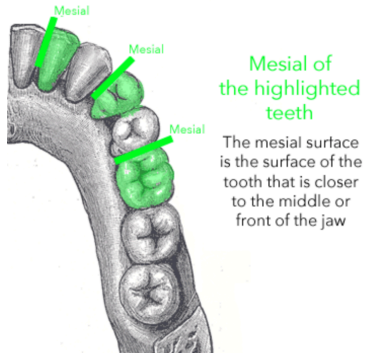

Figure 4 Representation of Mesial surface.

- **Distal surface** – surface away from the midline of the mouth.

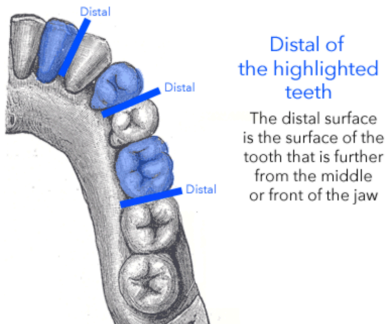

Figure 5 Representation of Distal surface.

- **Buccal/Vestibular/Facial surface** – surface facing the outside (cheek) of the mouth. The outer surface of the posterior teeth, premolars and molars, is commonly termed *buccal surfac*e.

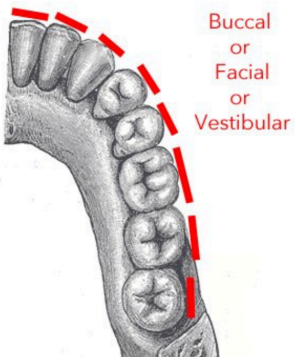

Figure 6 Representation of Buccal/Vestibular/Facial surface.

- **Lingual/Palatal surface** – surface facing the inside (tongue/palate) of the mouth. The surface of the maxillary teeth is termed *palatal surface* because it faces the palate, while that of the mandibular teeth is termed *lingual surface* because it faces the tongue.

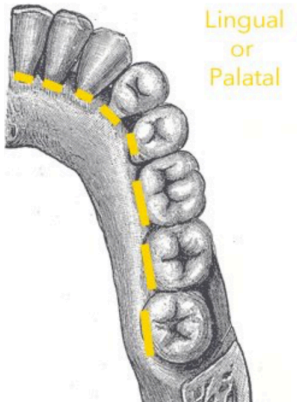

Figure 7 Representation of Lingual/Palatal surface.

For purpose of facilitating localization of various areas within a specific surface, the surface is divided into thirds in horizontal direction, as well as, in mesiodistal and bucco-lingual/palatal directions *(Figure 8).* [4]

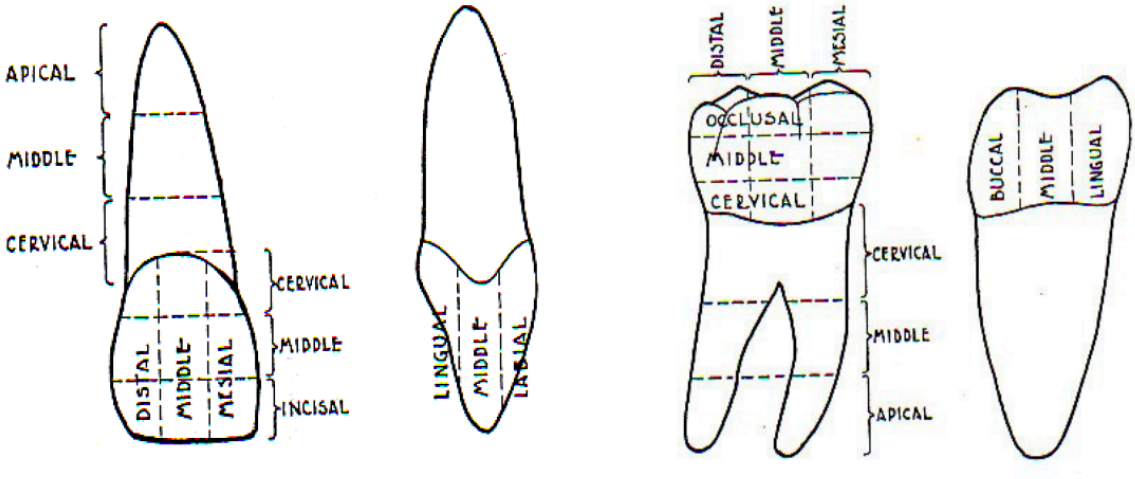

Figure 8 Division of tooth surfaces. Vertical divisions into thirds and buccal and proximal horizontal divisions.

2.2 Tooth Morphology

Teeth share general similarities in tooth structure (anatomy) but differ in morphology. In fact, the morphology depends on the type and position of the tooth. This paragraph provides a brief description of the dental morphology by analyzing each tooth making up the permanent dentition:

- **Incisors**;
- **Canines**;
- **Premolars**;
- **Molars**.

There are eight **incisors** *(Figure 10)* in the mouth, four in each jaw and two in each quadrant (central and lateral incisors) and they are placed one to each other. The maxillary and mandibular central incisors connect both arcades of the jaw, while the lateral/second incisors enter in contact with the canines on the distal side. Surface of incisors forms sharp edge and this feature characterizes the role of these teeth that is to shear, cut and separate pieces of food during mastication. *The maxillary central incisors* are characterized by a wide mesio-distal dimension, the widest one (Nelson and Ash, 2010) and a rectangular shape of the crown from the labial aspect, with a slightly convex surface. The mesial outline of the tooth forms a labial view and is usually straight or slightly convex. From the lingual aspect the tooth is concave in the upper part and shows mesial and distal borders creating marginal ridges that surround the concavity called lingual fossa, while the lower part is slightly curve, forming a structure called cingulum *(Figure 11). The maxillary lateral incisors* present similar characteristics to the central counterpart, even if they are smaller in dimensions and present differences in labial and lingual surfaces: the labial surface is more convex, while the lingual one has marked marginal ridges and a prominent cingulum. *The mandibular central and lateral incisors* are similar one to each other but compared with the maxillary ones they have very different morphology. They are the most mesio-distally narrow teeth in the whole set with the central incisors that are narrower than the lateral ones due to their small size. in fact, the mandibular central incisors are the smallest teeth in the whole oral cavity. The labial surface in these teeth is regular, extended and a little bit curved, while the lingual surface is not concave as in the maxillary incisors, but the cingulum is still present. All the incisors are characterized by a single root even if the length and the width may vary. [5]

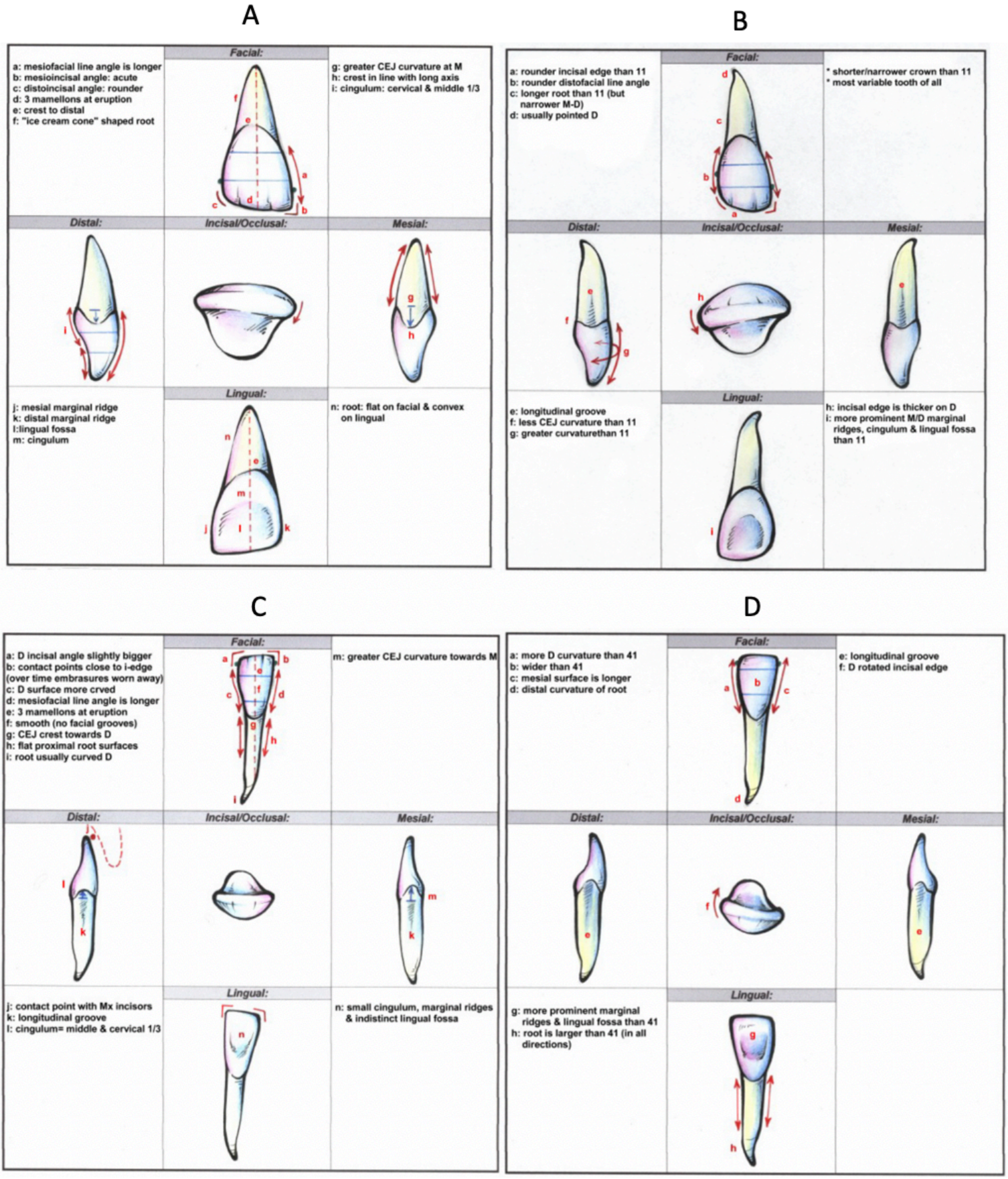

Figure 9 Dental morphology of the human incisors. A) right upper first incisor, B) right upper second incisor, C) right lower first incisor, D) right lower second incisor.[5]

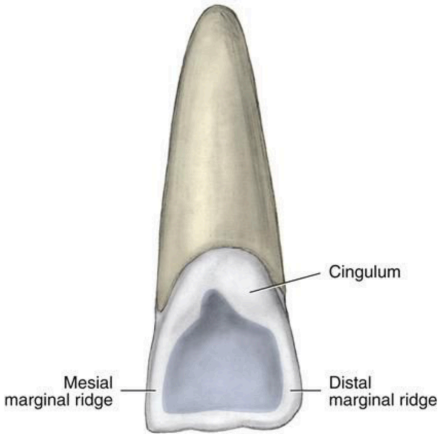

Figure 10 Cingulum: the lingual lobe of an anterior tooth that makes up the bulk of the cervical third of the lingual surface.

Canines are located between incisors and premolars and they have a dual function: to tearing pieces of food and to complement their neighbors in their actions. Maxillary and mandibular canines are similar in morphology but differ in size as the upper canines are wider than the lower ones *(Figure 12).* They only have one, prominent cusp and one root. That is the longest compared with all the other teeth. Their surfaces are strongly convex with marginal ridges visible on the lingual surface and show a prominent cingulum, especially in the upper canines. [5]

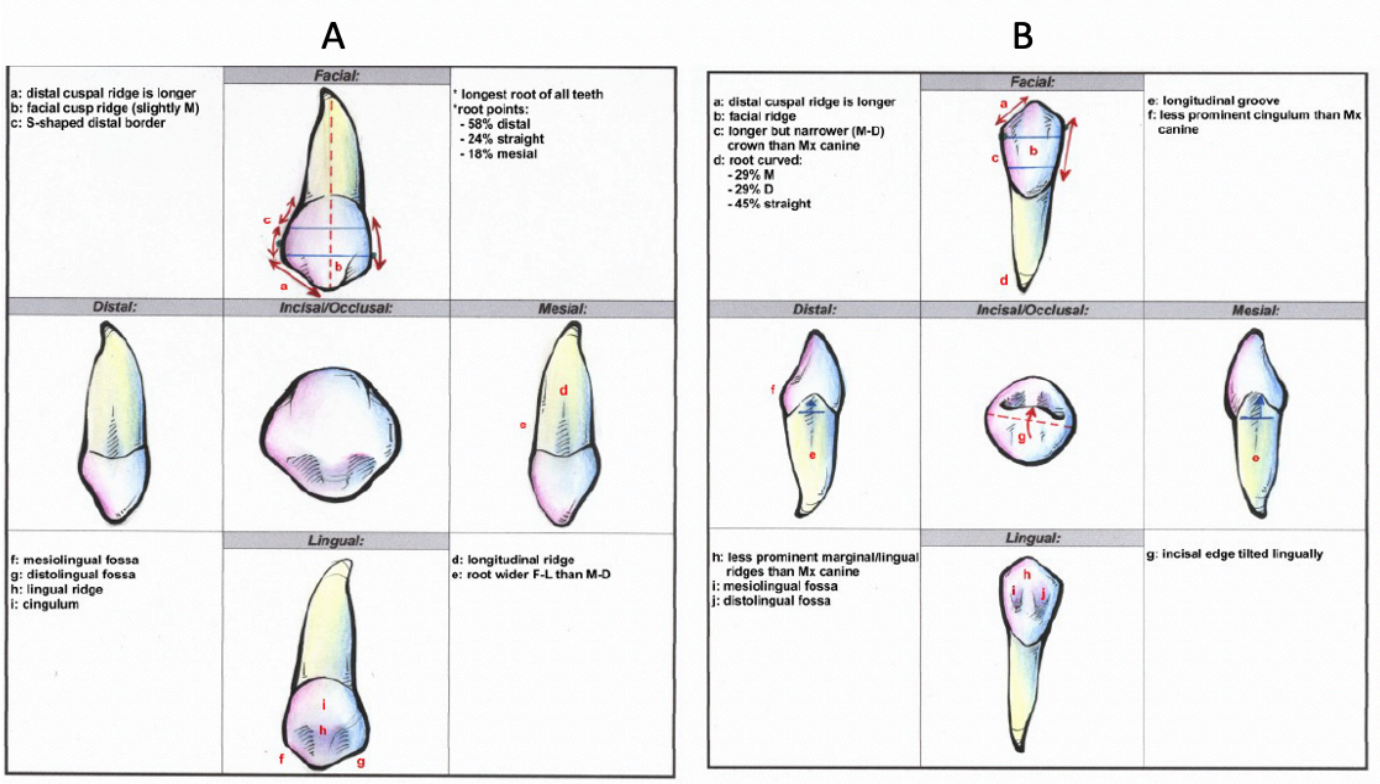

Figure 11 Dental morphology of human canines. A) right upper canine, B) right lower canine. [5]

Premolars are located behind the canines in the place of the deciduous molars and together with the molars are often referred to as posterior teeth. There are two premolars per quadrant, respectively referred to as third and fourth premolar, due to the fact that primitive mammals had four premolars, the first two were lost during evolution of the clade. These teeth have commonly two cusps (even if they can vary from one to three), one or two roots and a crown elongated specially in a bucco-lingual direction. The function of premolars is a combination of shearing and grinding food, the first action belongs to canines while the second one belongs to molars. Both premolar and molars lack in incisal cutting edges because their crown is flat and shows a broader occlusal surface. The maxillary third premolar is usually bigger than the maxillary fourth, both in crown and root dimensions. From a buccal view, the crown of premolars has a slightly pentagonal shape with a distal ridge longer than the proximal one. The buccal surface is curved and shows two facial grooves. The lingual surface is convex even if slightly narrower than the buccal one. The lingual cusp is sharp, but noticeably smaller than its buccal counterpart, with the tip bending mesially, except int the upper fourth premolar, in which they are similar in size. this cusp size difference is more evident in the mandibular premolars because the crown tends bends lingually, whereas it is strait in the upper premolars. The mandibular fourth premolar is frequently bigger than the third one, although its crown is usually a bit shorter. The buccal surface of the mandibular third premolar is convex and shows well-marked facial grooves, lees visible on the other premolars. From an occlusal perspective, the central groove and mesial and distal fossa are well marked, more centrally located int the upper premolars than in the lower ones which show a smaller lingual cusp and a diamond-shape occlusal contour. One or two roots may be present at the upper third premolar, though with a furcation at the apical third of the root, whereas the other premolars are single-rooted with a root often curved distally than mesially. [5]

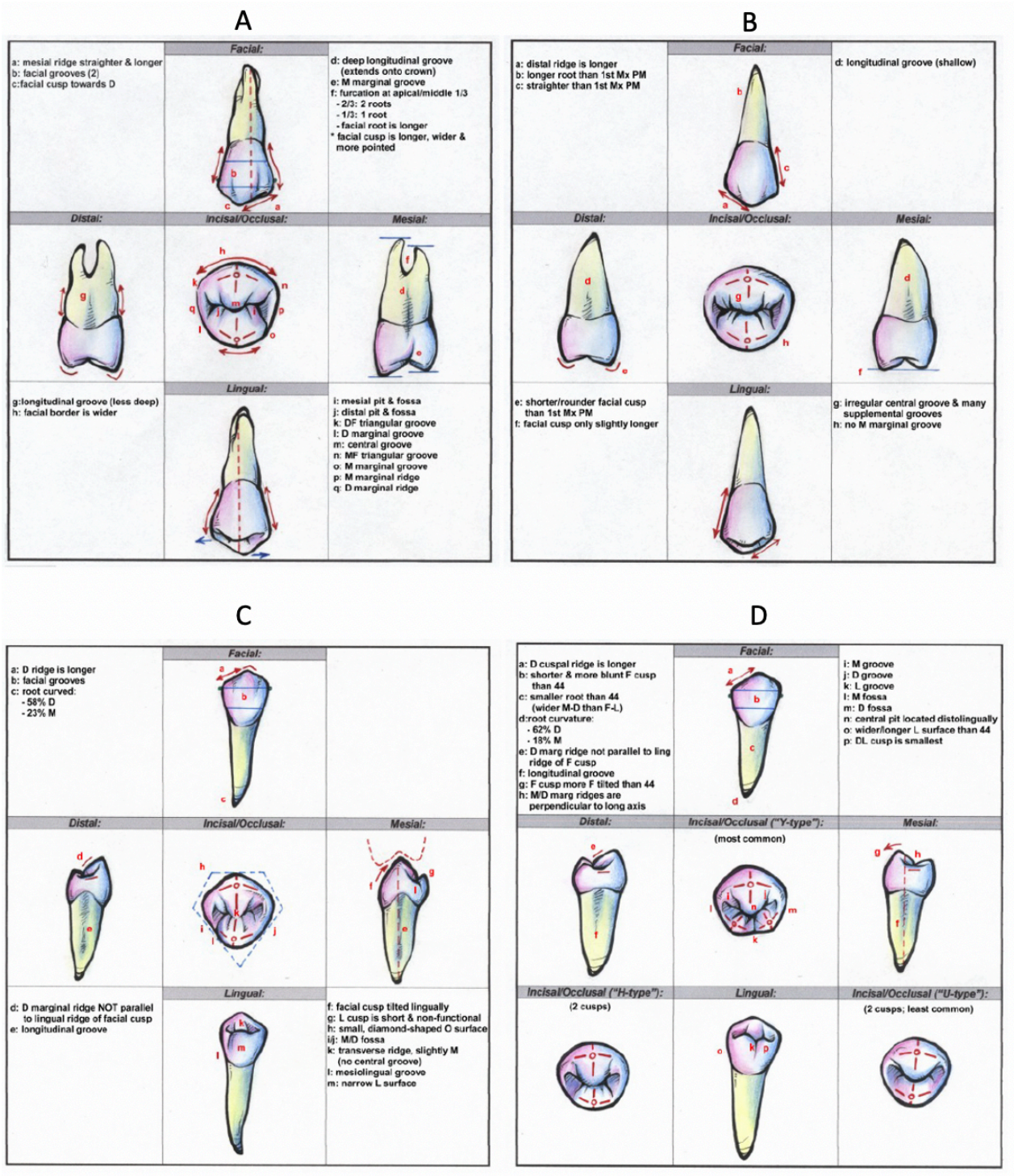

Figure 12 Dental morphology of the human premolars. A) right upper third premolar, B) right upper fourth premolar, C) right lower third premolar, D) right lower fourth premolar. [5]

Molars in the oral cavity are twelve, three for each quadrant. The chewing and grinding food particles during mastication are the main functions of these teeth, but they are also crucial in maintaining the verticality of the face and filling cheeks, a quality that molars shear with premolars. Molars are the biggest teeth in the mouth (summing up almost half of the dental arch length, 51%

in the mandible and 44% in the maxilla) and they have no antecedents in deciduous dentition. They show the most complicated morphology which notably changes between the jaws *(Figure 14)*. The first upper molar has the most stable morphology among all and it presents four main cusps, two buccal (protocone and paracone) and two lingual (metacone and hypocone). In this tooth the hypocone (disto-lingual cusp) is well defined by a distal oblique groove and the paracone and metacone are connected through a transverse groove of the oblique ridge that joins them. Most frequently the first upper molar has three roots of a similar length, two buccally and one lingually located. The tooth has a squared aspect larger bucco-lingually than mesio-distally if it is visualized from an occlusal view. The mesio-buccal cusp (protocone) is usually the biggest cusp and the disto-lingual one (hypocone) the smallest. The second upper molar that is generally smaller than the first one shows a more variable morphology. It is normally characterized by four cusps but sometimes hypocone seems to be reduced or even absent. From an occlusal view, the proximal side is wider than the distal. The mesio-lingual cusp is usually the biggest and the disto-lingual, if not missing, is the smallest. As in the first molar, the oblique ridge and the proximal and distal foveae are deep and well-marked. This tooth also has three, well-developed roots. The third upper molar is the last one in the dental arch and the last maxillary tooth to erupt. This tooth shows the greatest morphological variability of all the other teeth and is the smallest of the molars. The lower molars also have large occlusal surfaces but contrary to the upper ones, they are elongated mesio-distally, not bucco-lingually. This is because their morphology derives from a Y5 occlusal pattern with 5 main cusps (instead of 4), 3 buccal and 2 lingual. Their crown relief is relatively low and flat and the tooth has two roots (mesial and distal) that tend to curve distally. The lower first molar is the largest in the mandible with three buccal cusps (protoconid, paraconid and hypoconulid) and two lingual cusps (entoconid and hypoconid). The mesio-buccal (paraconid) is the biggest and the highest while the distal one (hypoconulid) is the smallest. The crown is usually wider on the buccal than the lingual side. The occlusal view shows three major fossae (central, mesial and distal) and several grooves as well as various ridges. The lower second molar is usually smaller than the first one and it only shows four cusps with the distal that are smaller than the mesial cusps. Here, the two roots are closer to each other than in the first lower molar and also tend to more pronouncedly bend distally. The lower third molar is the tooth with the highest morphological variation, characterized by convex buccal and lingual crown surfaces with three or four cusps. The groove pattern is very irregular with numerous pits and grooves that provide a wrinkled impression. The tooth roots are rather short and tend to fuse. [5]

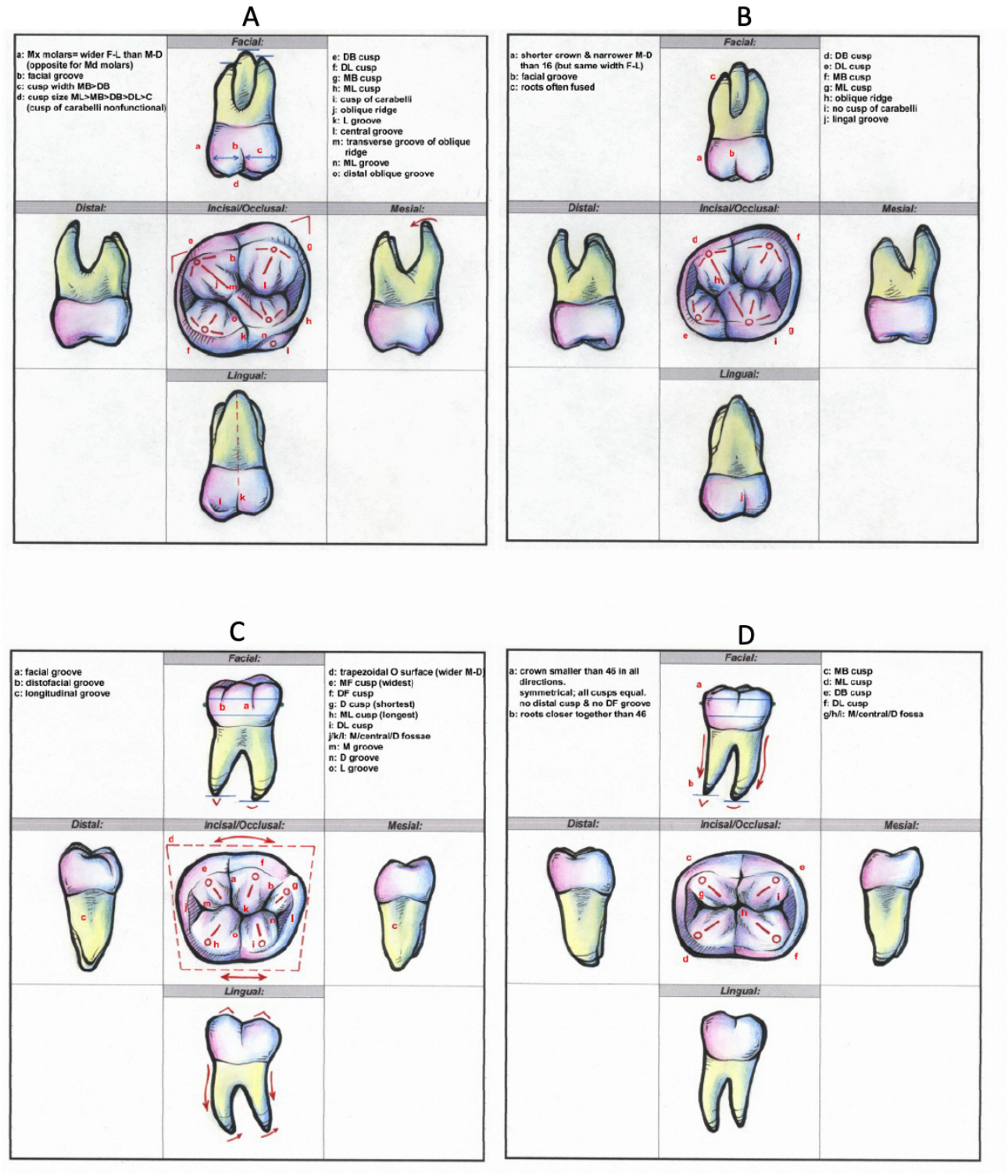

Figure 13 Dental morphology of the human molars. A) right upper first molar, B) right upper second molar, C) right lower first molar, D) right lower second molar. [5]

2.2.1 Dental Nomenclature

Dental professionals, in writing or speech, use several different dental notation systems for associating information with a specific tooth. The three most common systems are the:

- ISO System, FDI World Dental Federation notation.
- Universal Numbering System.
- Palmer notation method. The ISO system is used worldwide while the Universal is used widely in the United States.

The International Standards Organization Designation System (ISO System) by the World Health Organization notation system is widely used by dental professionals internationally to associate information with a specific tooth and it was used in this work during the analysis of the results. Based on the Fédération Dentaire Internationale (FDI), it is also known as ISO 3950 notation. Thus, the ISO System uses a two-digit numbering system in which the first digit represents a tooth's quadrant and the second digit represents the number of the tooth from the midline of the face *(Figure 14)*. For *permanent teeth*, patient's upper right teeth begin with the number, "1". The upper left teeth begin with the number, "2". The lower left teeth begin with the number, "3". The lower right teeth begin with the number, "4". For *primary teeth,* the sequence of numbers goes 5, 6, 7, and 8 for the teeth in the upper right, upper left, lower left, and lower right respectively. When speaking about a certain tooth such as the permanent maxillary central incisor, the notation is pronounced “one, one”. Beware of mixing up the teeth in written form such as 11, 12, 13, 14, 15, 16, 17, 18 between the Universal and ISO systems.

For example: retention of a primary molar tooth in the otherwise regular intact lower right jaw, position 5, would be noted as: 41, 42, 43, 44, 85, 46, 47, 48 *(Figure 15). [6]*

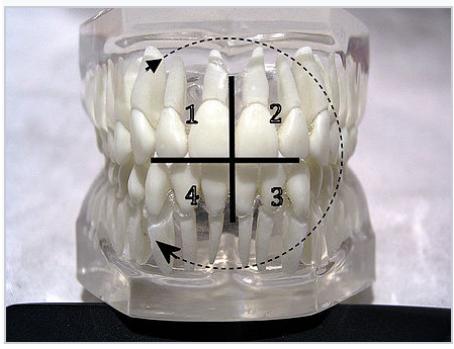

Figure 14 FDI Notation - teeth's quadrants.

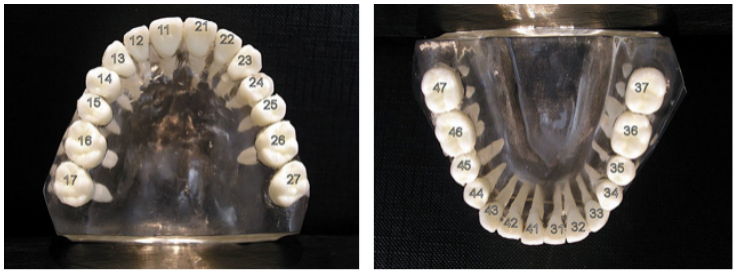

Figure 15 ISO notation, on the left the numbering system for the upper jaw, on the right the numbering system for the lower jaw.

The universal numbering system, although it is termed “universal”, is most commonly used in the United States and for this reason it is also called the "American system". The uppercase letters A through T are used for primary teeth and the numbers 1 - 32 are used for permanent teeth. The tooth designated "1" is the maxillary right third molar ("wisdom tooth") and the count continues along the upper teeth to the left side. Then the count begins at the mandibular left third molar, designated number 17, and continues along the bottom teeth to the right side *(Figure 16).* Each tooth has a unique number or letter, allowing for easier use on keyboards. *[6]*

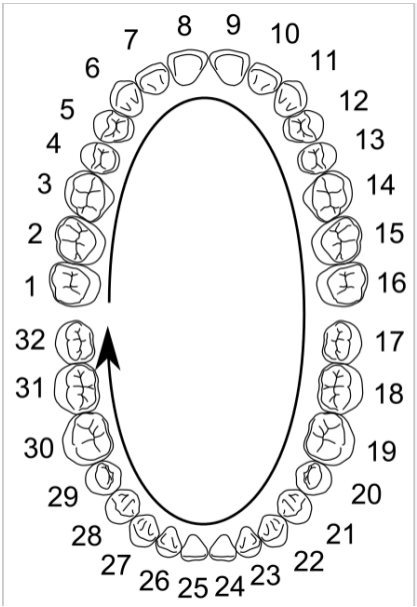

Figure 16 Universal numbering system. This is a dental practitioner view, so tooth number 1, the rear upper tooth on the patient's right, appears on the left of the map.

The Palmer notation is a system used by dentists to associate information with a specific tooth. Although supposedly superseded by the FDI World Dental Federation notation, it overwhelmingly

continues to be the preferred method used by dental students and practitioners in the United Kingdom. It was originally termed the "Zsigmondy system" after the Hungarian dentist Adolf Zsigmondy who developed the idea in 1861, using a Zsigmondy cross to record quadrants of tooth positions. Permanent teeth (adult) were numbered 1 to 8, and the child primary dentition (also called deciduous, milk or baby teeth) were depicted with a quadrant grid using Roman numerals I, II, III, IV, V to number the teeth from the midline distally. Palmer changed this to A, B, C, D, E.

The Palmer notation consists of a symbol (┘└ ┐┌) designating the quadrant of the tooth and a number indicating the position from the midline. Adult teeth are numbered 1 to 8, with primary teeth indicated by a letter A to E. Hence the left and right maxillary central incisor would have the same number, "1", but the right one would have the symbol, "┘", underneath it, while the left one would have, "└" *(Figure 17)*. *[6]*

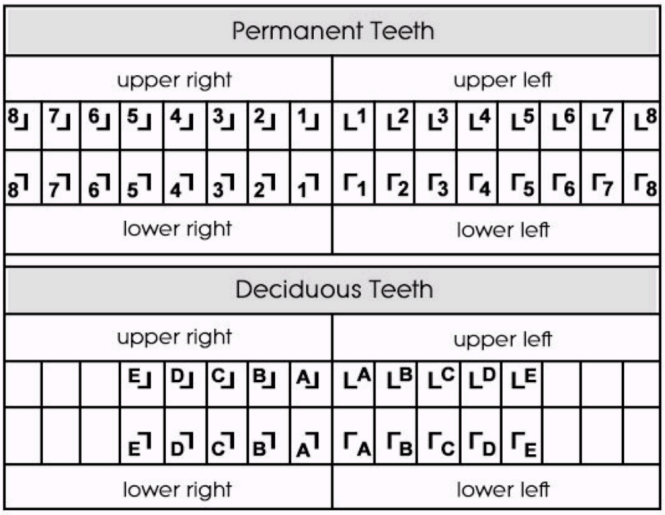

Figure 17 Palmer notation.

2.3 The Obstructive Sleep Apnea: Syndrome and Treatment

The Obstructive Sleep Apnea Syndrome (OSAS) is characterized by episodes of complete or partial obstruction of the upper airways during the sleep. This respiratory disorder is very common among the population and it can affect without any distinction young and old people, while it has been seen that OSAS distresses males more than females with a rate of 2:1. [7]

The factors related with OSA syndrome are multiple, first among all: the obesity. In fact, the obesity reduces the expansive force of the pharyngeal dilator muscles and it generates an accumulation of

adipose tissue in the neck region that provokes a reduction of the lumen of the airway tract. Secondary factors, linked to the respiratory disorder, are: the length of the soft palate, the pathologic increase of volume of tongue, the excess of pharyngeal mucosa and hypertonia of the tonsils. The symptoms shown by OSA patients are several and for discriminating a treatment therapy, it is fundamental to evaluate each of them in order to better recognize the gravity of the pathology. Moreover, for establishing a suitable treatment therapy it is necessary to investigate the origin of these symptoms in order not to confuse them with indicators of other pathologies. The symptoms originated from OSAS are divided into two categories: *day* and *night [8].* Daytime sleepiness, tiredness, cognitive disturbances and depression belong to the *day symptoms*, while snoring, apneas reported, non-restful sleep, insomnia and headache belong to the *night symptoms* category.

The diagnosis of OSA is very complex and the symptomatology is insufficient to determine this disorder, thus the polysomnography exams are useful for this aim since they evaluate the respiratory pattern during sleep [9]. For the *International Classification of Sleep Disorders: diagnostic and coding manual,* of the American Academy of Sleep Medicine the following two conditions are necessary for making a correct diagnosis: firstly, the combination between clinic criteria (symptomatology and clinic exams) and instrumental ones (polysomnography exams), then the evaluation obtained by using only the instrumental criteria. Once the diagnosis is carried out correctly, the successive element to investigate is the gravity of the pathology, evaluable through the apnoea-hypopnoea index (AHI) that represents the number of apnoea and hypopnoea events per hour of sleep. The threshold that indicates an OSA condition has to be equal or bigger than a value of 5 [10].

The treatment that follows the diagnostic procedure can be differentiated into two groups:

Behavioral therapy that suggests mainly changes in the life style of the patient (weight loss, change of position during sleep, limitation in alcohol abuse and oropharyngeal exercises).

Specific therapy, more invasive than the previous one. This latter one can be subdivided into different types:

- *Positive pressure in the upper airways (CPAP)*, represents the therapeutic choice that is first offered to patients, since, with some exceptions, it is the one that has brought the best results;

• *Endo-oral mandibular advancement devices (MAD)* are recommended for subjects who do not endure the first specific therapy or who in any case prefer them to it;

• *Surgical treatment*, it is very invasive and whose effectiveness is limitedly demonstrated;

• *Night oxygen therapy*, is not specifically recommended for the treatment of OSAS because it can prolong apneas, but it can be combined with CPAP (first point).

Whatever treatment is chosen the efficacy must be proved through the polysomnography exams and a clinic control has to be made after three months since the beginning of the treatment application [11, 12].

2.3.1 Overview of Mandibular Advancement Devices

The *Mandibular Advancement Devices (MADs)* take part of the nocturnal endo-oral devices together with the *Tongue Retaining Devices (TRDs).* Both these medical equipment are used for the treatment of the OSA syndrome but they have different strategies to prevent an upper airway collapse. The TRDs have the task of pushing forward the tip of tongue in order to allow the increase of the diameter of the pharynx, while the MADs promote a forward protrusion of the mandible, thus altering the jaw and tongue position. All the movements, achieved through the usage of MADs, are controlled thanks to the anchor of the devices over the teeth [13, 14].

The MADs have seen to be more desirable than the TRDs, mainly for the fact that they achieve higher levels of comfort and they continue to evolve their designs and functionalities in order to increase the comfortability and the mandibular mobility. Therefore, in this work a particular attention is given to MADs that meet a greater market demand. The MAD development initially starts with devices that had an acrylic monoblock design with a dental anchor, then going on with a design of hybrid devices that offered the suspension of soft palate in addition to the mandibular advancement. The most recent devices are the bi-maxillary MADs. They show innovations in the design and in the functionality in that they have geometries with several degrees of freedom in order to allow vertical and lateral motions. Nowadays, on the market a lot of bi-maxillary MADs are present.

Below, there is a brief description of just a few of these MADs, depicted in *Figure 18:*

- *Herbst*, a device in which a metallic and telescopic arm is present on both the lateral sides of the MAD. The length of the arm defines the entity of the advancement;
- *SomnoDent,* a device in which two vestibular flippers (in each lateral side of the inferior splint) lean to the two inclined planes of the superior splint. This splint can be advanced about 0.1 mm by means of an expansion screw located on the resin in order to achieve the activation. The mechanic behind this MAD is based on the principle of inclined slides;
- *Orthoapnea,* a device in which a small opening of the mouth occurs together with the mandibular advancement. The mechanic behind this MAD is based on the principle of reverse connecting rod;
- *New SomnoDent Avant,* a device in which two resin pins (on both the lateral sides of the inferior splint) act as an insertion point for a rod that goes to fit in a central support located over the superior splint. The length of the rod defines the entity of the advancement, smaller is the length and greater is the entity of advancement.

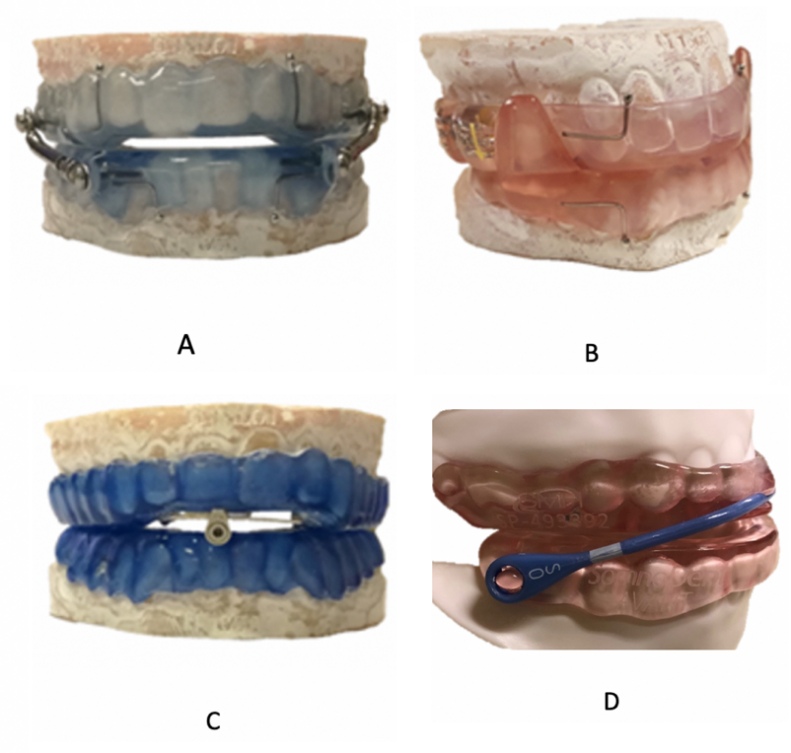

Figure 18. Different types of bi-maxillary Mandibular Advancement Devices. A) Herbst, B) SomnoDent, C) Orthoapnea, D) New SomnoDent Avant

The efficiency of the bi-maxillary MADs has been demonstrated through polysomnography and clinic exams like Axial Computer Tomography (TAC) and Magnetic Resonance Imaging (MRI) [15].

2.4 Dental Pathology: Periodontitis

The *Global Burden of Disease Study 2017* estimated that oral diseases affect close to 3.5 billion people worldwide, even if the majority of oral health conditions, as dental caries (tooth decay) or periodontal diseases, are largely preventable and treatable in their early stages. The prevalence of oral diseases continues to increase principally in the most low- and middle-income countries, where the urbanization is increasing and the living conditions are changing. This is primarily due to inadequate exposure to fluoride (in the water supply and oral hygiene products such as toothpaste) and poor access to oral health care services in the community. Marketing of food and beverages high in sugar, as well as tobacco and alcohol, has led to a growing consumption of products that contribute to worsening oral health conditions. [16]

One of the most common oral health conditions is the **periodontitis** *(Figure 19).*

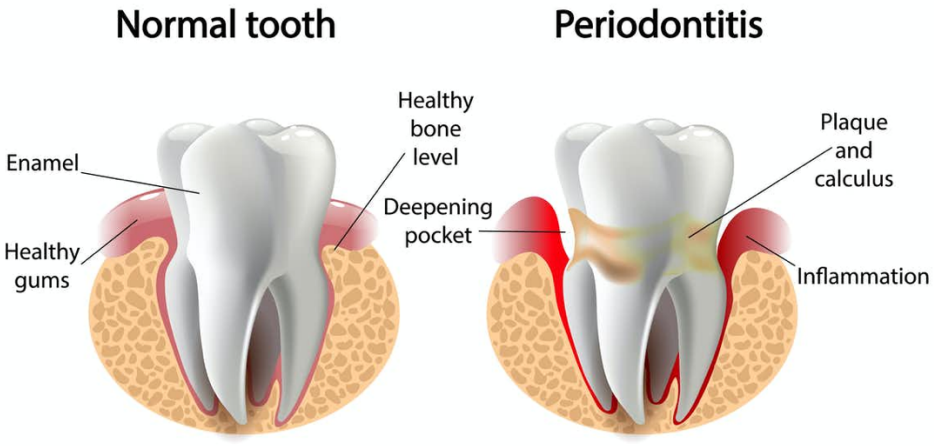

Figure 19 Comparison between a normal tooth and a tooth affected by periodontitis.

The periodontitis is characterized by microbially-associated, host-mediated inflammation that results in loss of periodontal attachment that can led to edentulism, the loss of tooth. The pathophysiology of the disease has been characterized in its key molecular pathways, and ultimately leads to activation of host-derived proteinases that enable loss of marginal periodontal ligament fibers, apical migration of the junctional epithelium, and allows apical spread of the bacterial biofilm along the root surface. The bacterial biofilm formation initiates gingival inflammation; however, periodontitis initiation and progression depend on dysbiotic ecological changes in the microbiome

in response to nutrients from gingival inflammatory and tissue breakdown products that enrich some species and anti-bacterial mechanisms that attempt to contain the microbial challenge within the gingival sulcus area once inflammation has initiated. Marginal alveolar bone loss – a key secondary feature of periodontitis – is coupled with loss of attachment by inflammatory mediators. Clinical presentation differs based on age of patient and lesion number, distribution, severity, and location within the dental arch. Based on pathophysiology, three different forms of periodontitis have been identified:

1. *Necrotizing periodontitis*, characterized by history of pain, presence of ulceration of the gingival margin and/or fibrin deposits at sites with characteristically decapitated gingival papillae, and, in some cases, exposure of the marginal alveolar bone;

2. *Periodontitis as a direct manifestation of systemic diseases*;

3. *Periodontitis*, characterized by a large range of phenotypes and damages to periodontium, the supporting structure of tooth. This typology is the most common form of periodontitis and it represents the majority of the clinical cases. In order to successfully manage these variety of cases several medical approaches are required together with a good knowledge of the pathology. [17]

Nowadays, a classification introduced in 2017 is used by the specialists in all over the world to better identify the periodontitis. This classification is based on a "staging" and a "grading" assessment. *The staging* has the aim to classify the severity of the periodontitis by measuring the extent of destroyed and damaged tissue. In addition, the staging is able to assess specific factors that may determine complexity of controlling current disease and managing long-term function and esthetics of the patient's dentition. There are four levels of staging related to periodontitis: Staging I, II, III and IV *(Figure 20).*

Stage I describes a borderline situation between gingivitis and periodontitis and it represents the early stages of attachment loss. Early detection and definition of a population of susceptible individuals offers opportunities for timely intervention and monitoring. Timing in diagnostics is the common goal of all specialists working in the field of dental practice. Assessment of salivary biomarkers and/or new imaging technologies may increase early detection.

Stage II represents established periodontitis in which a carefully performed clinical periodontal examination identifies the characteristic damages to the tooth support. At this stage of the disease process, however, management remains relatively simple for many cases as application of standard

treatment principles involving regular personal and professional bacterial removal and monitoring is expected to arrest disease progression.

At Stage III, periodontitis has produced significant damage to the attachment apparatus and tooth loss may occur. This stage is characterized by the presence of deep periodontal lesions that extend to the middle portion of the root and whose management is complicated by the presence of deep intra bony defects, furcation involvement, history of periodontal tooth loss/exfoliation, and presence of localized ridge defects that complicate implant tooth replacement. In spite of the possibility of tooth loss, masticatory function is preserved, and treatment of periodontitis does not require complex rehabilitation of function.

At the more advanced Stage IV, periodontitis causes considerable damage to the periodontal support and may cause significant tooth loss, and this translates to loss of masticatory function. This stage is characterized by the presence of deep periodontal lesions that extend to the apical portion of the root and/or history of multiple tooth loss; it is frequently complicated by tooth hypermobility due to secondary occlusal trauma and the sequelae of tooth loss: posterior bite collapse and drifting.

[17]

Periodontitis stage		Stage I	Stage II	Stage III	Stage IV
Severity	Interdental CAL at site of greatest loss	1 to 2 mm	3 to 4 mm	≥5 mm	≥5 mm
	Radiographic bone loss	Coronal third (<15%)	Coronal third (15% to 33%)	Extending to middle or apical third of the root	Extending to middle or apical third of the root
	Tooth loss	No tooth loss due to periodontitis		Tooth loss due to periodontitis of ≤4 teeth	Tooth loss due to periodontitis of ≥5 teeth
Complexity	Local	Maximum probing depth ≤4 mm Mostly horizontal bone loss	Maximum probing depth ≤5 mm Mostly horizontal bone loss	In addition to stage II complexity: Probing depth ≥6 mm Vertical bone loss ≥3 mm Furcation involvement Class II or III Moderate ridge defect	In addition to stage III complexity: Need for complex rehabilitation due to: Masticatory dysfunction Secondary occlusal trauma (tooth mobility degree ≥2) Severe ridge defect Bite collapse, drifting, flaring Less than 20 remaining teeth (10 opposing pairs)
Extent and distribution	Add to stage as descriptor	For each stage, describe extent as localized (<30% of teeth involved), generalized, or molar/incisor pattern			

Figure 20 Description of periodontitis staging taken from a table of the article of Tonetti et al. [17]

The grading, together with the staging, is fundamental for the classification of the periodontitis process because it estimates the future risk of progression of this pathology. Moreover, the grading has the goal to estimate the potential health impact of periodontitis on systemic disease and even the reverse, to guide systemic monitoring and co-therapy with doctors specialized in other medical branches. Irrespective of the stage at diagnosis, periodontitis may progress with different rates in individuals, may respond less predictably to treatment in some patients, and may or may not influence general health or systemic disease. This information is critical for precision medicine but has been an elusive objective to achieve in clinical practice. In recent years, validated risk assessment tools and presence of individually validated risk factors have been associated with tooth loss, indicating that it is possible to estimate risk of periodontitis progression and tooth loss.

Based on the rate of periodontitis progression, three different levels of grading are defined:

- Grade A, with a slow rate of progression.
- Grade B, with a moderate rate of progression.
- Grade C, with a rapid rate of progression.

For the definition of the grade, two primary criteria can be used: the direct and the indirect evidence of progression. The direct evidence is preferable and it consists on the evaluation of the radiographic bone loss or the clinical attachment loss (CAL). In absence of this direct evidence, the indirect estimation is made using case phenotype or bone loss as a function of age at the most affected tooth (radiographic bone loss expressed as percentage of root length divided by the age of the subject, RBL/age). Clinicians should initially assume grade B disease and seek specific evidence to shift towards grade A or C, if available. Once grade is established based on evidence of progression, it can be modified based on the presence of risk factors. These factors refer to increased risk that periodontitis may be an inflammatory comorbidity for the specific patient *(Figure 21).* [17]

	Progression		Grade A: Slow rate	Grade B: Moderate rate	Grade C: Rapid rate
Primary criteria *Whenever available, direct evidence should be used.*	Direct evidence of progression	Radiographic bone loss or CAL	No loss over 5 years	<2 mm over 5 years	≥2 mm over 5 years
	Indirect evidence of progression	% bone loss / age	<0.25	0.25 to 1.0	>1.0
		Case phenotype	Heavy biofilm deposits with low levels of destruction	Destruction commensurate with biofilm deposits	Destruction exceeds expectations given biofilm deposits; specific clinical patterns suggestive of periods of rapid progression and/or early onset disease
Grade modifiers	Risk factors	Smoking	Non-smoker	<10 cigarettes/day	≥10 cigarettes/day
		Diabetes	Normoglycemic/no diagnosis of diabetes	HbA1c <7.0% in patients with diabetes	HbA1c ≥7.0% in patients with diabetes

Figure 21 Description of the periodontitis grading taken from the article of Tonetti et al. [17]

3. Chapter 3: Engineering Background

The goal of this chapter is dealing with the theoretical principles that are needed for the creation of a 3D model and for performing a finite element simulation. The simulation has the aim to evaluate the stresses and deformations provoked by the interaction between the MAD and the anatomical structures building up the oral cavity that are affected from a staging I of periodontitis. The Reverse Engineering (RE) and the finite element analysis (FEA) take part of these theoretical references. The RE is used for the reconstruction of the tridimensional geometry of interest, built up by mandible, maxilla, PDLs and teeth, while the FEA is necessary to simulate as close as possible to reality the mechanical behaviors of the anatomical model during the MAD application.

Moreover, all the software used in the work are treated in this chapter and they are the following:

- Rhinoceros 6: general purpose CAD software for freeform surface modeling;
- NX 12: a Siemens CAM/CAD/CAE suite;
- Ansys: a program used for the finite element analysis.

3.1 Reverse Engineering

The *Reverse Engineering* is a process that allows to obtain a mathematical description of a model starting from its physical appearance. From the point cloud obtained from the acquisition of the geometry, it is possible to give a mathematical description of the object that allows its subsequent prototyping through processing systems, such as CAD software, favoring the generation of the related three-dimensional models. The term Reverse is used with the aim of emphasizing the opposition to traditional engineering methods which precisely start from a CAD model to produce a real object, while the RE on the contrary starts from a real object to produce a CAD model.

The Reverse Engineering finds application in various areas with the aim of speeding up production processes, optimizing overall design costs and finally storing all the information necessary for controlling and monitoring processes, ensuring greater competitiveness among companies. The application fields cover various sectors including: automotive, archeology and restoration, architecture, industrial design, web design and medicine.

The process that leads to a 3D model generalization is made up by a series of steps (*Figure 22*) [18]:

1. Acquisition of the point cloud of space belonging to the surfaces of the solid object to be modeled;

2. Management of the point cloud;

3. CAD model generation (mesh o NURBS);

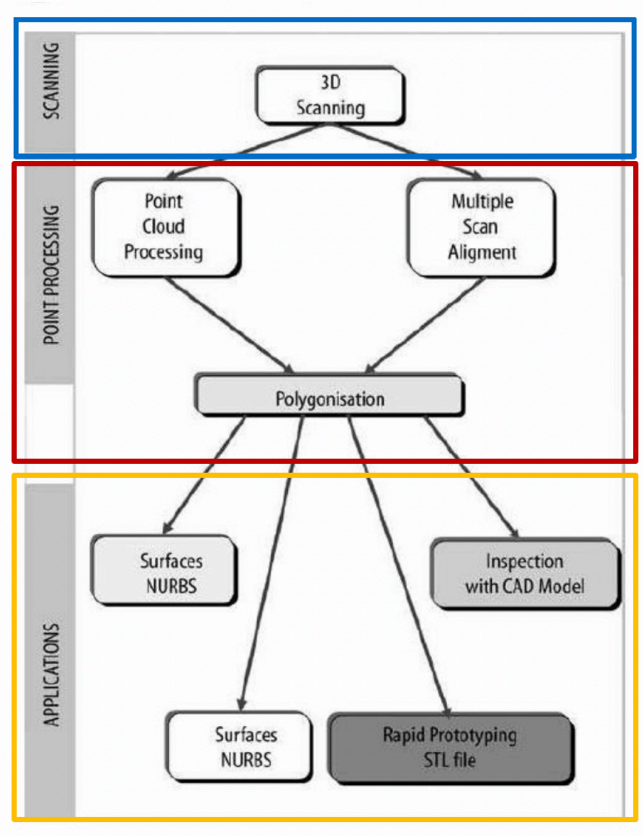

Figure 22 Phases of Reverse Engineering.

The acquisition represents the starting point of the process; in this phase the external shape of the object is detected and a cloud of points is reconstructed, each point is recorded in its spatial coordinates (first the x, then the y and finally the z) within an ASCII text file. According to the way in which the three-dimensional coordinates of the points are acquired and according to the different application cases it is possible to define two types of acquisition systems: with contact and without contact.

The acquisition systems with contact have the indisputable advantage of precision, high imperturbability to external disturbances and high repeatability of the measurements, but they also show a series of disadvantages including the high acquisition times, the high cost of the equipment, the support surface and the object to be measured. These instruments consist of two parts: feeler and handling system; when the probe comes into contact with the surface to be measured, it sends

a signal to the controller of the instrument which measures its position and outputs the coordinates of the detected point, thus building the cloud of points.

Contactless acquisition systems are indispensable when the morphology of the object to be acquired is complex, therefore with a high number of points to be acquired, or when the object is made of a yielding material that makes acquisition by contact impossible. These are classified into three categories according to the physical phenomenon used: acoustic, magnetic and optical.

- Acoustic methods: they are based on measurements of the time of flight of the sound reflected from the surface under examination, and it is for this reason that this method is very sensitive to acoustic interference;
- Magnetic methods: they are widely used in the medical sector, exploiting the oscillation of the atomic nuclei of hydrogen contained in the soft and liquid parts of the human body;
- Optical methods: these are the most popular for the speed of measurement, versatility of the field of use, precision and accuracy. They are divided into two categories: passive and active.

Passive systems do not use any light source and are based on image analysis, while active ones base their operation on artificial light and are classified according to this in structured light and interferometry laser systems. To obtain the coordinates of the points to be measured all active typologies use triangulation [19].

The acquisition methods widely used in the medical field are non-contact and magnetic ones, such as Computer Tomography (CT), Magnetic Resonance Imaging (MRI) and Cone Beam Computer Tomography (CBCT).

CT is a diagnostic technique that uses ionizing radiation to obtain detailed images of specific areas of the body. While the traditional radiographic image is the result of the analog transformation of a three-dimensional reality into a two-dimensional one, with computerized axial tomography the image undergoes a transformation from analog to digital.

During the diagnostic examination, the radiation passes through the body and is picked up by small ionization chambers; an electrical signal is thus obtained which, after being processed, provides detailed images which, if necessary, can be reconstructed into a 3D model of the body [20].

In *Figure 23* it is possible to observe a scan of a human massive facial through Computer Axial Tomography (CAT).

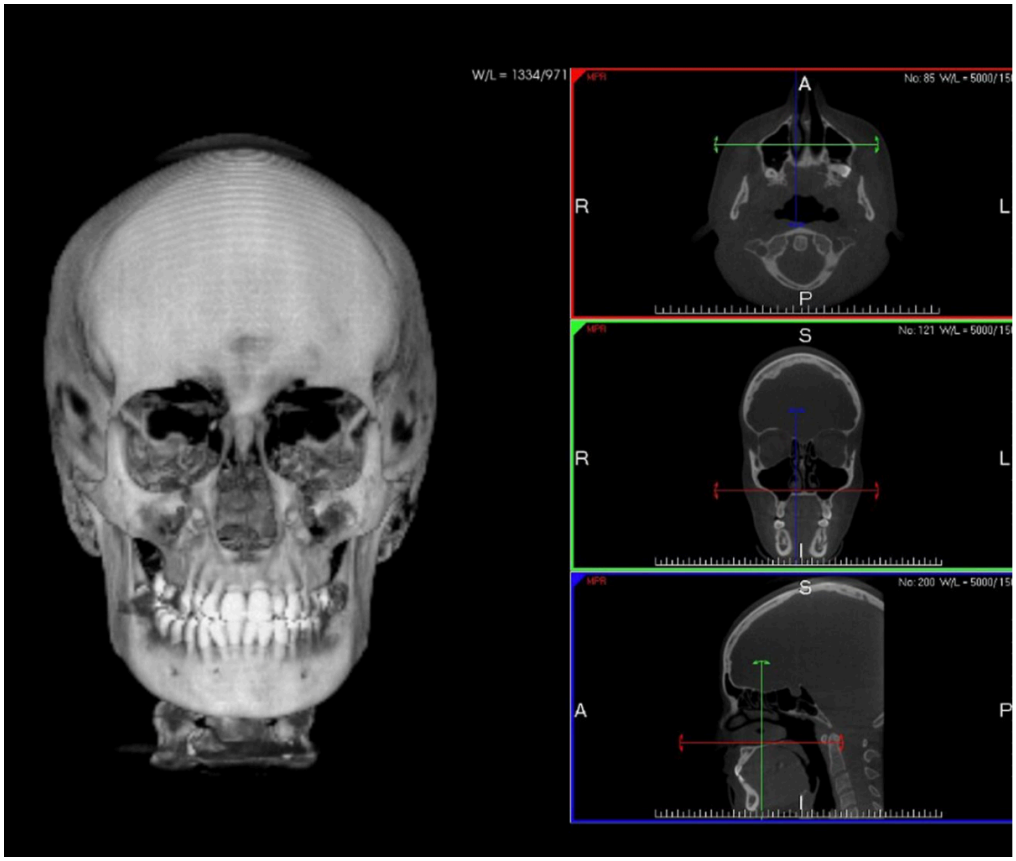

Figure 23 CAT image of the facial massif.

MRI is a diagnostic test that allows us to view the inside of our body without performing surgical operations and without the administration of ionizing radiation. Medical investigations using magnetic resonance provide different information than traditional radiological images: with MRI soft tissues are visible and discrimination between types of tissues is also possible, which is not appreciable with other radiological techniques [21].

In *Figure 24* it is possible to observe a scan of a human massive facial through Magnetic Resonance Imaging.

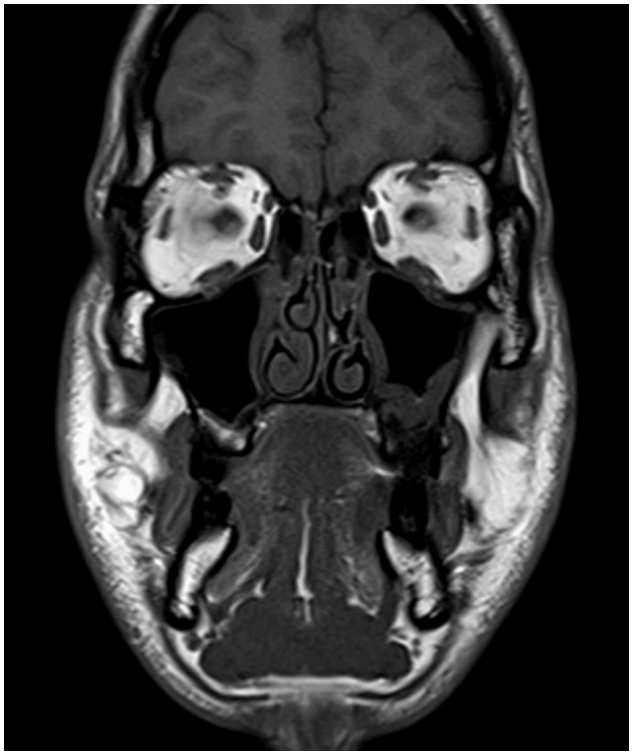

Figure 24 MRI image of the facial massif.

Comparing both the *Figure 23* and the *Figure 24,* it is possible to catch the principal difference between these medical methodologies; in fact, with the MRI it is possible to observe better the composition of the anatomical tissues while with the CAT the anatomical structure is better defined. The Cone Beam volumetric CT scan (CBCT) is a new CT technique dedicated to the massive facial study, in particular to the dental arches, useful in the preparatory phases for implantology. The Cone Beam technology uses a cone-shaped X-ray beam that allows to acquire a large volume, significantly reducing the radiation to which the patient is exposed, and is therefore preferred to other radiological techniques. Unlike other radiological images, this technique allows direct visualization of three-dimensionality, allowing the identification of anatomical details that are more difficult to obtain with other two-dimensional diagnostic images [22].

Diagnostic tools such as CT, MRI and CBCT produce related images in the digital DICOM format; acronym for Digital Imaging and Communications in Medicine, refers to a standard that defines the criteria, communication, visualization, archiving and printing of biomedical information such as radiological images. The points constituting the cloud acquired with the scans are joined to form polygons and the result of this operation is called a polygon mesh. The format used to save this solid model, now discretized into triangles, is the STL (acronym for Standard Triangulation Language file

format); this format represents binary or ASCII files and was created to interface with three-dimensional solid manufacturing machines.

The files that use this format can be viewed and corrected with the help of some specific programs for the treatment of meshes. Ultimately, the mesh approximates the reference of the real scanned object and the degree of detail of this approximation depends on the density of the acquired point cloud: the greater the number of points, the better the approximation.

What you want to get is a continuous solid model that represents the real scanned object, instead the mesh is discretized into polygonal elements so the representation by means of NURBS (acronym for Non-Uniform Rational Basis Spline) is necessary. They represent a class of geometric curves used for the representation of surfaces, the format responsible for saving the model approximated with the NURBS is the iges (acronym for Initial Graphics Exchange Specification) which represents a neutral data format that allows the exchange of data, graphic files and information between CAD systems.

3.2 Finite Element Analysis

Finite Element Analysis (FEA) is a computerized simulation technique used mainly in engineering analyzes and which exploits the Finite Element Method (FEM), whose goal is the solution, in discrete and approximate form, of systems of equations to partial derivatives. This method belongs to the class of Galerking methods, according to which a problem, drawn up in weak form, is approximated by the linear combination of some functions, called form. The linear combination of these functions constitutes the problem to be solved in the simulation phases, whose unknowns represent the degrees of freedom of the model [23-24]. With the FEM it is possible to carry out simulations on a previously created model; during the simulation the model undergoes both static and dynamic stresses as a result of which it can change or deform. The simulations in question take place in a virtual test bench, where the prototype (or model) is given directly by a three-dimensional CAD solid. In this context, one of the great advantages offered by this method is inserted, namely the reduction of physical prototypes to be created, reducing costs and design times. The experimental value of the data obtained by this method is very high, in fact the software suitable for the purpose have reached a degree of accuracy comparable, or even better, to that of traditional test benches, to the point of considering the real limit of the user and not the software used. In fact, as in

traditional test benches, it is the tester who verifies the correct execution of the simulation and the correct use of the software [23]. This type of simulations is useful for obtaining various types of information such as thermal, structural, instability, electrical analysis and many other types of analysis.

Currently, various software packages are available on the market that deal with carrying out this type of simulation, however the division of the analysis process into several steps is common to all *(Figure 25)*:

1. Pre-processing: in this phase the definition of the problem to be simulated with the finite elements is carried out; the geometric model (the prototype) is converted into a discretized finite element model (mesh) to define the properties of the material; the definition of the loading and boundary conditions;

2. Calculation: during this phase occurs the resolution of the finite element problem, by considering all the defined data in the pre-processing phase. In this step the identification of the nodal displacement occurs;

3. Post-processing: in this phase the calculation and display of the information related to the nodal displacements, such as deformation and stresses, is performed;

4. Mesh improvement: in this phase, the mesh is optimized, based on the previous analysis experience, in order to achieve the desired level of accuracy;

5. Report of the results: reports are generated containing a summary of the results and the deformations, stresses and displacements are displayed.

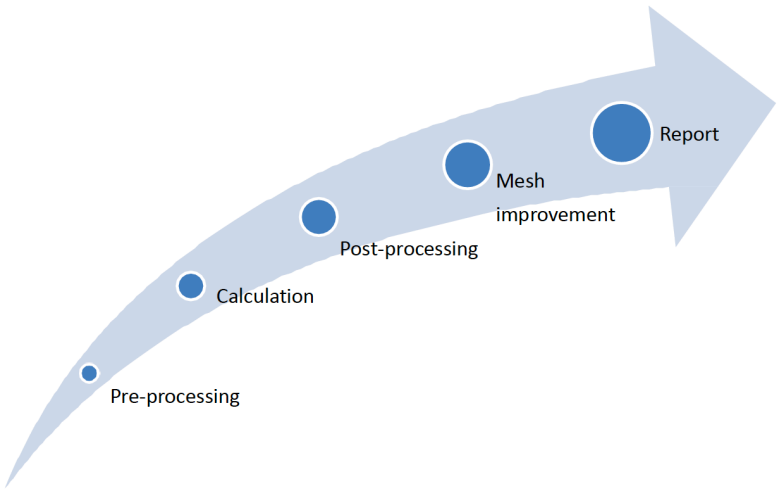

Figure 25 Phases of the Finite Element Analysis.

Among all the phases that lead to the execution of the finite element analysis, that of discretization is fundamental. In this phase, the model passes from the continuous world, characterized by an infinite number of degrees of freedom, to the discrete world, characterized by a finite number of degrees of freedom; the model is divided into a finite number, albeit very large, of basic elements and each of it is attributed a finite number of shape functions, the solution of which produces the resolution of the problem.

Each basic element is defined by nodes, the number of which can range from 2 to 27 [24], these elements are grouped into three macro-categories whose discriminant is the size, we have *(Figure 26)*:

- One-dimensional elements represented by the Lines and which are used for the discretization of reticular structures;
- Two-dimensional elements represented by triangle and quadrilateral elements which are used for the discretization of surface geometries;
- Three-dimensional elements represented by Tetrahedra, Triangular prisms and Hexahedra used in the discretization of solid geometries.

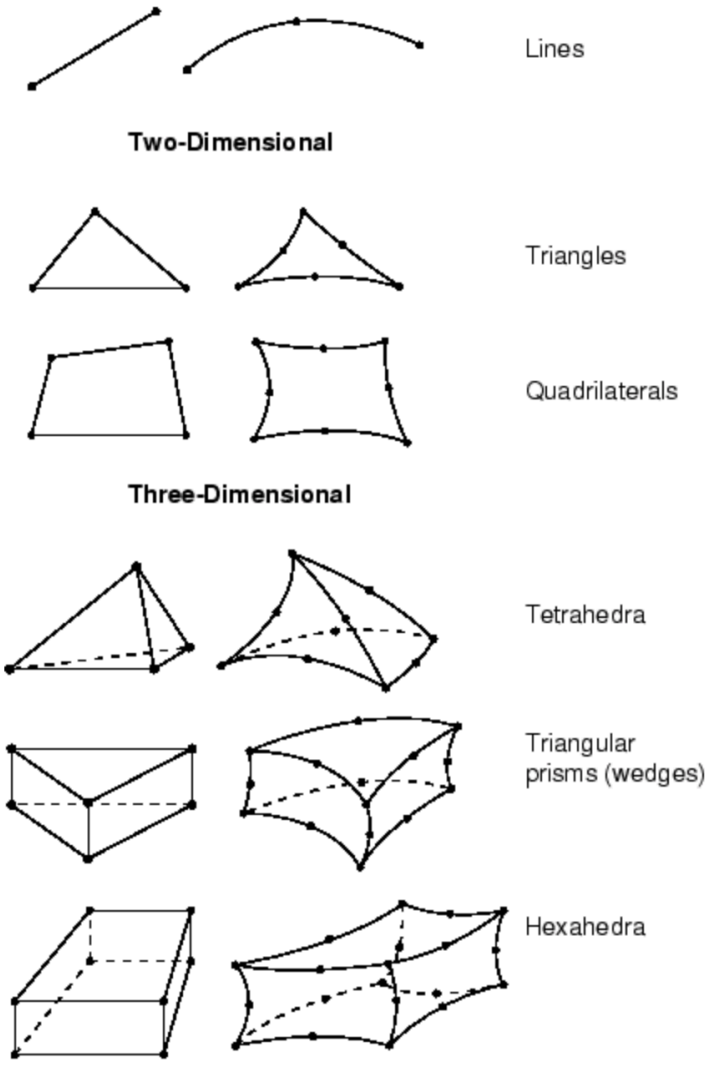

Figure 26 Elements for each step of Mesh.

Each node of the three-dimensional elements is assigned a field or gradient function that affects the entire structure. The application of the load condition, together with the other boundary conditions, acts on the individual nodes causing the variation of the functions associated with it; the solution of the system formed in this way is the goal of the Processing phase. This phase serves to reduce the potential energies and the consequent calculation of the nodal displacements; we therefore define a matrix known as the nodal forces, indicated with $[F]$, according to the following *equation (1)*:

$$[F] = [K] * [U] \qquad \textit{equation (1)}$$

$[K]$ matrix of the global stiffness of the model

$[U]$ nodal displacement matrix

This relationship identifies the duality between the external forces applied to the model and the nodal displacements [24], and it is linear if, as the load increases by a certain factor, the displacement also increases by the same factor otherwise, the relation is defined as non-linear [25]. A typical example of non-linearity is the non-linear behavior of the material, that is when the elasticity matrix of the material depends on the level of deformation, according to *equation (2),* and if there are large displacements or deformations. In these cases, the geometry of the structure must be updated at each movement, according to *equation (3).*

$$[\sigma] = [C] * [\xi]\, e \quad \textit{equation (2)}$$

$$[\xi] = [B] * [U] \qquad \textit{equation (3)}$$

$[\xi]$ effort matrix

$[B]$ stress-strain matrix

$[\sigma]$ matrix related to tensions

$[C]$ the matrix indicating the effort-tension

[23-24-25]

At the end of the simulation, reports are generated for the visualization of the stresses produced.

3.3 Rhinoceros

Rhinoceros is a CAD software for 3D modeling of surfaces in which all geometric entities are represented by NURBS which is widely used in numerous applications such as naval engineering, industrial design, rapid prototyping and reverse engineering. The program receives in input a great variety of formats including any file in the STL and iges format and outputs an equally wide range of formats including 3dm, iges and STL of which the first is the owner of the program. The latest version of this software is: Rhinoceros 7

. 

Figure 27 Logo of Rhinoceros 6.

3.4 NX

NX, formerly known as "unigraphics", is an advanced high-end CAD/CAM/CAE, which has been owned since 2007 by Siemens PLM Software. In 2000, Unigraphics purchased SDRC I-DEAS and began an effort to integrate aspects of both software packages into a single product which became Unigraphics NX or NX.

It is used, among other tasks, for:

- Design (parametric and direct solid/surface modelling)
- Engineering analysis (static; dynamic; electro-magnetic; thermal, using the finite element method; and fluid, using the finite volume method).
- Manufacturing finished design by using included machining modules.

[26]

It is a 3D mechanical design software, or modeler, which incorporates various modules for the creation of parts, assemblies or analyzes of various kinds. It allows the use, both in input and output, of the most common CAD formats as well as its proprietary extension .par

Figure 28 Logo of NX Siemens.

3.5 Ansys

Ansys is a program that is able to perform a variety of engineering simulations such as deformation, tensile and thermal simulations. A typical simulation involves the creation of the model to be tested and the identification of the loads to be applied to it; the objective to be pursued is the evaluation of the mechanical behavior of the prototype to the load applied to it.

The program has the entities organized according to a tree structure that guides the user through the different simulation steps. The latest version of Ansys is: Ansys R2.

Figure 29 Logo of Ansys.

4. Chapter 4: State of Art

In this chapter several themes are treated by reporting the literatures that have more scientific relevance. All the articles and studies mentioned below use a specific mathematical approach: The Finite Element Analysis which is a simulation of any given physical phenomenon using the numerical technique called Finite Element Method (FEM). In this method the physical phenomena are represented by mathematical equations that must be solved in order to make a structural analysis in which mechanical behaviors, like stress and strain, are estimated. The solutions obtained with the FEA are only approximations of the reality and they are usually depicted via a color scale that shows, for example, the pressure distribution over the object. [27]

The topics of interest are principally two: the effects of Obstructive Sleep Apnea treatments on people who suffer from this syndrome and the periodontitis. Both are pathologies that affect the oral cavity and although it is too early to declare a direct relationship between OSAS and periodontitis, the article [28] confirms a possible connection between OSAS and periodontitis via plasma and inflammatory salivary markers.

Another interesting topic covered in this chapter is the assignment of materials for anatomical parts such as mandible, maxilla, teeth and PDLs. The choice of materials is fundamental for a more realistic simulation, because each material with its mechanical properties can affect the reliability of the prototype. Hence, the material chosen for a specific anatomical part must reflect the biomechanical behaviors of that part, otherwise the simulation would lose trustworthiness.

4.1 Finite Element approach in the OSAS treatment

Mandibular Advancement Devices are non-invasive tools widely used worldwide for the treatment of OSAS. Their effectiveness has remained undisputed over time and many medical studies confirm that constant use of MAD leads to a reduction in OSA in the short and long term. [29] The benefits of MAD can be equally investigated in a young or old patient as these two reports [30, 31] can affirm where are respectively treated a 12-year-old and a 55-year-old patient. In both the clinical cases is shown a drastic reduction in the apnea-hypopnea index during the period of treatment.

Figure 30 Intraoral photographs of 55-year-old patient before treatment (upper panel) and after treatment (lower panel).[31]

Figure 31 Intraoral photographs of 12-year-old patient before treatment (upper panel) and after treatment (lower panel). [30]

Recently the need to investigate the side effects of these MADs has grown and many articles nowadays are looking for the negative consequences of OSAS treatment in order to make them sensitive to the problem so as to encourage solutions and improvements. A problem related to the MAD is the stress accumulated on the temporomandibular joint (TMJ), caused by the forced movement of the mandible forward. The article [32] analyzes the stress distribution over the TMJ through the Finite Element Analysis and it demonstrates that, although deformation and load values induced by MAD increase with the mandibular advancement, these are lower than physiological limits of the anatomical parts evaluated *(Figure 32)*.

Thus, slight mandibular advancement can be considered a harmless procedure even for the long period and should not cause permanent side effects.

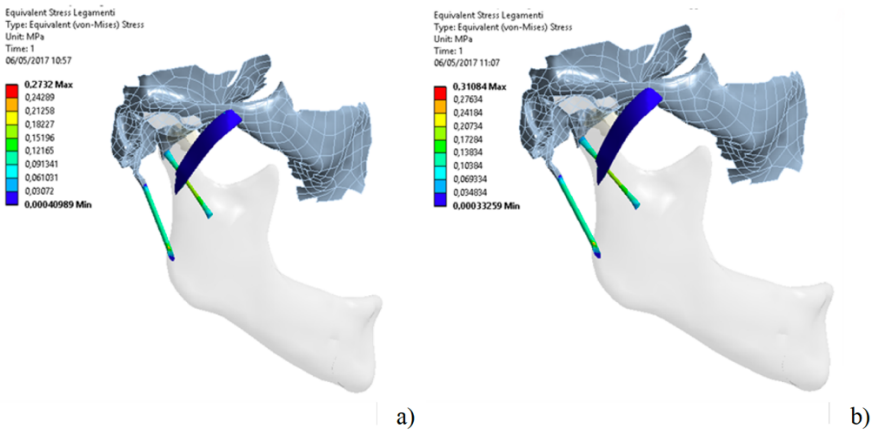

Figure 32 Von-Mises stress on temporomandibular, sphenomandibular and stylomandibular - results illustrated on the article of Brunzini et al. [32]

The same results are found in the study [33] in which a major focus was given to condyle and articular disc. Mandibular advancement causes a load distribution on the central area of the condyle and articular disc mainly. The central part of the anterior area of the condyle shows a higher stress for the contact with the articular eminence during mandibular protrusion movement. The articular disc shows a high load distribution in the central area too, but during the advancement movement the load distribution moves posteriorly. Deformation and load values induced by MAD are lower than physiological limits of the anatomical part evaluated.

The 3D reconstruction of TMJ in both the articles [32, 33] started with the CT images of the patient's skull and then proceed by transforming the bones in NURBS surface models through the RE techniques. Whereas all the soft tissues (articular disc and ligaments), which were able to be identified from CT scan, were modelled by means of specific CAD software *(Figure 33).*

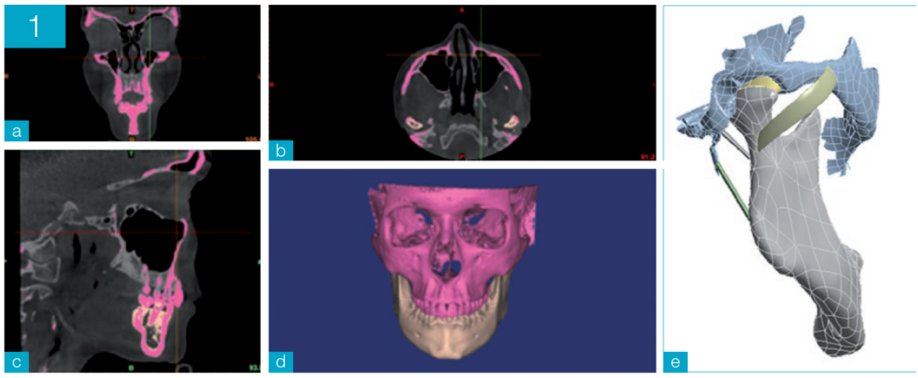

Figure 33 CT technique was used to obtain a three-dimensional model and the skeletal part of the temporomandibular joint using MIMICS software (a-d); three-dimensional model evaluated using Rapidform software (e).[33]

Subsequently another report, the [34], studied the motion during the mandibular advancement as for the [32, 33] articles. Although the [34] study defined a systematic method to assess the mandible roto translation caused by MADs according to a scan-to-CAD approach, starting from a closed mouth position and simulating the oral appliance at different settings. In this work was defined a digital workflow for the evaluation of TMJ kinematic at different settings of MAD in order to avoid involving patients in specific examinations as well as to reduce the invasiveness on the jaw movement.

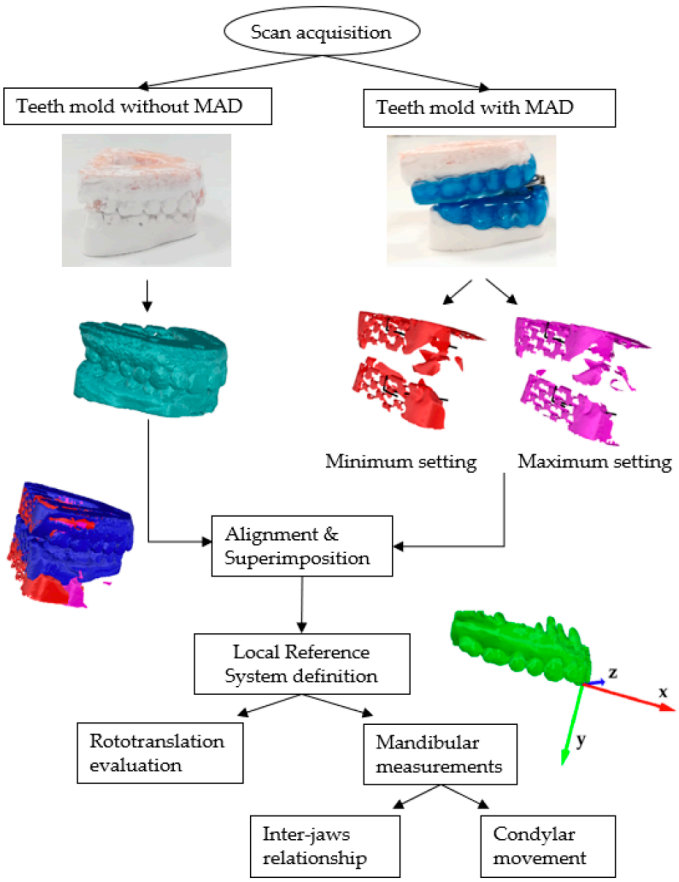

Figure 34 Digital workflow – a systematic method to assess the mandibular roto translation. [34]

The stress over the TMJ is not the only one that occurs during an OSA treatment. In fact, also the teeth and the PDLs record stress during the application of MAD. In the study [35] was demonstrated that the stress over teeth is proportional to the material with which a MAD is produced. Harder is the material of splint and higher is the stress over teeth. The results of this in vitro experiment led to the following clinical implications:

- Soft splints are more efficient in protecting teeth against the damage of bending forces, although there is an increase of compressive forces.

- The tooth opposing a hard splint is exposed to a higher risk of bending forces.

The stress over teeth and PDLs do not depend only on the material with which a MAD is composed, but also on the shape of this device. In the study [36] by means of the Finite Element Analysis was showed that the stress applied to the upper front teeth and the gingival area near the upper incisors differed between a newly prototype and a conventional one. Concentrated stress was relieved by inserting such a shield, helping to distribute the stress from the front teeth to the gingival area.

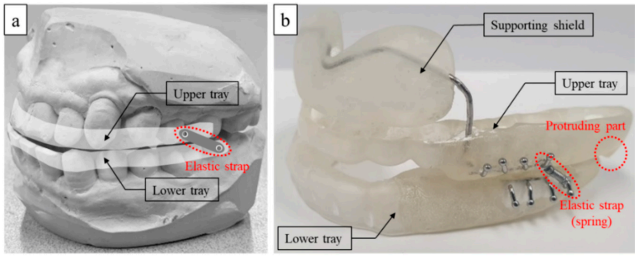

Figure 35 MADs compared in the article of Jonghun Yoon et al. a) conventional MAD; b) newly prototype. [36]

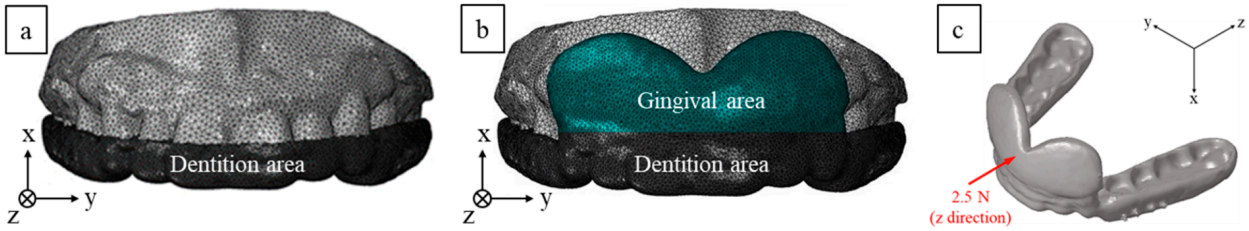

Figure 36 Finite Element Analysis. a) conventional MAD; b) newly prototype with shielded support; c) boundary condition. [36]

However, the literature presented above show some limitations in so much neither the new SomnoDent Avant nor the OSAS combined with periodontitis is treated.

4.2 Application of the Finite Element Method for the periodontitis

Periodontitis is an inflammatory disease that affects the oral cavity in several stages. This disorder begins to wear out the gum until it arrives to damage the alveolar bone, provoking a bone reabsorption. This reduction of the alveolar bone height represents more appropriately a secondary trauma from occlusion and even if it had little effect on the degree of tooth and the supporting

tissue stresses when 25% of bone support was lost, however, the stresses increased dramatically when 50% and 75% of bone support was lost, as the article [37] confirm.

In this work a combination within OSAS and periodontitis was done, but before treating it, it is important to clearly understand the effects provoked by this pathology over the dental arches. The following literature reports the most relevant biomechanical studies of the consequences of periodontitis, carried out also in this case through the finite element approach.

In the article [38] the stress and displacement evaluation were performed during the application of orthodontic forces in adult patients with different bone loss values. The results relating to displacements and tensions in the oral cavity showed that their greatest values were recorded in the same direction as the forces. Furthermore, it was found that the displacement values increased significantly with bone resorption. The same results were obtained for stress where it was verified that stress depends on the direction of the force and on the alveolar bone loss, lowering the center of resistance of the tooth and modifying the distribution of stress at the apex. In 2000, the same results on tooth displacement were obtained by Geramy A. [39] where a study was conducted on the displacement of the tooth with constant application of force (1 N amplitude) and with the reproduction of different stages of bone loss (from 1 to 8 mm), identifying the center of rotation and resistance for each stage. The results revealed that the moment / force (M/F) ratio required to produce body movement increases in association with alveolar bone loss. Bone loss causes the center of resistance to move towards the apex, decreasing the relative distance from the alveolar ridge. Furthermore, an increase in bone resorption resulted in greater displacements of the incisal edge and apex.

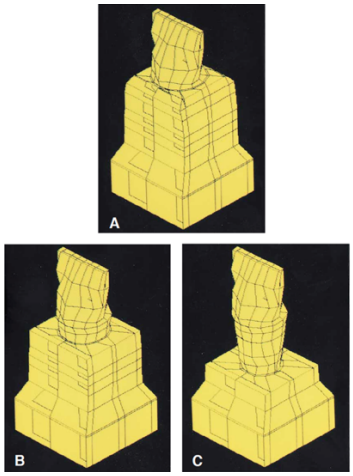

Figure 37 3-D models used in this study A) no alveolar bone loss; B) a bone loss of 0.5 mm; C) a bone loss of 8.5 mm (Geramy 391-396). [39]

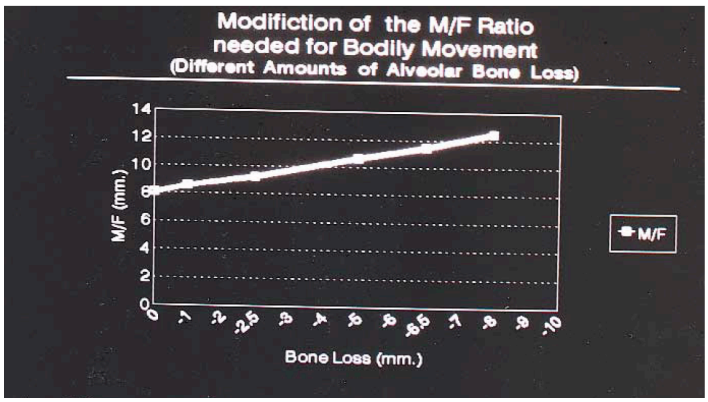

Figure 38 Change of the M/F ratio needed to maintain bodily movement with different alveolar bone [39]

In a recent study [40] the initial stresses in teeth, PDLs and bone were investigated in presence of different level of bone heights during the application of a force for intrusion and tipping on labial and lingual sides of the tooth. In this study six 3D finite element models of a maxillary central incisor with PDL were designed and at each model where applied the force on tooth. It was found that bone reabsorption caused an increase in the maximum the initial stresses relative to its heights. Moreover, the stress was studied based on the different forces applied. For the tipping force higher levels of stress are recorded in the cervical area, while for the intrusive force the stresses were higher in the apical region without any distinction if the force was applied on labial or lingual sides. In this work [50] were treated also the initial tooth displacements and as for the studies mentioned above, it is confirmed that a bone loss produced an increase of the displacement especially with the tipping and intrusive force application. The study [41] started from this latter awareness for illustrating the effects of force magnitudes on the long-term tipping movements of teeth under different levels of bone loss. For reaching this goal the study reproduced five finite element models of an incisor with different degrees of bone loss. The long-term tooth movements were simulated in a 4-week period based on a bone remodeling theory, characterized by a 1 N force for inducing and evaluating the tooth displacements and by forces 0.25 -1 N for evaluating the teeth rotations. The results of bone remodeling simulation confirmed previous studies that simulated initial tooth movement and indicated that when alveolar bone height reduced, under the same load, the long-term tooth movement was increased. Moreover, the results revealed that despite the fact that in all models the tipping degree in the tooth movement increased with increasing applied force, this increase was only pronounced in milder degrees of bone loss (<3.00mm of bone loss). It was also found that when there was more loss of alveolar bone, the tooth movement was less affected by

the magnitude of the orthodontic force. This study suggests that in the patients with more severe degrees of bone loss (>3.00mm of bone loss), the magnitude of force be reduced significantly (up to one quarter of the force applied to the tooth with healthy alveolar bone).

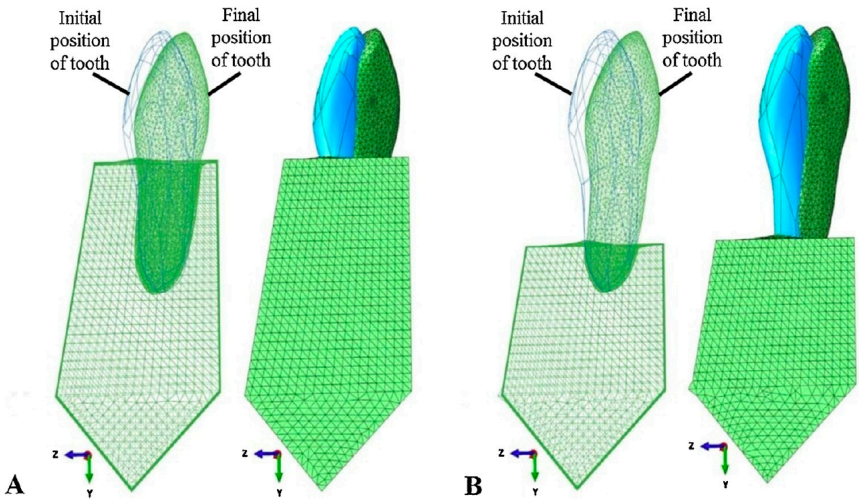

Figure 39 The orthodontic tooth displacement following 4 weeks of orthodontic treatment by the application of a 1.00N tipping force in the models of the incisors with: (A) a normal alveolar bone height, (B) a 6.00mm of height bone loss. The final positions of the tooth and bone can be seen in green (meshed model of tooth), and the initial position of the tooth can be seen in blue (unmeshed model of tooth). For a better comparison, root movement (A & B (left figure)) and crown movement (A & B (right figure)) are shown in two different views of the models. (For interpretation of the references to color in this figure legend, the reader is referred to the web version of this article.). [41]

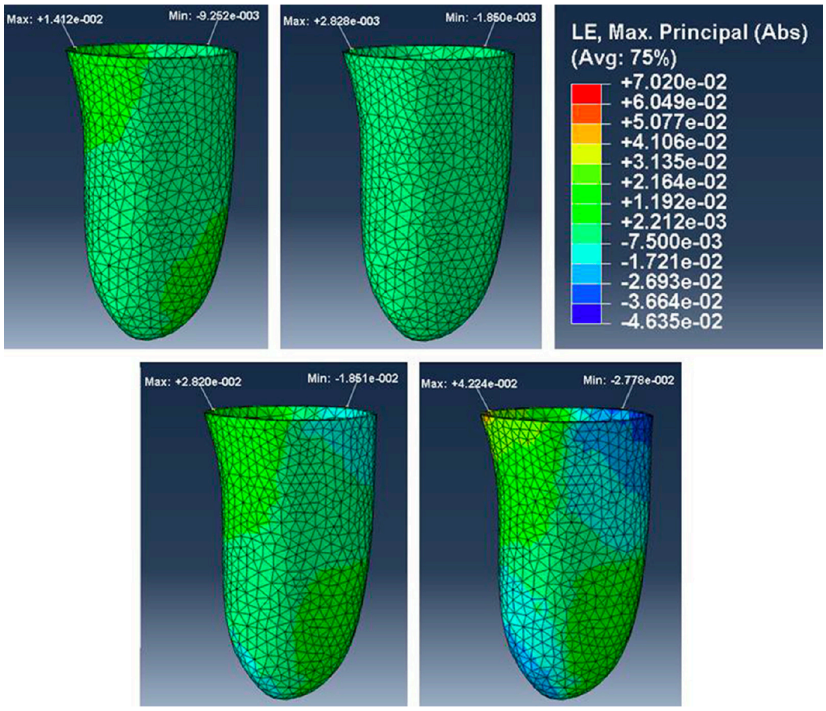

Figure 40 From up, counter-clockwise, maximum principal strains in PDL in teeth under orthodontic forces of 0.25, 0.50, 0.75 and 1.00N, respectively. [41]

Another factor that affects the stress over teeth and PDLs in condition of periodontitis is reported in the article [42] where the labiolingual inclination of a maxillary central incisor was studied. Here, the aim was to investigate whether labial tooth inclination and alveolar bone loss affect the moment per unit of force (Mt/F) in controlled tipping and consequent stresses on PDLs. For achieving this goal, three-dimensional models of maxillary central incisors were created with different labial inclinations (with a degree of: 5, 10, 15, 20) and several amounts of alveolar bone loss (0, 2, 4, and 6 mm). It was found that as bone loss increased, a given Mt/F imparted greater maximum tensile and compressive stresses on the PDL. Moreover, in teeth with greater alveolar bone loss, the stress changed more abruptly with changes in the Mt/F ratio. When the labial inclination of the incisor was increased without changing the amount of alveolar bone loss, the Mt/F ratio decreased for the lowest principal stress *(Figure 41 and 42).*

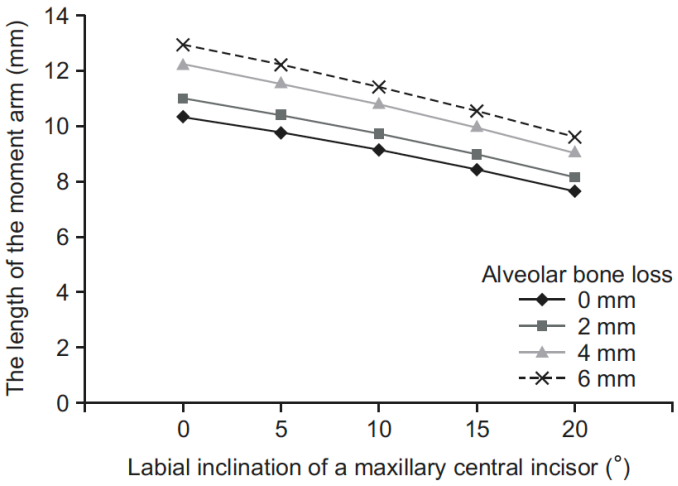

Figure 41 Changes in the length of the moment arm (the perpendicular distance between the line of action of the force and the center of resistance) according to changes in maxillary central incisor inclination and surrounding alveolar bone loss. [42]

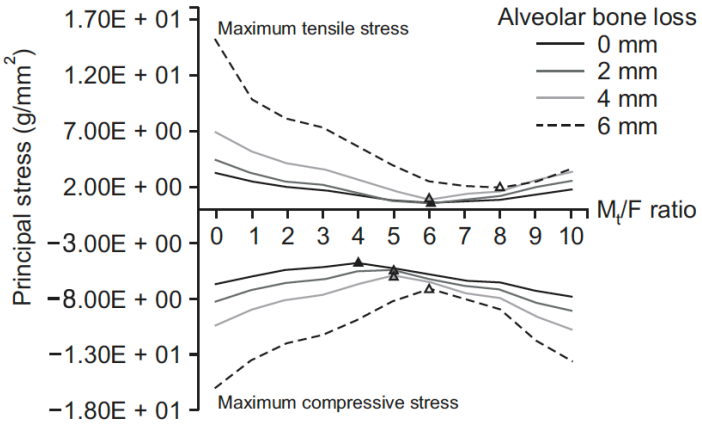

Figure 42 Relationship between the Mt/F ratio and principal stresses in tooth models with 20o of labial inclination. The minimum principal stress levels are indicated by triangles. [42]

Even in the literature presented above some limitations are highlighted since nobody has developed a simulation model by means of FEM for studying all the periodontitis staging that affect in a general way the dental arches of both the mandible and maxilla. In addition, also in this case no one has studied the combination between OSAS and periodontitis and the effects of MADs over the patients.

4.3 Materials

For a correct and reliable simulation with the finite element analysis, the definition of materials is fundamental because each material mimics a specific anatomical part (tissues or bony structures) and as a consequence it mimics also the mechanical properties. Hence in a structural analysis the principal components that must be expressed are: The Young's modulus and the Poisson ratio.

The article [43] reports the most used mechanical properties for the description of TMJ bony components and here were treated separately the cortical and the cancellous bone at which were assigned a young's modulus of 13700 and 7930 MPa respectively and a Poisson ratio of 0.4 for each. These same values were reported in the article [44] which had the goal to determine the most stable fixation method for mandibular symphysis fractures by comparing the mechanical characteristics of models fixed at different positions *(Figure 43).*

	Elastic Modulus (MPa)	Poisson's Ratio
Cortical Bone	8700–15000	0.3–0.33
Cancellous Bone	500–1500	0.3
Titanium	105000–110000	0.34–0.35

MPa; Mega Pascal.

Figure 43 range of values for cortical and cancellous bone. [54]

TMJ has been extensively treated in studies [45, 46], where the mechanical behaviors of the joint were obtained through a neo-Hookian hyper-elastic model. Basically, the articular disc was considered as a solid element of hyper-elastic material whose deformation curve is non-linear. Using the Neo-Hookean method, the elastic modulus is not evaluated, but the strain energy density. Together with the discussion of the materials constituting the bony parts, it is of fundamental importance to describe the material constituting the periodontal ligament. The PDL is a thin layer of soft connective tissue that connects the tooth root to the alveolar bone and its main role is to transfer loads from the tooth to the mandible and maxilla.

In article [43] the periodontal ligament has been reconstructed with the following mechanical properties: Elastic Modulus of 0.49 MPa and Poisson's Ratio of 0.49. The modeling of periodontal ligaments was explained in the article [47] where a hyper-elastic, non-linear model was chosen for trying to approach all those transitory characteristics belong to PDLs. In order to better reflect the properties of the PDLs material, characterized by areas of greater stress in correspondence of the application of a traction force over the tooth, a third-order Ogden model was used.

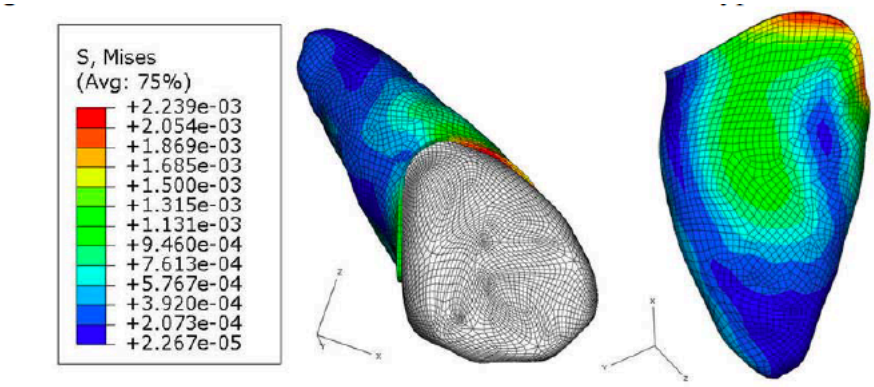

Figure 44 The stress distribution of the PDL based on Ogden hyper-elastic model. [48]

5. Chapter 5: Materials and Methods

In the following chapter all the phases that constitute the core of this work are treated. the first step is the acquisition of physical devices and anatomical parts that belonged to OSA patients, and then continues with a geometric reconstruction of the model using CAD software. Subsequently the 3D model is implemented in Ansys, a software for structural analysis, where the definition of materials and boundary conditions are made. One of the most important steps for a structural analysis is the idealization of the structure that allows to pass from a physical to a numerical model. This idealization involves the reduction of the degrees of freedom from an infinite to a finite number and this operation that allows to pass from a real structure to an idealized one by means of FEM is called discretization. The discretization of the model occurs in the Ansys workspace in which the definition of a mesh applied to the model allows to divide the 3D solid into a finite number of smaller elements. The elements into which the geometric model is divided can be both tetrahedral and hexahedral. The discretization with tetrahedra is certainly faster to implement and realize but requires a particularly high number of elements and nodes to obtain satisfactory results, extending the calculation times. The discretization with hexahedron is very difficult for models with strong irregularities and asymmetries, such as the one in question, but at the same time requires a much lower number of nodes and elements than the discretization with tetrahedra, thus streamlining the calculation phases [49]. In general, a discretization with tetrahedrons is preferred during the mesh phase due to its higher degree of precision. The figure below describes visually the workflow just described.

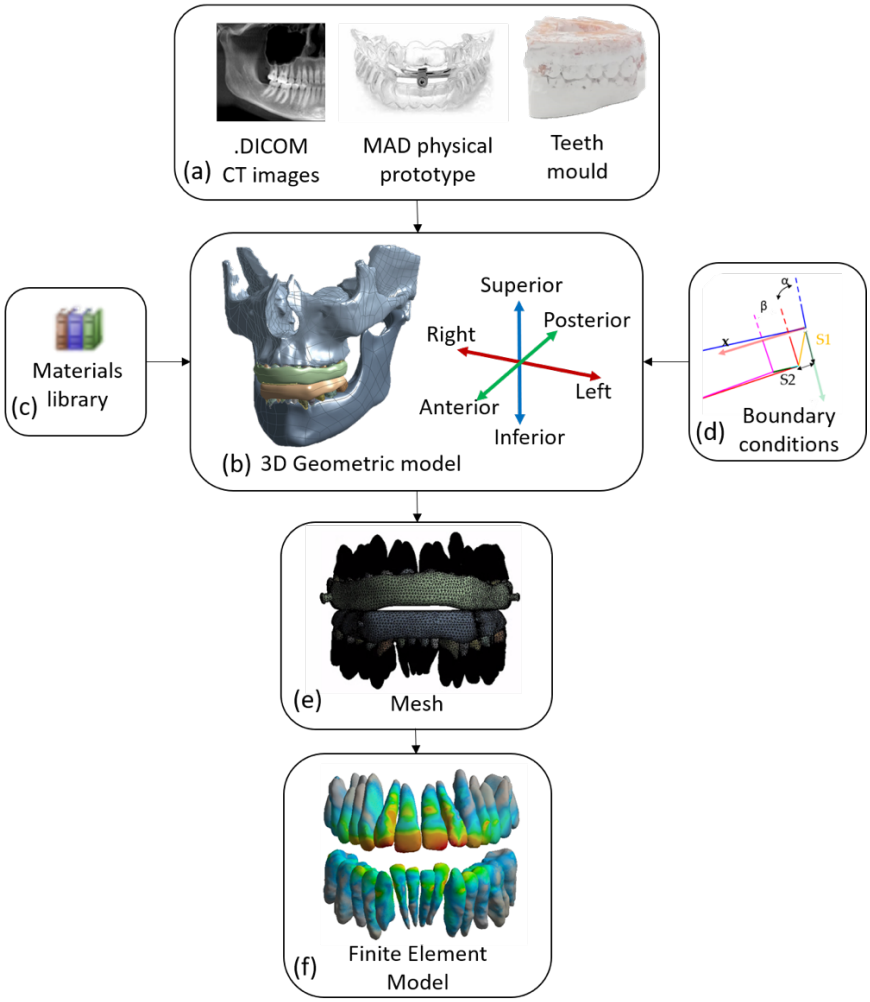

Figure 45 Workflow required to develop the finite element model. a) CT imaging system, the optical scans of the teeth and the mold allow to acquire the patient's anatomy skull; b) the reconstruction of the 3D geometric model; c) definition of a proper set of materials applied to discretized model; d) definition of boundary conditions applied to discretized model; e) setting of mesh for the geometry processing; f) finite element model, the last step of the simulation. [50]

5.1 Model acquisition

The acquisition represents the starting point of the workflow *(Figure 45 a),* in which the 3D reconstruction of the model is achieved through a RE approach starting from a physical object. In this phase the external shape of the object is detected and a cloud of points is reconstructed by recording the spatial coordinates of each point. For the model taken into analysis two types of acquisition were performed, one for the anatomical components and the other for the structural features of the MAD.

5.1.1 Anatomical components

Bony components were 3D reconstructed starting from the Cone Beam Computed Tomography (CBCT) images of a female patient affected by OSA syndrome through a 3D reconstruction software. The CT images were segmented by defining thresholds for the bony components and the teeth in terms of greyscale values. The triangular mesh model was furtherly processed for noise removal, data editing and cleaning.

The anatomy consists of maxilla, mandible, and a full set of teeth. Since the PDLs are soft tissues, they cannot be identifiable through CT scan. Thus, PDLs have been modelled in a 3D surface modelling software for NURBS reconstruction by offsetting the tooth-root surface of 0.3 mm in a thin homogeneous layer. [50]

5.1.2 3D scans of the new SomnoDent Avant

As a first operation for the scanning and acquisition of the geometry of new SomnoDent Avant, the MAD was disassembled in all its components so that each part was visible to the laser scanner; to facilitate scanning, each piece was coated with a white spray in order to highlight its shapes. The acquisition was carried out with the Range7 *(Figure 46),* a laser scanner that allows the acquisition of the cloud of points belonging to a real reference; since the physical principle of scanning is the optical one, the laser scanner belongs to the type of active and therefore contactless optical acquisition systems.

Figure 46 Konica Minolta Range 7.

The operation of the scanner is associated with a software, the *Range Viewer*, whose role is to recognize the scanner, manage the scan and reconstruct the three-dimensional image of the object. The software has two interfaces: one for the scanning phase and the other for the modification phase which can be accessed through the relevant tabs located on the right of the default interface, namely the scan one. The Range Viewer offers several features, in fact in addition to performing a scan it is also able to manage and modify any scans previously made.[51]

The format of the input files must be of the type rgv in the case of single scans, rvm in the case of multiple scans.

As for the output file formats, the software offers various solutions allowing the saving of files in the formats: STL, rvm and rgv, the latter two are the default formats typical of the program, and rmk, with the latter type it allows to save the typical information produced by the markers.

In order to obtain the best possible scans, the splits of the MAD were acquired from both sides, right and left, and in both directions, up and down; during the acquisition, the 'Exposure' parameter was reduced in order to prevent the software from acquiring surfaces other than those of interest. The density of the scanning was also reduced using the “Scan setting” command as well as the markers as reference points *(Figure 47)*. In order to improve the final alignment for each scan, the "Registration" command was used and finally each scan was saved before and after the overlay in the STL format.

Figure 47 ranger Viewer's interface during the scan of the splint.

Subsequently the acquisition and the procession of the scans were proceeded by Rapidform XOR3, a high-performance Reverse Engineering software that offers a whole series of specific tools to convert the point clouds of real objects created through scans into solids. This procedure was done in order to model the external structures of a general MAD and reconstruct the dental arches acquired in reverse engineering. [52]

5.2 Model reconstruction

The reconstruction of a prototype follows the acquisition of the physical model. In this phase a tridimensional geometrical model is developed by means of CAD software starting from two-dimensional data acquired before. For the model taken into analysis several types of geometrical reconstructions were performed:

- 3D model for the anatomical structures easily investigated through CT scan (mandible, maxilla and teeth);
- 3D model for anatomical soft tissues (PDLs);
- 3D model for splints and main features that build up the new SomnoDent Avant device;

- 3D model for the reproduction of a generalized periodontitis that affects both the dental arches.

In this work are treated deeply the 3D reconstruction related to the new MAD and the reproduction of periodontitis, since no one has done it before. Whereas, the geometrical model related to the anatomical structures such as maxilla, mandible, teeth and PDLs have been resumed from the article [44] in which the volumetric image of the anatomy was reconstructed in Mimics (v.12.11, Materialise NV, Leuven, Belgium). The periodontal ligaments were reconstructed through the 3D modelling software Rhinoceros (v.5.0 by McNeel & Associates, Seattle, WA) and modelled by offsetting each tooth root surface of 0.3 mm to fill the space between each tooth and the alveolar socket, although the average thickness of periodontal ligament is 0.15 to 0.38 mm and its shape is thinnest at the middle third of the root (hourglass shape).

5.2.1 CAD of the new SomnoDent Avant

The modelling process for this new MAD did not differ much from other MADs taken into account in previous articles like [44, 50, 52]. In fact, the process of reconstruction for the inferior and superior splint was exactly the same. The surfaces related to the splints were imported and unified in Rhinoceros in order to obtained a single object. Starting from this object were drawn two curves that were taken as rails for some profile curves that defined the shape of these splints. Subsequently with a sweep2 command some surfaces were generated from these curves. Then the surfaces were closed at their extremities and they were aligned in order to have the coplanarity between the superior and the inferior part. Afterwards, was made a superimposition between the upper and lower splint with the dental arches acquired in reverse engineering in order to obtain the accommodation locations of teeth by Boolean subtraction.

Then the attention went on the modelling of those parts which distinguish the new SomnoDent from the other MADs treated previously in literature, like the Orthoapnea and the Herbst. The parts that distinguish the MAD treated in this work are the following:

- two pins on the lateral sides of the lower splint *(Figure 48 A);*
- a rod *(Figure 48 B);*

- a central support in which the rod goes to fit *(Figure 48 C).*

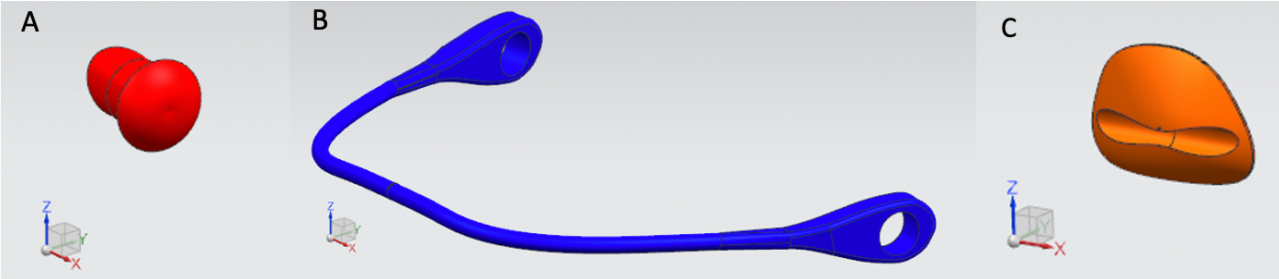

Figure 48 Details of the New SomnoDent Avant device. A) lateral pin. B) rod. C) central support.

The pin was modeled on Rhinoceros through a revolution of a profile along an axis. The profile contained a line parallel to the axis of revolution in order to generate a cylindrical surface which was then made to fit with the rod *(Figure 49).*

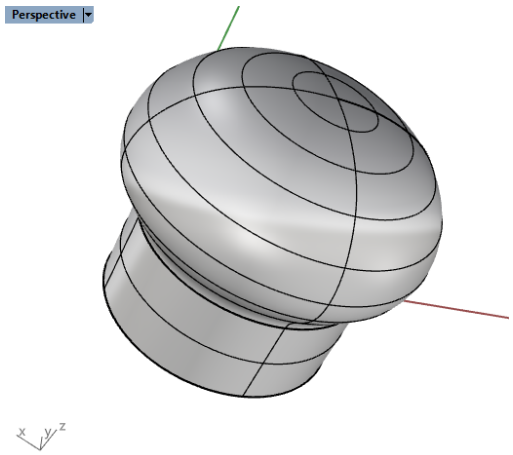

Figure 49 The perspective view of the pin in Rhinoceros.

The modeling of the rod was extremely complex, due to the irregular shape at its ends. First, the axis of the rod was defined through several sections and then a circumference was passed along this axis using the “sweep” command, in order to generate the tubular shape that characterized the rod in its regular part. Subsequently, the ends of the rod were modeled starting from the offset of a planar surface characterized by a hole coaxial with the pins. For the rod to match perfectly with the pins of the lower splint, the width of the hole had to be perfectly equal to the width of the cylindrical surface of the pins. The regular and irregular parts have been combined together by the "loft" action, resulting in a unified rod shape.

The last component of the MAD is the central support. The support was created from a Boolean difference between an extruded curve and a cylinder. It was essential to model a cylinder with the same radius of the rod because otherwise the rod would not have been able to adapt to the support and consequently the MAD would not have been able to function properly.

In *Figure 50* it is possible to observe the MAD with all the components assembled together.

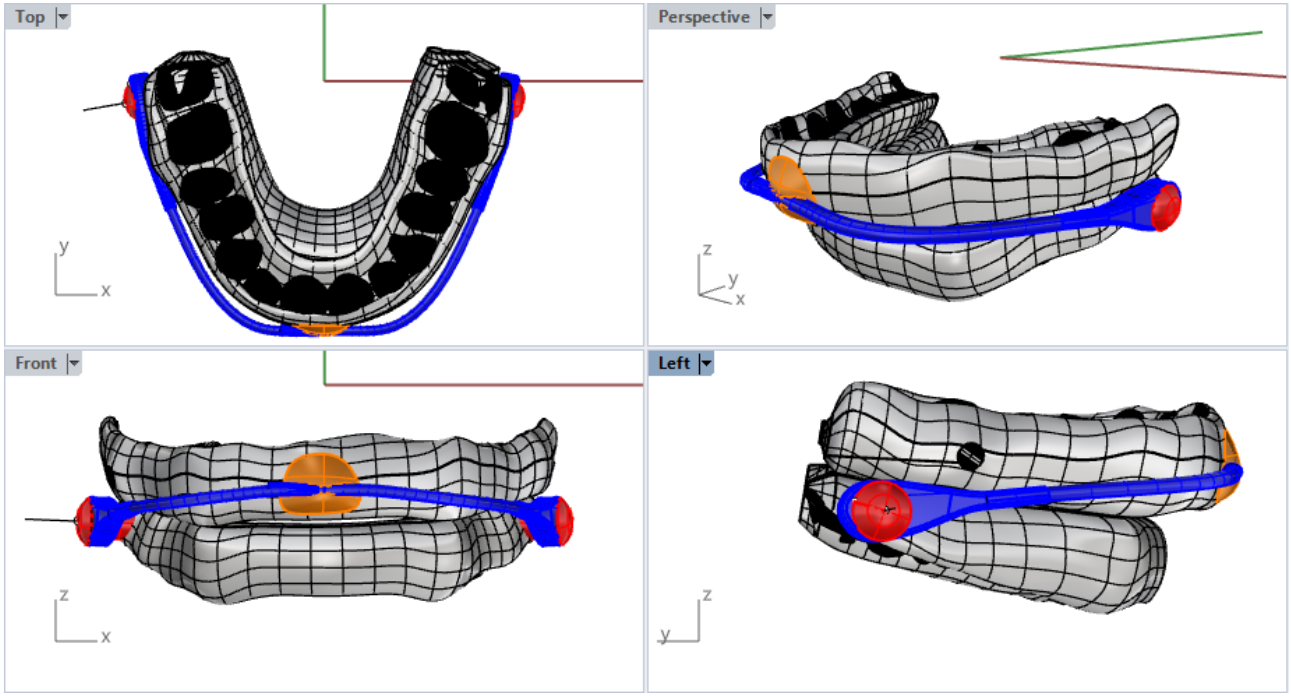

Figure 50 MAD with all the assembled components in the four views of Rhinoceros.

After the assembly, the MAD was exported in STEP extension file in order to be acquired by Ansys for the subsequent phases of the analysis.

5.2.2 Geometric modeling of periodontitis

The reconstruction phase did not stop at the modelling of MAD since in this work the combination between OSAS and periodontitis has been treated. It is important to point out that the periodontitis was not modelling starting from CT images as it was not possible for privacy reasons. Hence, were led simulations about the major periodontitis staging starting from data collected from literature, previously analyzed in chapter 4. The simulations were carried out using two different CAD

software: Rhinoceros and NX where the anatomical prototype (completed with maxilla, mandible, PDL and teeth) was modified to reproduce different stages of alveolar bone loss.

Based on the article of Tonetti et al. [17] the simulations tried to mimic the physiological behaviors of alveolar bone during the staging I, II, III and IV which are respectively characterized by a reabsorption of 15%, 30% and 45% (for both the most severe staging) without, however, considering the loss of teeth in cases of more severe periodontitis.

The process for the modeling of the three degrees of alveolar bone loss began in the Rhinoceros workspace with the measurement of the roots for each tooth and the subsequent calculation of the percentage at each specific periodontitis stage. The procedure for the measurement was standardized in all the teeth even if they have a single root or multiple ones. The actions listed below describe step by step what was done for the computation of the root length *(Figure 51)*:

- Draw points over the alveolar tooth bone in order to outline the upper part of the root (in the neck area) by means of “multiple points” command;
- Draw a circumference that passes through the points with the command “circle: fit points”;
- Generate a surface from the circumference by “surface from planar curves” command;
- Draw a point over the surface that corresponds to the center of the circumference;
- Through the command “polyline normal to surface” generate a line with its origin corresponding to the center of the circumference and its ending point corresponding perpendicularly to the end of the root;
- Measure the length of the traced segment by using “Analyze - length”.

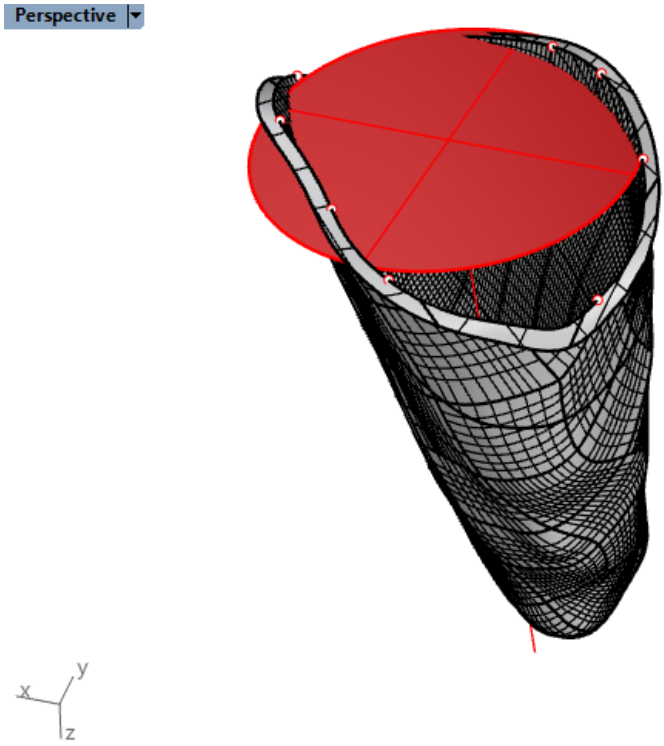

Figure 51 Perspective view of the maxillary right canine - in red a summarizing of all the actions that build up the root measurement procedure.

Below, *Table 1 and Table 2* report the length of the roots for both the maxillary and mandibular arch and together with the length, the values to be removed from the total length of each root are also reported to adequately simulate the resorption of the alveolar bone corresponding to each phase of periodontitis.

Table 1 Measurement of maxillary dental roots and evaluation of periodontitis staging.

Maxillary teeth	Root length (mm)	15% of loss (mm)	30% of loss (mm)	45% of loss (mm)
II molar (left)	11.609	1.741	3.483	5.224
I molar (left)	12.210	1.832	3.663	5.495
II premolar (left)	11.643	1.747	3.493	5.239
I premolar (left)	11.988	1.798	3.596	5.395
Canine (left)	15.903	2.386	4.771	7.156
Lateral incisor (left)	12.973	1.946	3.892	5.838

Central incisor	12.094	1.814	3.628	5.442
Central incisor	11.867	1.780	3.560	5.340
Lateral incisor (right)	14.234	2.135	4.270	6.405
Canine (right)	15.222	2.283	4.567	6.850
I premolar (right)	12.029	1.804	3.609	5.413
II premolar (right)	10.353	1.553	3.106	4.659
I molar (right)	11.943	1.792	3.583	5.374
II molar (right)	10.983	1.648	3.295	4.942

Table 2 Measurement of mandibular dental roots and evaluation of periodontitis staging.

Mandibular teeth	**Root length (mm)**	**15% of loss (mm)**	**30% of loss (mm)**	**45% of loss (mm)**
II molar (left)	11.567	1.500	3.470	5.205
I molar (left)	13.432	2.015	4.030	6.044
II premolar (left)	12.421	1.863	3.726	5.590
I premolar (left)	13.246	1.987	3.974	5.961
Canine (left)	12.146	1.822	3.644	5.466
Lateral incisor (left)	10.077	1.512	3.023	4.535
Central incisor	11.866	1.780	3.560	5.340
Central incisor	10.944	1.642	3.283	4.925

Lateral incisor (right)	11.520	1.728	3.456	5.184
Canine (right)	10.405	1.561	3.122	4.682
I premolar (right)	15.306	2.296	4.592	6.888
II premolar (right)	11.925	1.789	3.578	5.366
I molar (right)	12.601	1.890	3.780	5.671
II molar (right)	11.708	1.756	3.512	5.269

At this point, continuing to work in Rhinoceros workspace, a cutting surface was modeled for each level of periodontitis, starting from 15% and then continuing with 30% and 45%. The procedure for generating this cutting surface follows iterative and also standardized actions. First of all, as in the measurement procedure, a circumference was generated passing through points that indicated the top of the root and then a surface was created from this circumference. Subsequently the surface was moved perpendicularly towards the apex of the tooth, by a value corresponding to the percentage of the bone loss taken into consideration. Then the surface was extended in order to make visible intersections with maxilla or mandible (depending on the part that was considered). the visibility of these intersections was given thanks to curves that highlighted the edges in both the sides of the anatomical structure as shown in *Figure 52.*

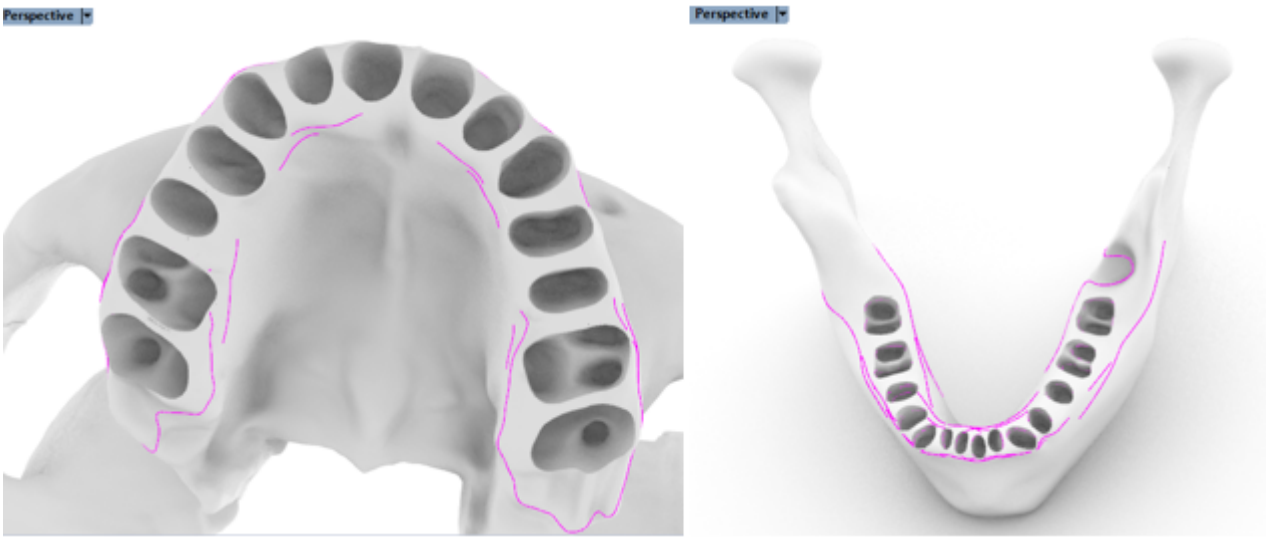

Figure 52 Rendered views of both maxilla and mandible that describe the intersection areas, highlighted by magenta curves.

By activating the Osnap commands, a point has been inserted at the center of the extended surface and through this point a curve has been passed that interpolates all the centers of the circumferences constructed in each tooth. Subsequently, this interpolated curve was extended at its ends in such a way as to come out of the bone and then through the "Fair" command the shape was smoothed, in order to make it less angular and more linear. At this point some profile curves, of parabolic shape, were drawn in correspondence with the major changes in angle of the teeth. These profile curves have been constructed starting from three points: one on the first intersection curve (magenta curve), one perpendicular to the interpolated curve (red curve) and one perpendicular to the second intersection curve (magenta curve), as can be seen in the *Figure 53*.

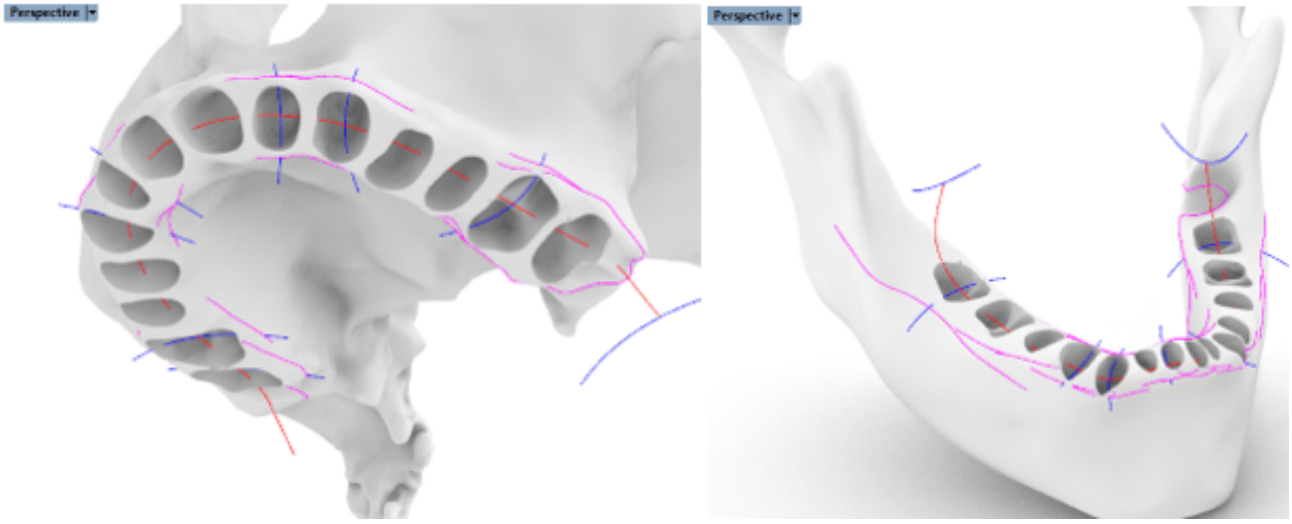

Figure 53 Rendered views of the profile curves (blue curves) meeting both the intersection curves (magenta curves) and the interpolated curve (red one) for both maxillary and mandibular cases.

The cutting surface at this point was easily created, since its shape is defined by the profile curves previously drawn. The generation of this surface occurred by using "sweep1", a command that fits a surface through a series of profile curves that define the surface cross-sections and one curve that defines a surface edge. In this case the curve that defines the surface edge was the interpolated curve (red one), while the surface cross sections were defined by the profile curves (blue ones). The *Figure 54* reports the cutting surface created for the simulation of the stage I of periodontitis.

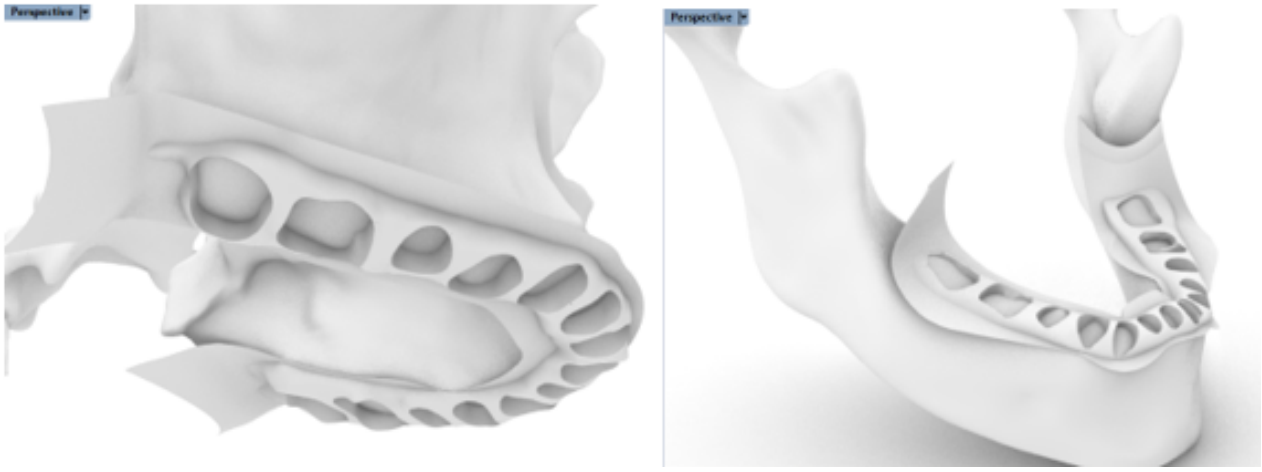

Figure 54 Rendered views of the cutting surfaces at 15% of bone resorption in both the maxilla and mandible.

At this point, after the generation of the three cutting surfaces (one for each periodontitis stage), the files of Rhinoceros were saved with the STEP extension and imported in NX for executing the

Boolean difference between the surface and the anatomical structure, composed by PDLs, cortical and cancellous bone. *Figure 55* shows the mandible before and after the application of the Boolean difference.

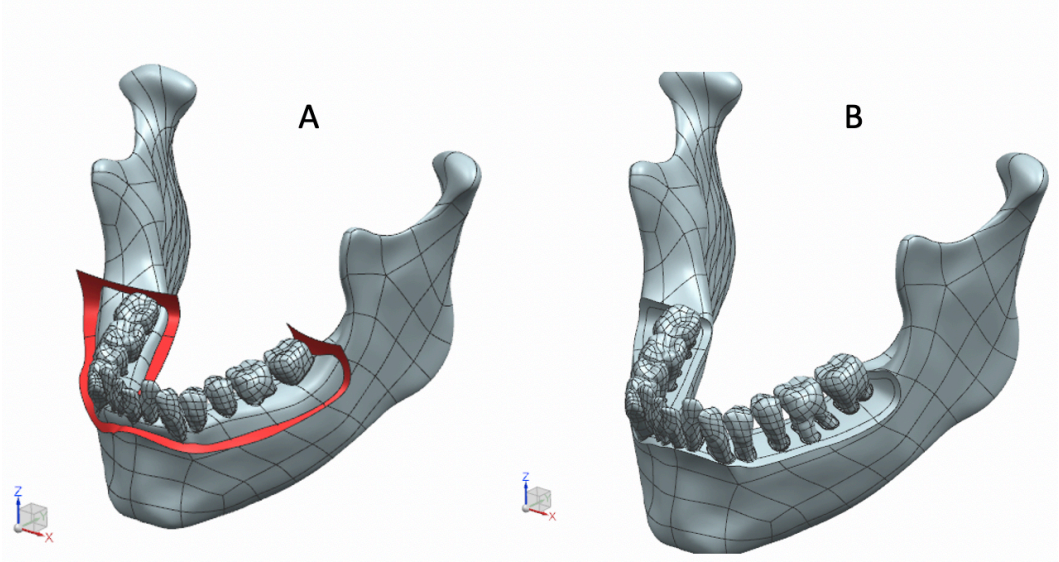

Figure 55 The representation of the Boolean difference in NX for a 30% of alveolar bone loss. A) The cutting surface with which to cut the mandible; B) The mandible without its portion cut by the surface and subtracted by means of Boolean action.

Below, are reported two panels for both mandible and maxilla in which it is possible to observe the different level of alveolar bone loss reproduced through these CAD software, Rhinoceros and NX.

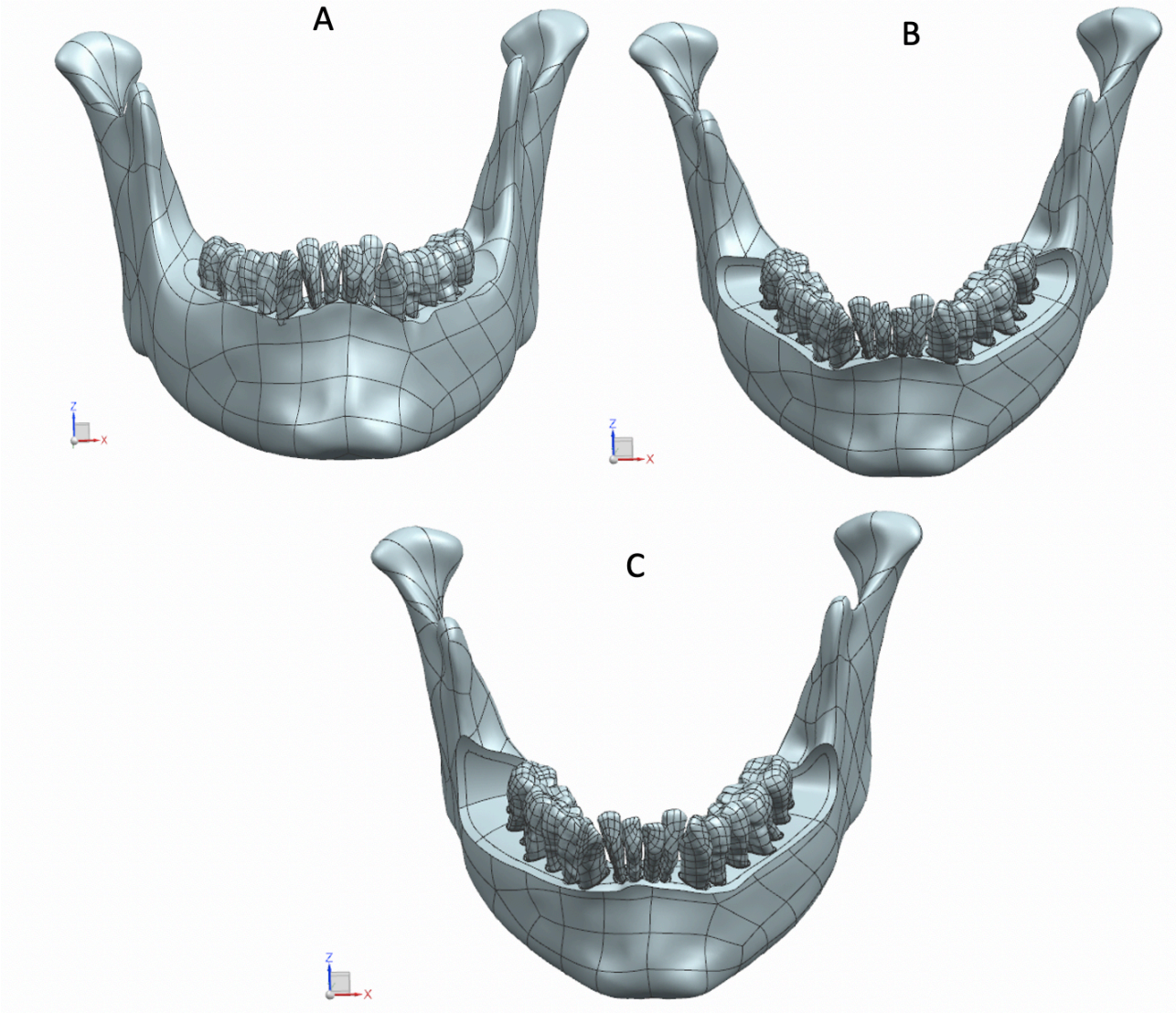

Figure 56 The panel shows three different levels of alveolar bone resorption in the mandible. A) 15% of bone loss; B) 30% of bone loss; C) 45% of bone loss.

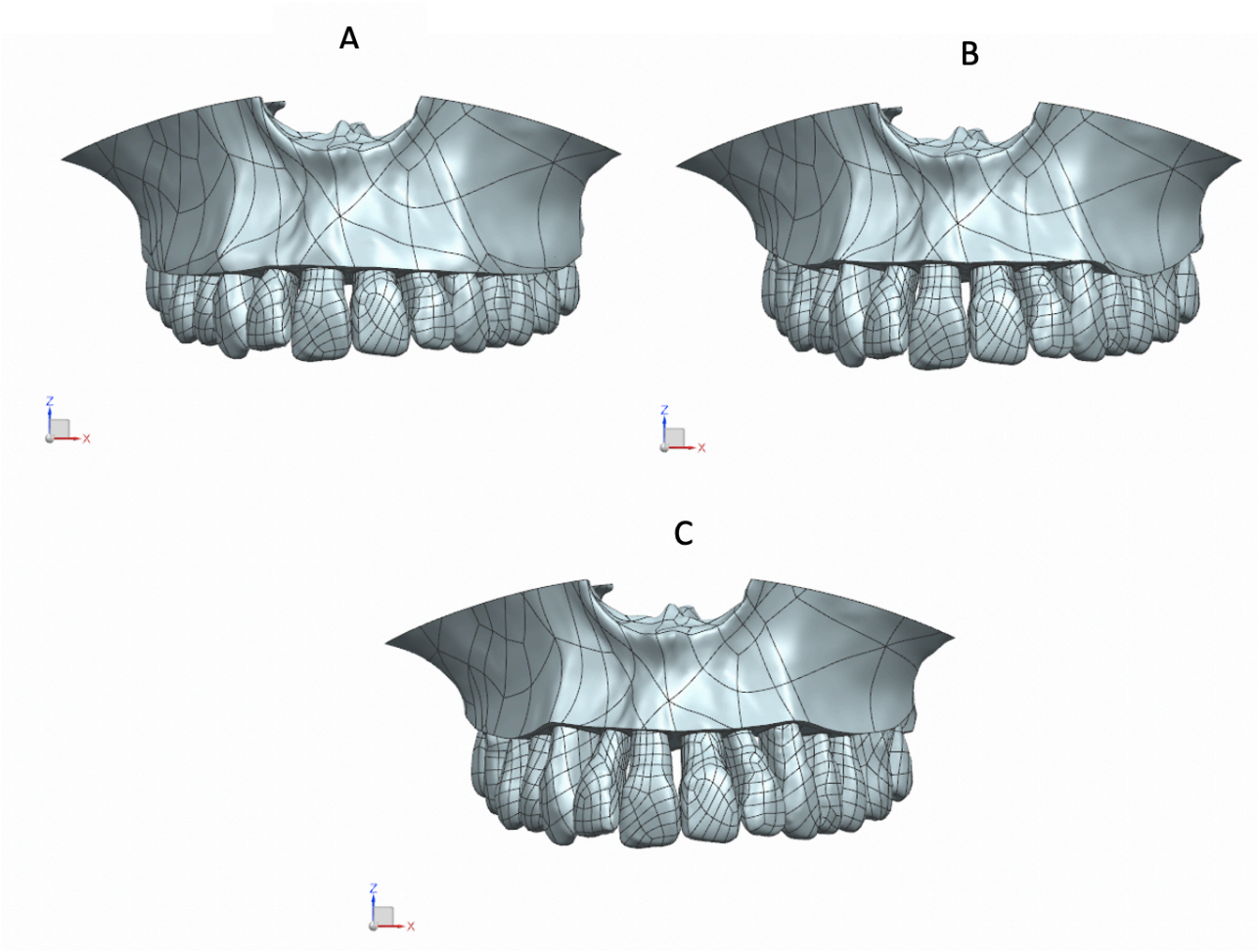

Figure 57 The panel shows three different levels of alveolar bone resorption in the maxilla. A) 15% of bone loss; B) 30% of bone loss; C) 45% of bone loss.

5.3 Finite element model processing

The discretization phase follows the CAD approach, as it can be observable in *Figure 45* and it consists mainly in the transferring of continuous data into discrete counterpart. Hence, it is a process that allows to pass from a physical to a numerical model. From the numerical model a structural analysis is carried out, in order to evaluate the mechanical behaviors of it. However, in order to carry out this analysis, it is essential to specify some conditions to make the analysis as close to reality as possible. The conditions to introduce are basically the materials with which the model is built up, the definition of the contacts between bodies and the forces applied to the model for better simulating a more realistic situation.

5.3.1 Properties of materials

The definition of the materials, as previously mentioned, is fundamental for a realistic simulation of the model, since the materials determine the mechanical behavior of the prototype. Thus, in this work, a careful choice of the material was made and particular attention was given to Young's modulus (E) and Poisson's ratio (υ), features that describe the elastic properties of solids. To better describe the assignment of each material it is good to take a look at the article of Caragiuli et al. [50] in which the same assumptions were made, with the exception of cancellous bone, which was not treated in the article.

The material properties of the components representing MAD, teeth, cortical and cancellous bone were assumed to be homogeneous, isotropic, and linearly elastic as listed in *Table 3*. About the MAD two material behaviors have been assumed: a softer material (nylon 6/6 with E=1480 MPa) for the rod and a stiffer behavior for all the other components (acrylic with E=8300 MPa). For what concerns the PDLs, they were represented by a hyperelastic model based on a strain-dependent energy function, expressed in *Equation 1*.

$$\boldsymbol{W = \sum_{i=1}^{N} \frac{2\mu_i}{\alpha_i^2}\left(\bar{\lambda}_1^{\alpha_i} + \bar{\lambda}_2^{\alpha_i} + \bar{\lambda}_3^{\alpha_i} - 3\right) + \sum_{i=1}^{N} \frac{1}{D_i}(J-1)^{2i}} \qquad \textit{Equation 1}$$

W is the strain energy function, **λ1, λ2, λ3** the principle stretches of the left Cauchy-Green tensor and **J** the determinant of the elastic deformation gradient. The parameter **N** is the order of the polynomial, while the constant **μi** is related to the initial (around the undeformed configuration) shear modulus of the material. The coefficients **Di** refer to the initial bulk modulus of the material and since the PDLs have almost incompressible behavior these coefficients were considered equal to 0. Lastly, the parameters **αi** affect the non-linearity of the stress-strain relationship and make the model capable of fitting experimental stress-strain curves that show a strong non-linearity.

For the best fitting of uniaxial test data, a 2nd order Ogden model was chosen in order to represent the behaviors of PDLs. [50]

Table 3 Mechanical properties of the model's components.

Material	Model	E*	υ*	Coefficient values
MAD	Linear elastic	8300 1480	0.28 0.41	
Tooth	Linear elastic	18300	0.31	
Cortical Bone	Linear elastic	13700	0.3	
Cancellous Bone	Linear elastic	1370	0.31	
PDL	Hyperelastic Ogden 2nd order	---	---	α_1=-3.4761 α_2=18.679 μ_1=-0.034004 MPa μ_2=0,00088691 MPa d_1=0 d_2=0

*E: Young's modulus (MPa); υ: Poisson's ratio.

5.3.2 Boundary conditions and loading

The simulation model aims to evaluate the interactions between the new SomnoDent Avant and anatomical structures, both in health and pathological conditions. To this end it is important to define the stress state and the deformation that occurs during the OSAS treatment that causes a mandibular protrusion for MAD millimeter adjustment (measured on the occlusal plane). It is important to say that during the simulations only a half model (right side) was considered which includes PDL (for both arches), teeth (for both arches), MAD splints (connected via a flexible rod), mandibular cortical bone and mandibular cancellous bone. Therefore, the definition of the boundary conditions was carried out on these components for both the healthy model and the one with periodontitis.

In this work, all the defined boundary conditions are the same both for the simulation involving healthy anatomical structures and for the one involving pathological ones, since the results obtained can only be compared in this way. Thus, in both the simulations the connections used for linking the anatomical elements were described by **bonded contacts** which were defined between the following bodies:

- Teeth –PDLs (for both maxilla and mandible);
- Cortical bone – cancellous bone (only for mandible);
- Cortical bone – PDLs (only for mandible, since in the maxillary PDLs was applied a fixed support).

For what concerns the connection between MAD and teeth was used the **share topology** which is the only way to achieve a conformal mesh where bodies meet, and it is the only way to be certain that the intersection of bodies is meshed perfectly. Whereas, there were several connections used for describing the interactions between MAD components and they are listed below:

- **Frictionless contact** between rod and central support and between rod and pins;
- **No separation contact** between upper and lower splint;
- **Cylindrical joints** between rod and pins, with Z the rotational axis as shown in *Figure 58*.

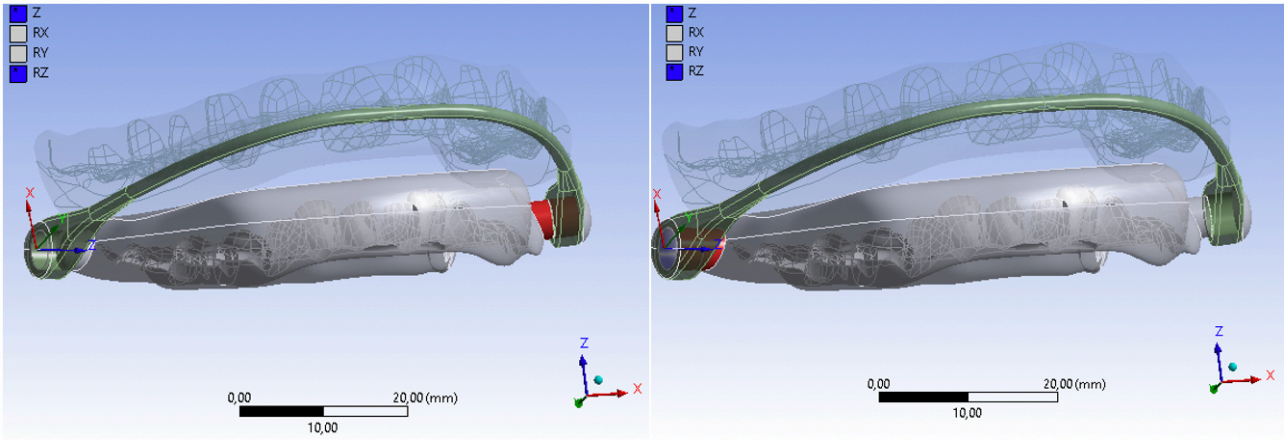

Figure 58 A representation of the cylindrical joints – in red the contact body while in blue the target one.

According to the article of Since Cohen-Levy et al. [53] in which was reported a force of 1.18 N/mm for the advancement due to MAD application, also in this work a total load of 11. 18 N was applied in relation to the extent of mandibular protrusion along the occlusal plane. Half of the total load was applied to each condyle, with an amplitude of 5.59 N, in order to best describe the operating principle of the MAD.

5.3.3 Mesh setting

For fastening the simulations, the maxilla was removed from both the models and these latter ones were also divided into half, analyzing only the right parts of the prototypes as shows *Figure 59*.

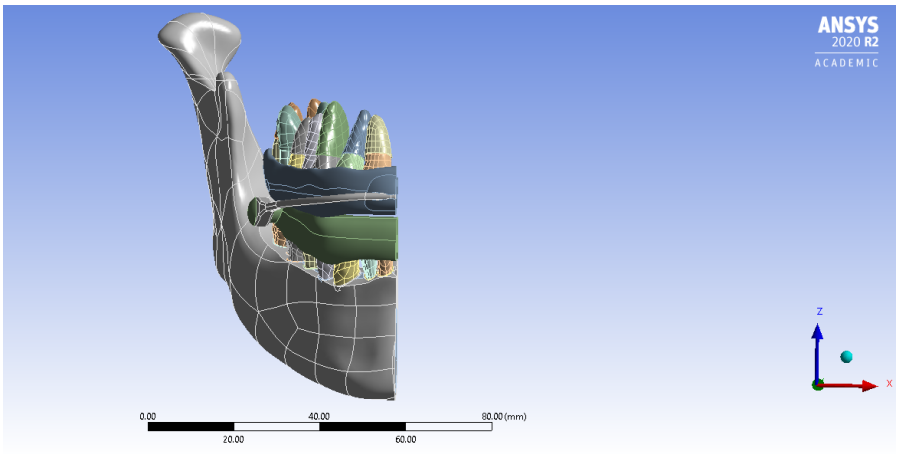

Figure 59 The examined geometry in the static structural analysis.

The models were discretized using three-dimensional, linear, four-node tetrahedral elements which are the suitable elements for modelling complex shapes, such as the irregular surfaces of teeth and PDLs. In both the simulations was defined a general setting with the same growth rate of 1.85 and a capture curvature which is often used in bodies full of holes and curvatures in order to increase the fitting in these parts through a finer mesh. This setting was chosen to increase accuracy in areas of interest such as PDL and teeth. in fact, in these regions a much finer mesh was chosen than that used in the mandible where a coarser mesh was chosen, so as to reduce nodes and elements and consequently the computational complexity of the model (Figure 60).

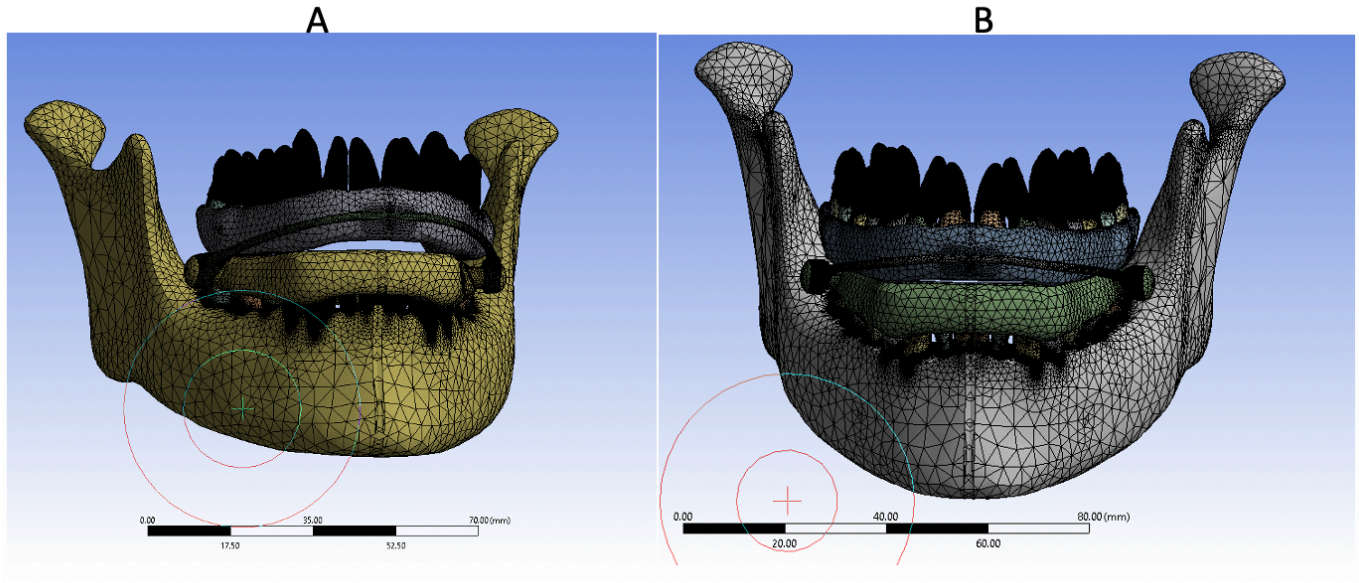

Figure 58 A) mesh in the healthy model; B) mesh in the periodontitis simulation model.

The choice of the element size is strictly related to the thickness of a body; smaller is the thickness, finer is the size. This concept is extremely important for understanding how the values were decided for the sizing of the mesh over each model component. In fact, for the PDLs (with a thickness of 0.3 mm [44]) was chosen, in both the simulations, an element size of 0.2 mm for higher accuracy, since they are very thin components. This setting was not used only for the PDLs but also for the alveolar cortical bone in both the prototypes. This choice was made since it was discovered in the article [54] that this anatomical component is characterized by a thickness of 0.2 mm in the alveolar area. By considering the sizing for the cancellous bone in the same area, the alveolar zone, finer elements of 0.1 mm dimension were taken into account in both the prototypes. The setting in both the alveolar

cortical and cancellous bone was characterized by the curvature proximity function which is used to generate a finer surface mesh and also a higher number of cells across a gap for increasing the accuracy in the more complex surfaces of the models. The *Figure 62* shows the inner parts of the meshed models so that is easier to understand the thickness of each component and also it is possible to appreciate the local mesh setting given in order to increase the accuracy.

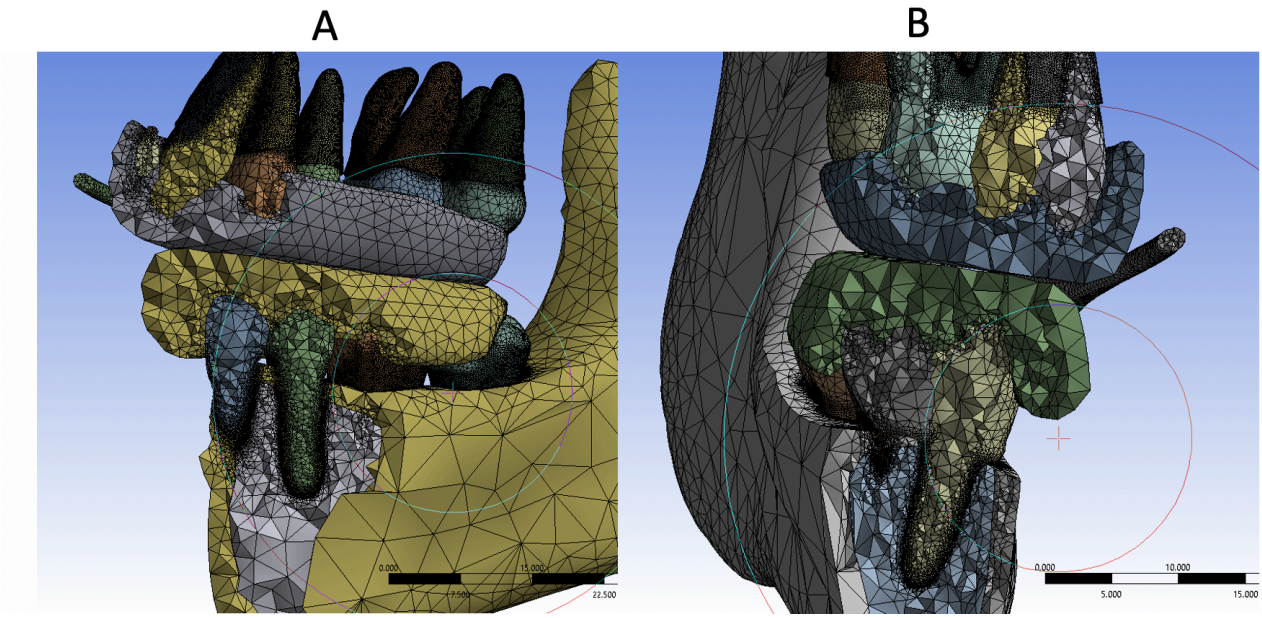

Figure 59 The transition of the mesh from an area to another of the model is appreciable; a finer mesh is found in the areas with high curvature or less thickness. A) The inner view of the healthy model; B) The inner view of the periodontitis simulation model.

Each discretized simulation model, both the healthy and the pathological one, includes a specific number of elements and nodes, listed in *Table 4.* The node count was reduced by creating matching element faces that share nodes on the surface common to both bodies. The FEA was performed on the finite element software Ansys Workbench 2020 R2.

Table 4 Mesh statistic for both the models.

	Healthy anatomical model	**Model for 15% of bone loss**
nodes	1300732	1192725
elements	5676993	5208661

6. Chapter 6: Results and Discussion

In this chapter the results obtained from the simulations of both the models are treated. Principally the attention goes to the stresses and the deformations that occur during the application of the new SomnoDent Avant in both the healthy and inflammatory condition. The material deformation is caused by a volumetric change and a distortion that can be investigated thorough von Mises Stress, since the deviatoric stress is responsible for changes in the shape in the material. The stress is the internal pressure that develops to counteract the applied external load; therefore, it is strictly related to the load distribution. As it has been already said in *the paragraph 5.3.2*, the external loads were applied to the condyles in order to reproduce the advancement of the mandible. In each condyle a force of 5.89 N was applied in the y direction.

These observed parameters are especially evaluated in teeth and PDLs, since they directly enter in contact with the MAD and they are the main subjects of periodontitis.

In this work a comparative analysis between the healthy and the periodontitis model was carried out in order to underline the main differences during the MAD application.

The most relevant information is achieved by considering the deformation over the teeth and the stress over PDLs.

From the **deformation**, a generalized increase in tooth deformation can be observed for the periodontal model, as shown in *Figures 60* and *61*. An evaluation of both the maxillary and mandibular arch deformation was performed on the right side of the simulated models. The results obtained from both dental half arches cannot be compared, as two different constraints were applied for the mandibular and maxillary PDLs. In fact, in the maxilla the PDLs were constrained limiting the deformation in teeth and PDLs themselves, while for the mandible was defined a BONDED contact between Cortical bone and PDLs.

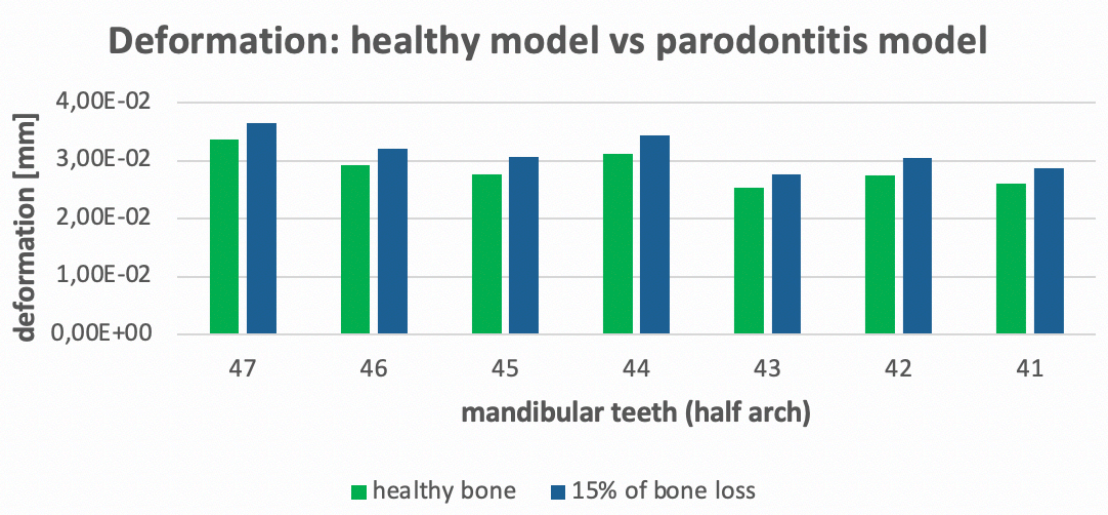

Figure 60 Comparison of deformation over mandibular teeth (with the ISO system numeration) in both the healthy and periodontitis model.

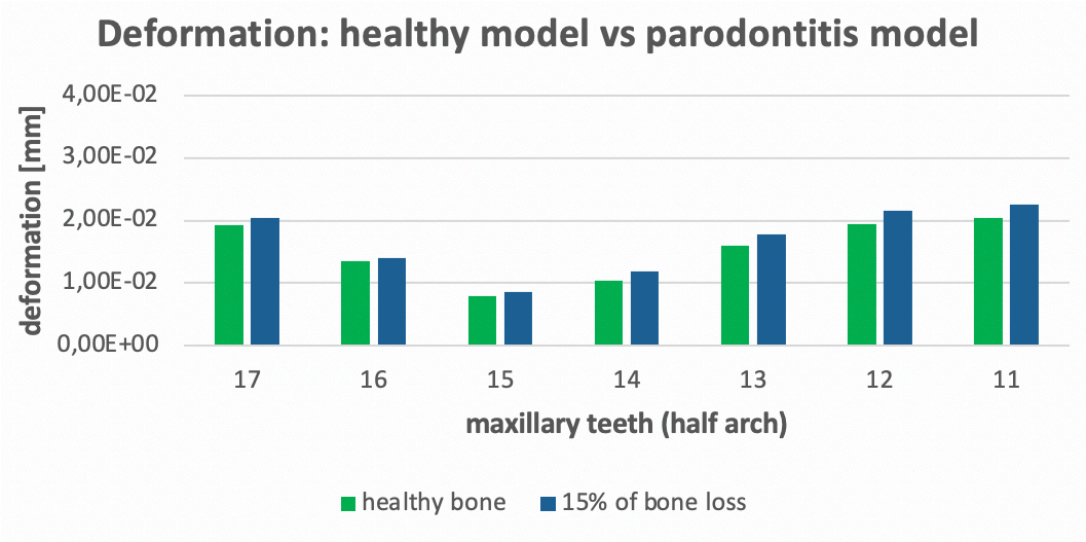

Figure 61 Comparison of deformation over maxillary teeth (with the ISO system numeration) in both the healthy and periodontitis model.

By analyzing *Figure 60,* it is clear that the greatest deformation value is recorded in tooth 47, since in the CAD model *(Figure 56 A)* this tooth is more exposed during periodontium wear. Subsequently, observing the graph, high deformation values are recorded on teeth 44, 45, 42 and 41. It is interesting to analyze the percentage that describes the trend of deformation from the healthy model to the periodontitis one. In fact, this trend defines an increment of deformation in correspondence of the 15% of alveolar bone reabsorption and this increment oscillates in a percentage range of 9% to 11%. The 9% is recorded in teeth 47 and 43 while the 11% in tooth 45, for all the other teeth an increment of deformation for 10% is documented.

By analyzing *Figure 61,* it is clear that the greatest deformation value is recorded in the tooth 11, since (as for the mandibular tooth 47) in the CAD model *(Figure 57 A)* this tooth is more exposed during periodontium wear, following by teeth 12, 17 and 13. Also in this case the trend of deformation describes an increment during the bone reabsorption, but this trend is not as uniform as that in the mandible. In fact, the increasement oscillates from a 3% to a 14%. The tooth 16 records a deformation increasement of 3%, while the tooth 14 an increasement of 14%. Going on with 7% in tooth 17, 8% in tooth 15, 10% in tooth 12 and 11% in teeth 13 and 11. These low differences in percentage for maxilla and mandible in both the healthy and periodontitis model are shown in the figure below, while a representation of the distribution of displacements over the teeth in both the models is presented in *Figure 63.*

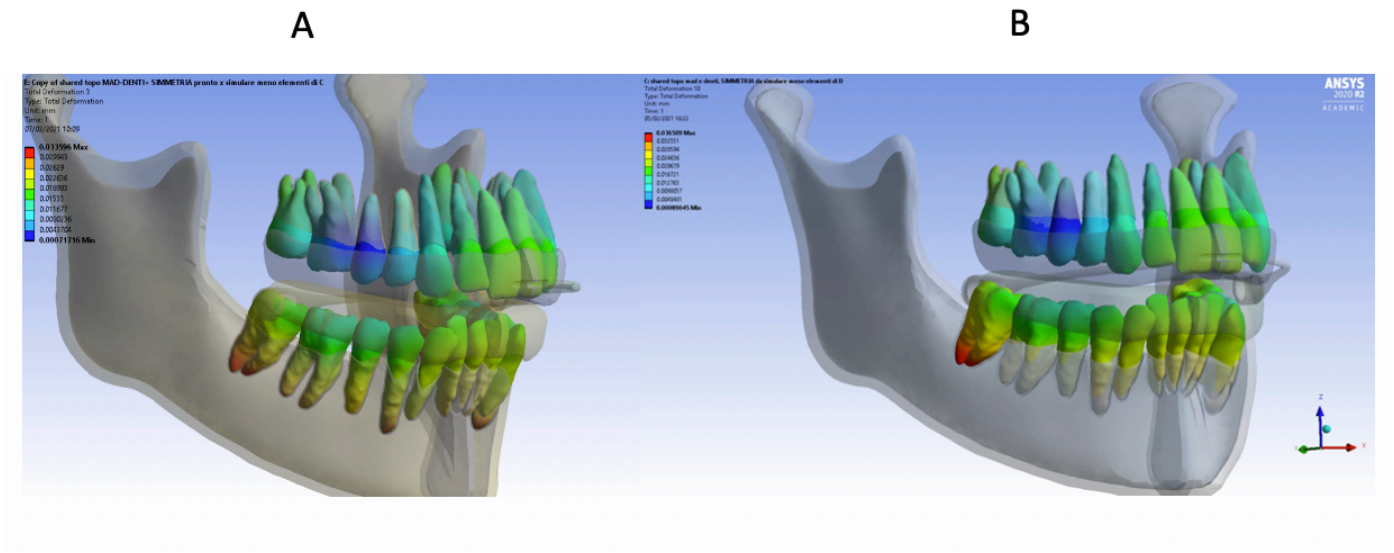

Figure 62 Deformation over teeth in the right part of the model. A) healthy model; B) 15% of alveolar bone loss.

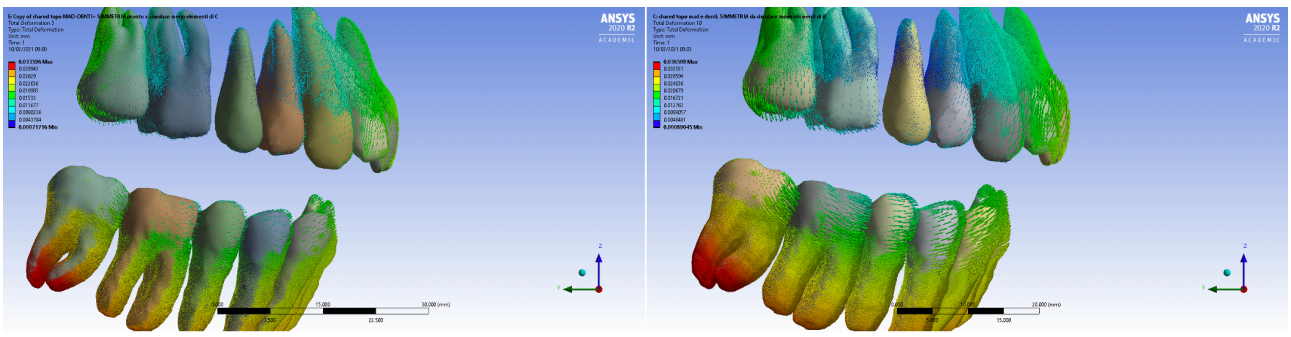

Figure 63 Distribution of displacements over teeth through arrows that indicate from left to right the direction of deformation respectively in the heathy model and in the periodontitis one.

All the deformations were evaluated at the tip of the teeth and they were a product of an orthodontic force applied over the condyles and not directly over the teeth. Precisely, for this reason it is very difficult to compare these results with others presented in literature, since almost all the articles take into account a force applied directly over teeth and they specify the typology of the applied force (intrusion force, tipping force etc..).

In spite of it all, the following consideration could be made by considering the article [50] of Geramy, in which the deformation over tooth 11 was studied. In this study a deformation over the incisal edge of this tooth was evaluated during the application of 1N force in two different conditions: healthy and alveolar bone loss conditions.

In the healthy condition the tooth deformation was about $4.7e^{-3}$ mm whereas during the bone loss condition it was recorded a deformation of $6.80e^{-3}$ mm, thus a 45% of deformation increasement occurs during the bone loss. This percentage is considerably higher than that recorded in this work for the maxillary central incisor, which is around 11% (deformations of $2.04e^{-2}$ mm and $2.26e^{-2}$ mm respectively in healthy and bone loss conditions) and this is probably related to several factors like the root length of the considered tooth, the considered bone loss and the condition in which is evaluated the deformation. For example, in this work the deformation is considered during the application of a MAD that probably limits the tooth deformation and it is also considered a situation in which a force is applied over all the teeth that composed dental arch and not only over one tooth. Even if there are several differences between the article and this work, it is possible to affirm that a condition of bone loss increases the deformation over teeth.

In *Figure 63* and *64* are reported also the deformations over PDLs. The graphs in both the arches represent conforming trends with the graphs of teeth deformations. In maxilla the highest deformation is recorded in the VII PDL (corresponding to tooth 17) and then goes on with II and I PDLs (corresponding to the incisor teeth 12, 11). In mandible an exception to the teeth trend is recorded over the III PDL (corresponding to tooth 43), where a higher value of deformation is recorded compared to the IV PDL (corresponding to tooth 44). This can be explained by the fact that the canine (43) in the mandible has a lower root length of 10.405 mm while the I premolar (44) has a root length of 15.306 mm. Thus, the deformation is higher in the III PDL, since the length of PDL is smaller than that of the IV PDL.

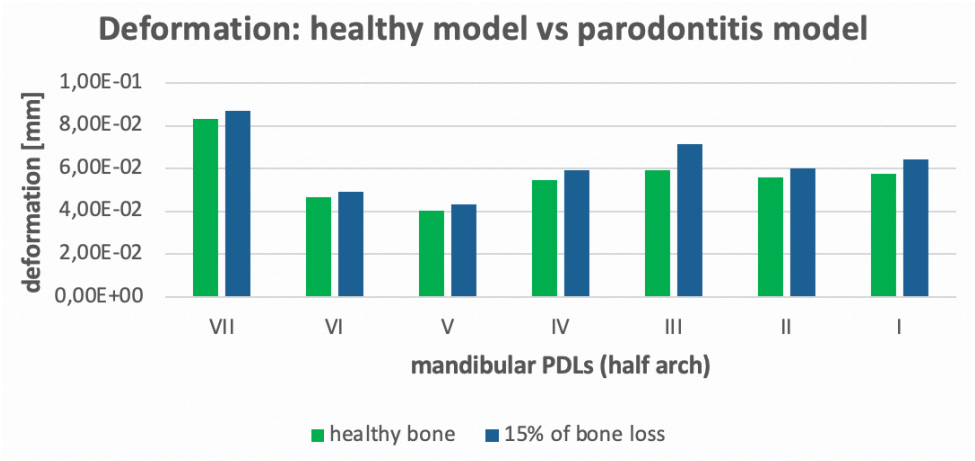

Figure 64 Comparison of deformation over mandibular PDLs in both the healthy and periodontitis model.

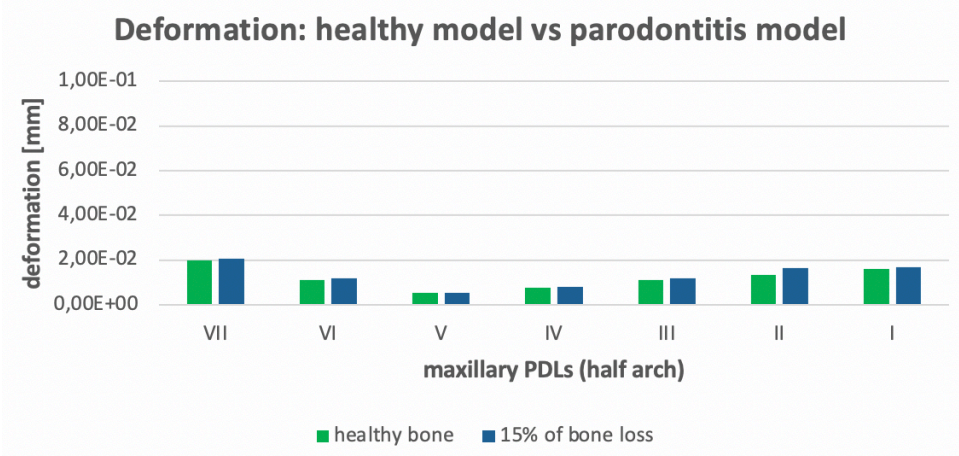

Figure 65 Comparison of deformation over maxillary PDLs in both the healthy and periodontitis model.

Going forward with **stress** it is important to focus on PDLs, since, constituting the periodontium (structural unit of the tooth), they register, even in healthy conditions, tensions that help to understand if there is something wrong and that limits its functioning. *Figures 66* and *67* respectively show the trend of stress on the mandibular and maxillary PDLs, but even in this case only a comparison is made between the models, since different constraints for both PDLs are taken during the simulations.

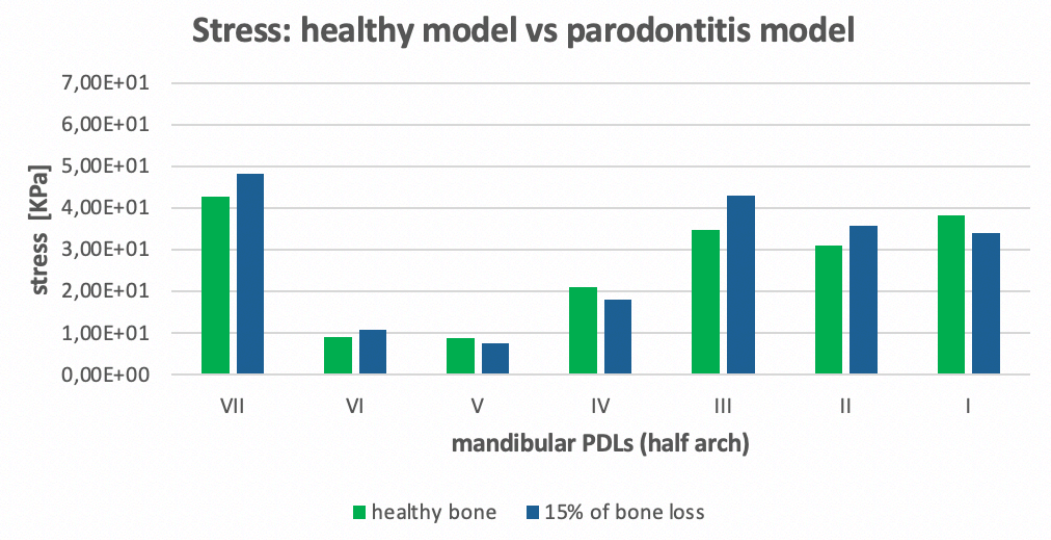

Figure 66 Comparison of stress over mandibular PDLs in both the healthy and periodontitis model.

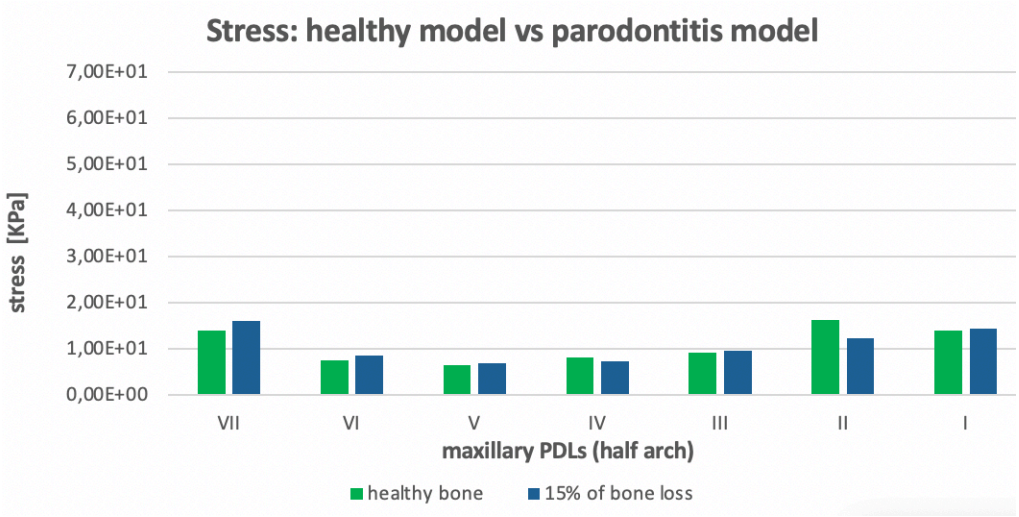

Figure 67 Comparison of stress over maxillary PDLs in both the healthy and periodontitis model.

By observing *Figures 66* it is visible that there is not a generalized increasement of stress over the periodontitis model, since in V, IV and I PDLs (corresponding to teeth 45, 44 and 41) a decreasing of stress respectively of 16%, 14% and 11 % is recorded. In all the other PDLs, passing from the healthy to the periodontitis model, it is recorded an increase of stress mostly over the III PDL (corresponding to tooth 43) where it is registered the greatest increment, about 24%. The percentage of increment over the VII PDL is about 13%, not so higher with respect to the III PDL, but this PDL (corresponding to tooth 47) presents the highest value of stress found in the periodontitis model. These considerations led to analyze locally the PDLs in question, since a non-homogeneity in the results is found and it suggests errors caused by a mistake during the mesh setting or by singularity points.

Starting by analyzing the VII mandibular PDL, it is possible to affirm that in neither model these high values of stress are associated to a coarse mesh, even if in the periodontitis model (*Figure 69*) the mesh quality presents some rare coarse elements. Moreover, it is possible to say that these high values of stress do not depend by singularity points, as it can be observed in the images below.

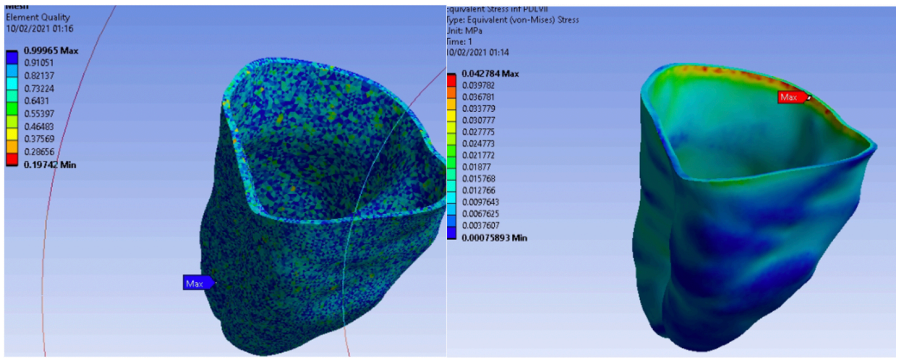

Figure 68 Comparison between mesh (on the left) and stress distribution (on the right) over the VII mandibular PDL for the healthy model.

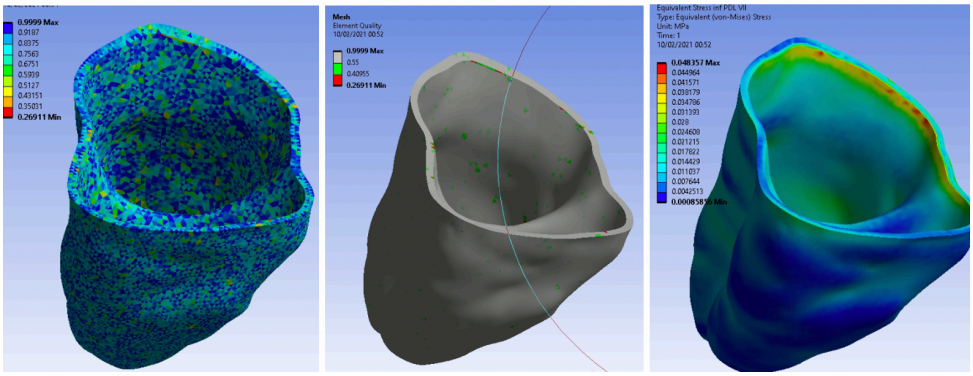

Figure 69 Comparison between mesh (on the left and the center) and stress distribution (on the right) over the VII mandibular PDL for the periodontitis model.

Subsequently, passing to analyze the III PDL in both the models it is possible to observe from *Figure 70* and *71* that also in these cases the mesh quality does not influence the values of stress and these values do not depend on singularity points as it can be observed by considering locally the stress distribution.

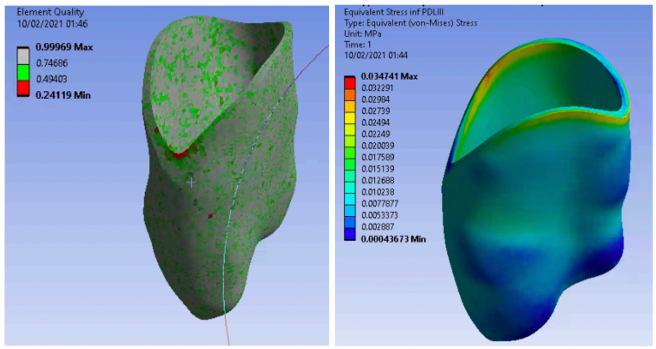

Figure 70 Comparison between mesh (on the left) and stress distribution (on the right) over the III mandibular PDL for the healthy model.

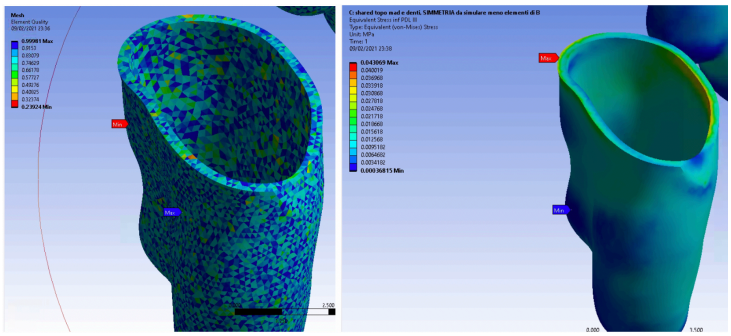

Figure 71 Comparison between mesh (on the left) and stress distribution (on the right) over the III mandibular PDL for the periodontitis model.

At this point, the focus goes on the analysis of stress over the maxillary PDLs *(Figure 67)*. Similarly, to the stress trend in the mandibular ligaments, also in the maxillary ones it is found a non-homogeneity by comparing the results of both the models. The percentage evaluated between the healthy and the periodontitis model oscillates also in this case from negative values to positive ones, thus describing a decrement of stress in the periodontitis model over II and IV PDLs (corresponding to teeth 12 and 14), respectively of 24% and 10%. For what concerns the stress recorded over the VII PDL (corresponding to tooth 17) of the periodontitis model, an increment of 14% is established. For this PDL also the greatest value of stress is defined among all the maxillary ligaments of the periodontitis model. Also in this case, it is necessary to visualize the local distribution of stress over the VII PDL for excluding mistakes in mesh setting.

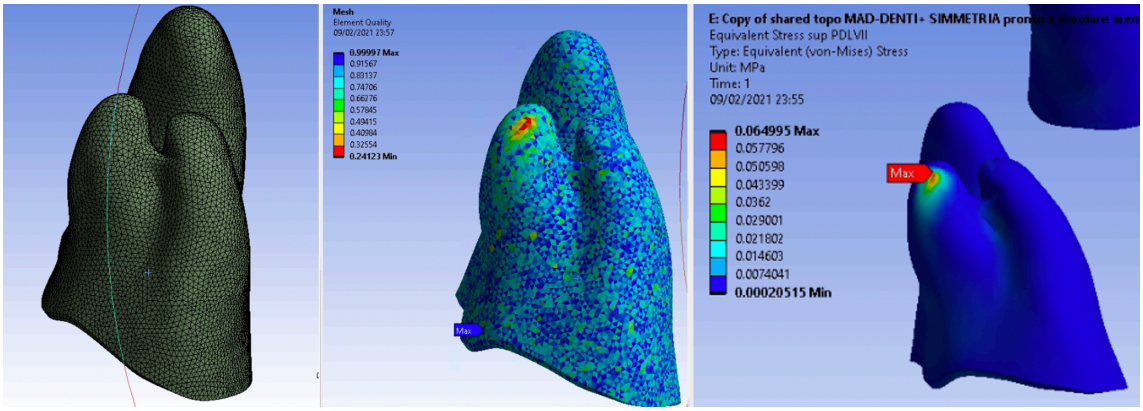

Figure 72 Comparison between mesh (on the left and the center) and stress distribution (on the right) over the VII maxillary PDL for the healthy model.

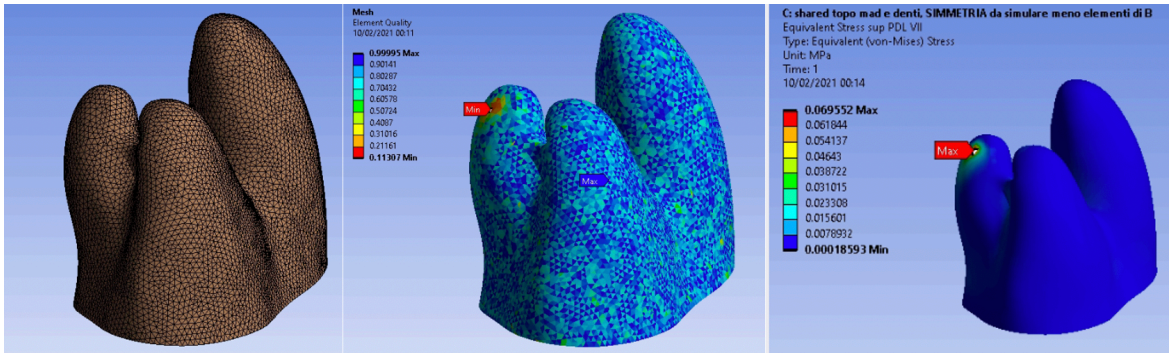

Figure 73 Comparison between mesh (on the left and the center) and stress distribution (on the right) over the VII maxillary PDL for the periodontitis model.

By observing *Figure 72* and *73*, it is possible to visualize a poor - quality mesh over the apex of the VII PDL and this provokes a higher stress concentration over that area which leads to record unrealistic stress values. In both these cases an average value is taken to represent the stress over the PDL: 14 KPa (healthy model) and 16 KPa (periodontitis model). Thus, in these conditions it is possible to appreciate how the mesh quality influence the results and how it is important to compare the obtained values with images that describe the stress distribution in order to avoid mistakes in the interpretation of results.

In *Figure 74* and *75* are also reported the values of stress for the teeth as a comparison between healthy and periodontitis model.

The stress in the mandible increases with the bone resorption, since the application of the force over teeth creates a higher stress, localized especially in the cervical area of teeth. This aspect is underlined by a more uniform stress trend than that recorded over the PDLs. There is only an exception for tooth 46, where a decrease of stress in the periodontitis model is recorded around

1%. Whereas in all the other teeth of the periodontitis model the percentage oscillates from 4% to 86%. A 4% in tooth 41, 11% in tooth 45, 12% in tooth 47, 23% in tooth 44, 29% in tooth 42 and 86% in tooth 43 (the same tooth in which the PDL deformation is the greatest). The concentration of stress over this tooth could be explained by observing the CAD model *(Figure 56)* in which the canine is subjected to a major exposure due to periodontium damage. In maxilla *(Figure 75)* the percentage that describes the stress path oscillates more with a range of -14% to 29%. The lowest percentage is recorded in tooth 12, and then goes on in tooth 15 with -7%. The highest percentage is recorded in teeth 11 and 14. By observing *Figure 76* it is possible to visualize the stress distribution over the teeth in both the arches.

It must be said that the results describing the stress over teeth and especially over PDLs cannot be compared with any article in literature, since the actual studies report values of stress in relation to a specific orthodontic force like tipping, intrusion and extrusion. In this case the applied force, provoked by the MAD functioning, generates over PDLs and teeth a stress which is a product of the action of several forces.

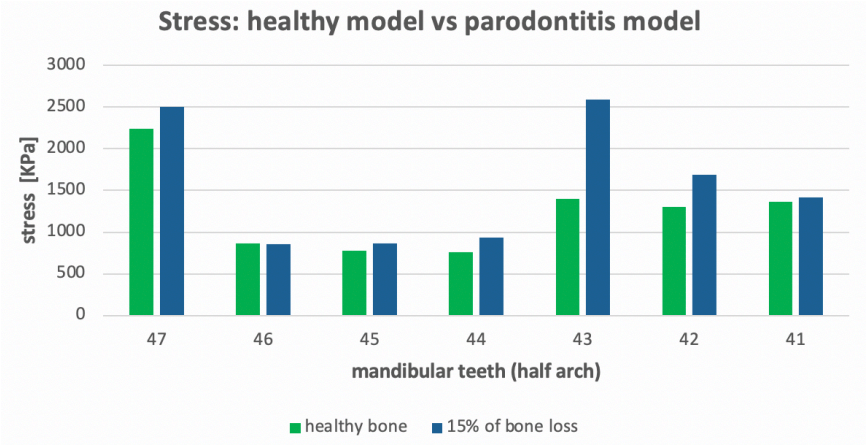

Figure 74 Comparison of stress over mandibular teeth (with the ISO system numeration) in both the healthy and periodontitis model.

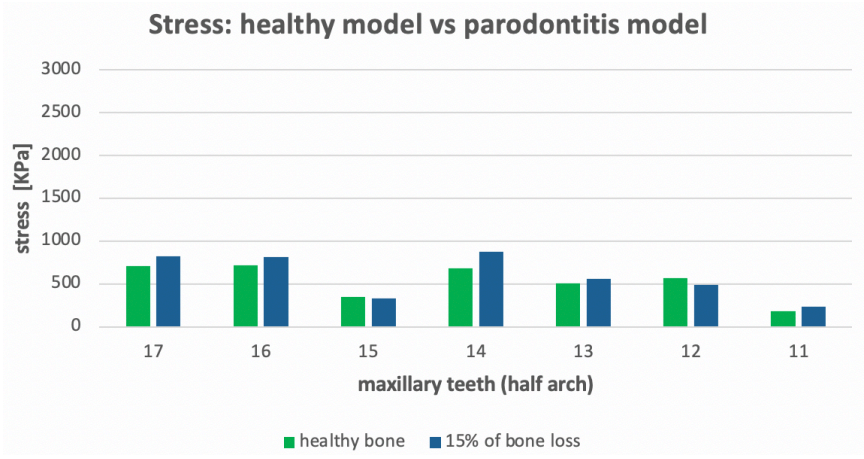

Figure 75 Comparison of stress over maxillary teeth (with the ISO system numeration) in both the healthy and periodontitis model.

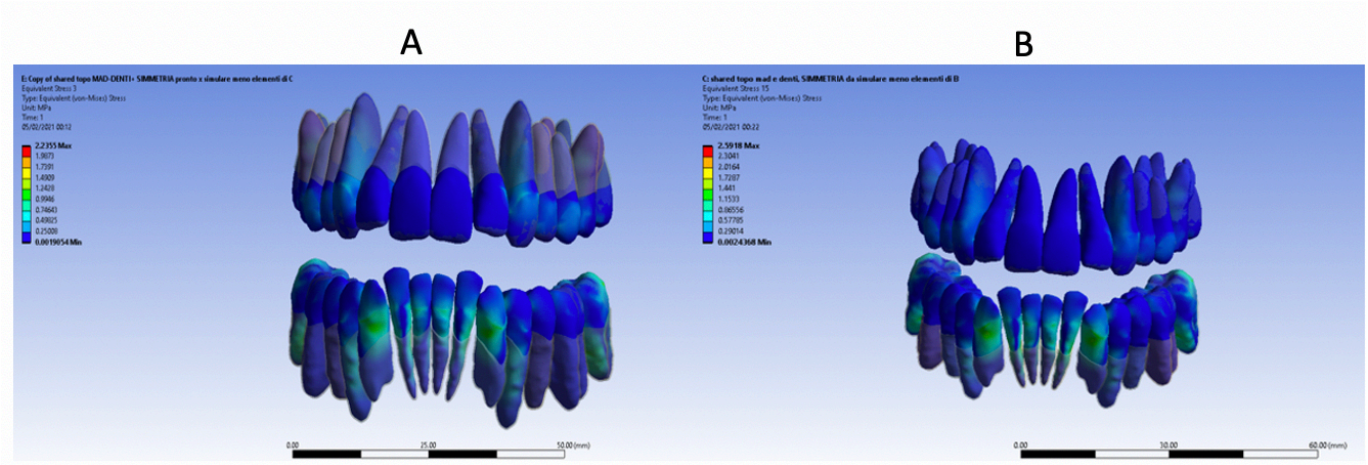

Figure 76 Stress distribution over the teeth. A) in healthy model; B) in periodontitis model.

7. Chapter 7: Conclusion

To conclude,

In this work through the RE approach and the FEM it was possible to reproduce and evaluate the mechanical interactions between the new SomnoDent Avant device and the anatomical components of oral cavity in two different conditions: with the 15% of alveolar bone loss (due to periodontitis) and without any loss. The results that came out from the comparison of these two different conditions, simulated by means of CAD software, underline that teeth and PDLs are affected by higher values of stress and deformation during bone reabsorption. For the deformation evaluated over the teeth a positive trend is recorded passing from the healthy to the periodontitis model in both the dental arches. In the mandible the increasement of deformation, passing from the heathy to the periodontitis model, ranges between the 9% and the 11%, while in the maxilla the increment of deformation ranges between the 3% and the 14%. For what concern the stress over PDLs, the trend is a little bit swinging with values that variate from negative to positive in both the arches. In the lower arch the maximum increment of stress of the 24% is recorded over the III PDL that corresponds to tooth 43, while in the upper arch the maximum increment of the 14% is recorded over the VII PDL that corresponds to tooth 17. The results of this work are in line with the articles describing a situation of bone resorption, since greater deformation and stress values are documented in the most worn areas as might be expected. However, not all the results of this work are comparable with the results found in the literature, since in this study OSAS and periodontitis are combined together and this aspect makes this work innovative. In fact, until now, no one has studied this combination because these two pathologies have always been treated separately. This work has therefore helped to shift attention to the effects caused by the application of MAD in an already delicate oral health condition. Obviously, this is only the beginning of a series of works that will focus on this topic, going to better investigate the stages of periodontitis associated with OSAS (since in this work only the first stage is evaluated) and also introducing the edentulism which is a direct consequence of the most advanced stages of periodontitis.

References

[1] Berkovitz B.K.B., Moxham B.J., Newmann H.N., 1995. The periodontal ligament in health and disease, Mosby-Wolfe, London.

[2] Christina Dorow, Natasˇa Krstin, Franz-Günter Sander. Determination of the Mechanical Properties of the Periodontal Ligament in a Uniaxial Tensional Experiment. J Orofac Orthop 2003; 64:100–7.

[3] Risorsa web: http://www.datgenius.com/predental/dental-anatomy/

[4] Prof Maged Lotfy, "Tooth Morphology & Physiology", Oral Biology Dept., Faculty of Dentistry, Ainshams University, Cairo, Egypt, 2012.

[5] Katarzyna Gorka, "Dental morphology and dental wear as dietary and ecological indicators: sexual and inter-group differences in traditional human populations", Doctorat en Biodiversitat, Universitat de Barcelona, 2010/11.

[6] Risorsa web: https://en.wikipedia.org/wiki/Dental_notation

[7] Karl A. Franklin, Eva Lindberg "Obstrictive Sleep Apnea is a common disorder in the population-a review on the epidemiology of sleep apnea" Jouranal of Thoracic Disease 2015;7(8):1311-1322.

[8] Eva-Azagra Calero, Eduardo Espinar-Escalona, Josè-Maria Barrera-Mora, Josè-Maria Llamas Carreras, Enrique Solano Reina "Obstructive Sleep Apnea Syndrome (OSAS). Review literature". Med Oral Patol Oral Cir Bucal 2012 Nov 1;17(6): e925-9.

[9] Braghiroli A, Marrone O, Sanna A, et al. "Linee guida di procedura diagnostica nella sindrome delle apnee ostruttive nel sonno nell'adulto". Commissione paritetica Associazione Italiana Pneumologi Ospedalieri (AIPO) - Associazione Italiana Medicina del Sonno (AIMS). Rassegna di Patologia dell'Apparato Respiratorio. 2001; 16:278-280. 116

[10] Won Lee, Swamy Nagubadi, Meir H. Kryger, Babak Mokhlesi "Epidiemology of Obstructive Sleep Apnea: a Population-based Perspective", Expert Rev Respir Med 2008 June 1; 2(3): 349–364. doi:10.1586/17476348.2.3.349.

[11] Remmelink HJ1, Hoeke A "Dutch national guidelines for diagnosis and treatment of obstructive sleep apnea syndrome in adults". Ned Tijdschr Tandheelkd. 2010 Apr;117(4):227-31

[12] Ngiam J1, Balasubramaniam R, Darendeliler MA, Cheng AT, Waters K, Sullivan CE. “Clinical guidelines for oral appliance therapy in the treatment of snoring and obstructive sleep apnoea”, Aust Dent J. 2013 Dec;58(4):408-19.

[13] Sutherland K, Deane SA, Chan AS, Schwab RJ, Ng AT, Darendeliler MA, Cistulli PA. “Comparative effects of two oral appliances on upper airway structures in obstructive sleep apnea” 2011 Apr 1;34(4):469-77. 117

[14] Shadi Basyuni, Michal Barabas, Tim Quinne “An update on mandibular advancement devices for the treatment of obstructive sleep apnoea hypopnoea syndrome”, Journal of Thorcic Disease, 2018 Jen.

[15] Chan AS, Lee RW, Srinivasan VK, Darendeller MA, Grunstein RR, Cistulli PA. “Nasopharingoscopic evaluation of oral appliance therapy for obstructive sleep apnoea”. Eur Resp J 2010; 836-42.

[16] Risorsa web: www.who.int

[17] Maurizio S. Tonetti, Henry Greenwell, Kenneth S. Kornman, “Staging and grading of periodontitis: Framework and proposal of a new classification and case definition”, Journal of Clinical Periodontology - WILEY, 2018 Feb.

[18] Risorsa web: *https://it.wikipedia.org/wiki/Finite _Element_Analysis*

[19] Rhinoceros 6 – User’s Guide.

[20] Risorsa web: *http://www.my-personaltrainer.it/salute/tac.html*

[21] Risorsa web: *https://it.wikipedia.org/wiki/Nuclear _Magnetic_Resonance*

[22] Risorsa web: *http://www.centroradiologicopotito.it/radiologia-odontoiatrica2/24-giagnostica-odontoiatrica/82-tc-3d-conebeam*

[23] Risorsa web:
www.ingenioweb.it/Articolo/4844/Cosa_si_intende_per_analisi_agli_elementi_finitie.html

[24] Risorsa web: https://it.wikipedia.org/wiki/Finite_element_analysis

[25] Risorsa web:

http://www1.unipa.it/antonio.pantano/2012SN_Lezione_11_del_25-10-2012.pdf

[26] Risorsa web: *https://it.wikipedia.org/wiki/Siemens_NX*

[27] Risorsa web: https://www.simscale.com/docs/simwiki/fea-finite-element-analysis/what-is-fea-finite-element-analysis/

[28] Charles Tremblay, Pascale Beaudry, Caroline Bissonnette et al. , "Periodontitis and Obstructive Sleep Apnea: A Literature Review", Journal of Dental Sleep Medicine, 2017;4(4):103–110.

[29] Pirelli P, Saponara M, Guilleminault C., "Rapid maxillary expansion (RME) for pediatric obstructive sleep apnea: a 12-year follow-up", Sleep Med 2015;16:933-5.

[30] Denis Bignotti, Alberto De Stefani, Luca Mezzofranco, Giovanni Bruno, Antonio Gracco, "Multidisciplinary Approach in a 12-Year-Old Patient Affected by Severe Obstructive Sleep Apnea: a Case-Report", Sleep Med Res 2019;10(2):103-107.

[31] Alberto De Stefani, Giovanni Bruno, Ludovica Agostini, Luca Mezzofranco, Antonio Gracco, "Resolution of a Severe Grade of Obstructive Sleep Apnea Syndrome with Mandibular Advancement Device: A Case Report", Sleep Med Res 2020;11(1):44-48.

[32] Agnese Brunzini, Marco Mandolini, Steve Manieri, Michele Germani, Alida Mazzoli, "Finite elements analysis of the stress distribution on temporomandibular joint due to the use of mandibular advancement devices", 15th International Symposium on Computer Methods in Biomechanics and Biomedical Engineering and 3rd Conference on Imaging and Visualization CMBBE 2018.

[33] Alberto De Stefani, Giovanni Bruno, Marco Mandolini, Alida Mazzoli, "Strength distribution on TMJ using mandibular advancement device for OSAS treatment: A finite element study", Dental Cadmos, September 2018.

[34] Giovanni Bruno, Alberto De Stefani, Edoardo Conte, Manila Caragiuli, Marco Mandolini, Daniele Landi, Antonio Gracco, "A Procedure for Analyzing Mandible Roto-Translation Induced by Mandibular Advancement Devices", Materials 2020, 13, 1826.

[35] M. Halachmi, A. Gavish, E. Gazit, E. Winocur, T. Brosh, "Splints and stress transmission to teeth: an in vitro experiment", Journal of Dentistry 28 (2000) 475–480.

[36] Jonghun Yoon, Sang Hwa Lee, Yuhyeong Jeong, Dong-Hyun Kim, Hyun-Il Shin and So Yun Lim, "A Novel Mandibular Advancement Device for Treatment of Sleep-Disordered Breathing: Evaluation of Its Biomechanical Effects Using Finite Element Analysis", Applied Science 2020, 10, 4430.

[37] Kharidhi Laxman Vandana, Mittal Deepti, Muneer Shaimaa, Karnath Naveen, Desai Rajendra, “A finite element study to determine the occurrence of abfraction anddisplacement due to various occlusal forces and with differentalveolar bone height”, Journal of Indian Society of Periodontology 2015.

[38] Cristina Bica, Ligia Brezeanu, Dorin Bica, Mircea Suciu, “Biomechanical reactions due to orthodontic forces. A finite element study”, 8th International Conference Interdisciplinarity in Engineering 2014.

[39] Allahyar Germany, “Alveolar bone resorption and the center of resistance modification (3-D analysis by means of the finite element method)”, American Journal of orthodontics and Dentofacial Orthopedics, April 2000.

[40] Jayam Bharath Kumar, Gudimetla Jaisekhar Reddy, Moturi Sridhar, T. Jayasimha Reddy, Pyata Jaipal Reddy, Sadam Srinivasa Rao, “A finite element analysis of initial stresses and displacements in the tooth and the periodontium in periodontally compromised simulations: Labial versus lingual force application”, Journal of Dr. NTR University of Health Sciences 2016;5(1) 34-43.

[41] Azin Zargham, Allahyar Geramy, Gholamreza Rouhi, “Evaluation of long-term orthodontic tooth movement considering bone remodeling process and in the presence of alveolar bone loss using finite element method”, orthodontic waves 2016.

[42] Sung-Hwan Choi, Young-Hoon Kim, Kee-Joon Lee, Chung-Ju Hwang, “Effect of labiolingual inclination of a maxillary central incisor and surrounding alveolar bone loss on periodontal stress: A finite element analysis”, the Korean Journal of orthodontic, 2015.

[43] Agnese Brunzini, Antonio Gracco, Alida Mazzoli, Marco Mandolini, Steve Manieri, Michele Germani “Preliminary simulation model toward the study of the effects caused by different mandibular advancement devices in OSAS treatment”

[44] Tomohisa Nagasao, Tsuyoshi Kaneko, Junpei Miyamoto, “A comparative study of most suitable miniplate fixation for mandibular symphysis fracture using a finite element model”, The Keio Journal of Medicine, April 2006.

[45] A. Pérez del Palomar, M. Doblaré, “On the numerical simulation of the mechanical behaviour of articular cartilage”, International Journal for Numerical Methods In Engineering 2006.

[46] A. Pe´rez del Palomar, M. Doblare´, “Finite element analysis of the temporomandibular joint during lateral excursions of the mandible”, Journal of Biomechanics 39 (2006) 2153–2163.

[47] Giovanni Bruno, Alberto de Stefani, Manila Caragiuli, Francesca Zalunardo, Alida Mazzoli, Daniele Landi, Marco Mandolini and Antonio Gracco, “Comparison of the Effects Caused by Three Different Mandibular Advancement Devices on the Periodontal Ligaments and Teeth for the Treatment of Osa: A Finite Element Model Study”, Applied Science 2020.

[48] Wu Bin, Yan Bin,” Study on Stress Distribution in Periodontal ligament of Impacted Tooth Based on Hyperelastic model”, 2009.

[49] B. O'Malley, J. Kópházi, M.D. Eaton, V. Badalassi, P. Warner, A. Copestake, “Pyramid finite elements for discontinuous and continuous discretizations of the neutron diffusion equation with applications to reactor physics”, Progress in Nuclear Energy 105 (2018), 175–184

[50] Manila Caragiuli, Marco Mandolini, Daniele Landi, Giovanni Bruno, Alberto De Stefani, Antonio Gracco, “A finite element method for evaluating mandibular advancement devices”

[51] Range Viewer – User’s. Guide

[52] Finocchio Matteo, “Dispositivi di avanzamento mandibolare: Studio e valutazione degli effetti su articolazioni e legamenti”, Master Degree in Mechanical Engineering (2018/19), paragraph 5.2

[53] Cohen-Levy J, Pételle B, Pinguet J, Limerat E, Fleury B. 2013. Forces created by mandibular advancement devices in OSAS patients A pilot study during sleep. Sleep Breath. 17: 781–789.

[54] Porto Oc, Silva Bs, Silva Ja, Estrela Cr, Alencar Ah, Bueno Mr, Estrela C; “CBCT assessment of bone thickness in maxillary and mandibular teeth: an anatomic study”; Journal of applied oral science 2020.

[21] [17] Yaser M. Alkiary, Tamer M. Nassef, Inas A. Yassine, Seham B. Tayel, Abd ElSalam kh. Ezzat, “A New Numerical Model to Analyze Stress Distribution of TMJ Disc from 2-D MRI Scan”, Advances in Computing 2012, 2(5):66-75.

[22] [18] A. Pèrez del Palomar, M. Doblarè, “Finite element analysis of the temporomandibular joint during lateral excursions of the mandible”, Journal of Biomechanics 39 (2006), 2153-2163.

[24] [20] Alkhiary YM, Nassef TM, Yassine IA, Tayel SB, Ezzat AE., “A new numerical model to analyze stress distribution of tmj disc from 2-D MRI scans”, 2012, AC. 2(5):66–75.

[37] Kharidhi Laxman Vandana, Mittal Deepti, Muneer Shaimaa, Karnath Naveen, Desai Rajendra, “A finite element study to determine the occurrence of abfraction an displacement due to various occlusal forces and with different alveolar bone height”, Journal of Indian Society of Periodontology 2015.

[53] Cohen-Levy J, Pételle B, Pinguet J, Limerat E, Fleury B. 2013. Forces created by mandibular advancement devices in OSAS patients A pilot study during sleep. Sleep Breath. 17: 781–789.